UNIVERSITÀ
DEGLI STUDI
DI TRIESTE

UNIVERSITÀ DEGLI STUDI DI TRIESTE

XXXVIII CICLO DEL DOTTORATO DI RICERCA IN

AURORA KINASE A IN CHRONIC LIVER DISEASE AND HEPATOCELLULAR CARCINOMA: DISTINCT MECHANISMS AND ROLES

Settore scientifico-disciplinare: **MED/12**

DOTTORANDO / A
CLARISSA GARCIA

COORDINATORE
PROF. ALESSANDRO TOSSI

SUPERVISORE DI TESI
PROF. CLAUDIO TIRIBELLI

SUPERVISORE DI TESI
DOTT. DEVIS PASCUT

ANNO ACCADEMICO 2024/2025

Table of Contents

List of Figures and Tables

Summary

This study investigated the potentially distinct role of Aurora Kinase A (AURKA) in chronic liver disease (CLD) and hepatocellular carcinoma (HCC), revealing context-dependent regulatory mechanisms that remain poorly investigated in CLD and HCC contexts.

Analyses of 56 paired HCC samples revealed a striking mRNA-protein discordance. While *AURKA* mRNA was significantly elevated in tumors, AURKA protein demonstrated the opposite pattern, with marked upregulation in the adjacent, non-tumoral tissues. Immunohistochemical (IHC) validation confirmed the overexpression of AURKA with predominantly hepatocytic expression within the chronically injured liver tissues across various etiologies. Notably, phospho-AURKA (Thr288), the activated form of the enzyme associated with cell cycle control, was elevated in 61% of the tumors, suggesting that enhanced regulatory activity of the cell cycle, rather than the total expression, is linked to neoplastic transformation.

In the adjacent tissues, AURKA protein levels significantly correlated with the expression of Yes-associated protein 1 (YAP1), while no correlation was found in HCC. YAP1 protein was also significantly increased in both adjacent and metabolic dysfunction-associated steatotic liver (MASLD) tissue samples. Functional validation through AURKA silencing in JHH6 cells demonstrated a marked reduction in total YAP1 protein with minimal effect on phospho-YAP1 (Ser397) expression, suggesting AURKA modulates YAP1 stability rather than phosphorylation-dependent activation, potentially affecting liver regeneration, DNA damage response and apoptosis.

AURKA has emerged as a positive regulator of PD-L1 expression in HCC cells. Both pharmacological inhibition (AK-01) and knockdown (siRNA) consistently reduced PD-L1 protein levels in HCC cells. With distinction, while silencing primarily affects newly synthesized PD-L1, AK-01 reduces the stability of PD-L1 inducing a proteasome-dependent degradation.

Different cell lines exhibit varying PD-L1 stability: JHH6 cells showed the longest PD-L1 half-life, while HLE and Hep3B demonstrated the shortest, which was also associated with very low PD-L1 levels.

Contrary to what has been reported in literature, PD-L1 proteasomal degradation appears to be GSK-3β independent. Neither AURKA inhibition nor knockdown altered p-GSK-3β (Ser9) levels. Furthermore, GSK-3β knockdown failed to recapitulate PD-L1 accumulation, suggesting cell-specific effects rather than the predicted GSK-3β-mediated PD-L1 reduction.

Comparative gene expression profiling revealed that AURKA and GSK-3β operate through largely independent regulatory networks. In JHH6 cells, AURKA knockdown downregulated proliferation markers (*CTNNB1*, *AXIN2*) and glycolytic genes (*GLUT1*, *PKM2*), while in HuH7 cells, AURKA demonstrated broader control over metabolism, fibrosis, and inflammatory pathways. GSK-3β showed a more focus, cell-specific effects. Notably, *CDKN1A* emerged as a convergent target, with its expression positively regulated by both AURKA and GSK-3β, as evidenced by consistent downregulation following knockdown of either kinase across cell lines.

These findings establish AURKA as a context-dependent regulator with distinct functions in CLD and HCC. In chronically injured liver, AURKA-YAP1 signaling may coordinate tissue repair responses, while in established tumors, AURKA promotes immune evasion through PD-L1 stablization. The correlation between AURKA and YAP1 in adjacent tissues further suggests potential biomarker utility for CLD progression, while AURKA's role in PD-L1 regulation positions it as a compelling target for combination immunotherapy strategies in HCC.

This work fundamentally reframes AURKA from a simple oncogenic driver to a key hub in a complex network of signaling pathways whose functions adapt to pathophysiological context, offering new therapeutic opportunities across the liver disease spectrum.

Chapter 1

Introduction

Liver cancer remains the sixth most diagnosed cancer and the third leading cause of cancer-related mortalities worldwide, with approximately 866,136 new cases and 758,725 deaths recorded globally in 2022 [1]. The high mortality-to-incidence ratio (MIR) of 0.86 underscores the persistently high mortality of this disease globally [2]. Recent projections based on GLOBOCAN 2020 data indicate that new cases and deaths from liver cancer will increase by more than 55% in 2040, with an estimate of 1.4 million new diagnoses and 1.3 million deaths expected in that year [3]. Liver cancer also demonstrates a strong male predominance globally, with males accounting for approximately 69.35% of all cases and 68.78% of all deaths in 2022 although the male-to-female ratio varies across regions but consistently demonstrates male predominance, ranging from 2.03 to 3.78 in very high human development index (HDI) nations [1,2].

1.1. The adjacent tissue paradox in HCC

Hepatocellular carcinoma (HCC) represents the predominant form of primary liver cancer, accounting for around 90% of all liver malignancies worldwide [4]. HCC remains a progressive disease that predominantly develops in patients with chronic liver disease (CLD), with approximately 80-90% of cases occurring in the context of chronic liver inflammation, fibrosis, and cirrhosis [5]. Despite significant advances in overall patient management, early diagnosis remains a challenge, and prognosis particularly for advanced cases remains poor with a five-year survival rate of less than 20% [1].

A critical but often overlooked aspect of HCC pathogenesis is the nature of the "adjacent, non-tumoral" tissues. While conventionally considered as representative of normal liver parenchyma for comparative studies due to the lack of healthy tissue samples, emerging evidence suggests that these tissue samples represent a field of

chronic injury and aberrant signaling—a microenvironment that may actively contribute to disease progression and therapeutic resistance [6,7]. Our preliminary investigations revealed an unexpected finding that challenges the conventional assumption about tumor biology: *Aurora Kinase A (AURKA) protein expression was significantly upregulated in paired, adjacent non-tumoral tissues of HCC patients compared to the tumor nodules themselves*. This result prompted the fundamental re-examination of this kinase's functions across the liver disease spectrum and forms the central thesis of this investigation.

This paradoxical finding suggests that the molecular alterations driving liver diseases are more complex and context-dependent than previously understood, with regulatory proteins exhibiting distinct functional profiles depending on the specific pathological microenvironment. Understanding these context-dependent regulatory mechanisms could provide crucial insights into disease progression mechanisms and reveal novel therapeutic targets that have been overlooked by conventional tumor-centric approaches.

1.2. Aurora kinase A: from cell cycle control to disease pathogenesis

AURKA, a serine/threonine kinase primarily known of its essential role in cell cycle regulation and mitosis, has emerged as a critical regulatory molecule with diverse functions beyond cell division [8,9]. While AURKA's oncogenic functions are well-established across many solid tumors, including HCC, its broader regulatory mechanisms and downstream targets in liver pathophysiology remain incompletely understood [8–10].

1.2.1. Aurora kinase A: Structure and canonical function

The AURKA gene is located on human chromosome 20q13.2 and encodes for at least 16 known transcript variants. The reference transcript encodes for a protein consisting of 403 amino acids (403 aa). This protein contains a central kinase domain flanked by two regulatory regions that lack catalytic activity (Figure 1). Indeed, the N-terminal region (amino acids 39-139) and a the C-terminal region

(amino acids 15-20) contain most of the regulatory sequences [10,11]. AURKA protein has a complex structure, its kinase domain adopts a tertiary structure consisting of a β-sheet at the N-terminal and an α-helix at the C-terminal, linked by a flexible hinge region and an ATP-binding site where the ATP molecule attaches to the hinge region through hydrogen bonds [12] (Figure 2). An intermolecular reaction within the AURKA domain triggers autophosphorylation on the catalytic residue Threonine 288 (Thr288) of the C-terminal lobe, leading to a 3D conformational change that opens the catalytic loop and activates kinase activity [13]. The N-terminal domain facilitates AURKA interactions with other proteins, controlling its localization and functions. Both the N-terminal and C-terminal domains contain specific degradation sequences known as A-box/D-box activating domain (DAD) and destruction box (D-box), respectively, which are recognized by the Cdc20 homologue 1 (CDH1) protein that activates the Anaphase-promoting complex/Cyclosome (APC/C) complex. Additionally, the N-terminal domain contains the KEN motif, which is also targeted by CDH1-APC for AURKA degradation [14–16] (Figure 1).

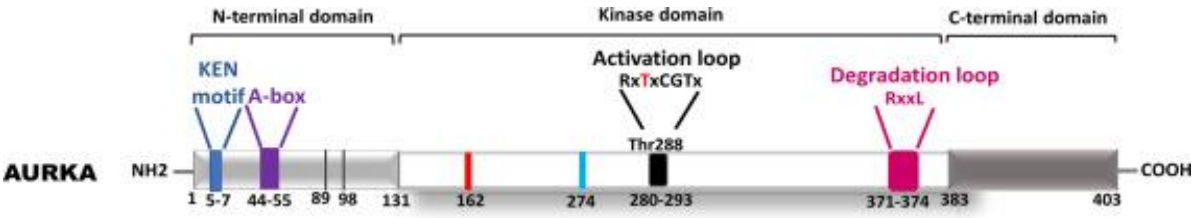

Figure 1. AURKA Protein Structure. The 403-amino acid AURKA protein features a central kinase surrounded by N-terminal and C-terminal non-catalytic regions. The catalytic Thr288 residue essential for AURKA activation is located within the activation loop. Degradation regulatory elements also known as degrons include KEN motif (blue), A-box/Dad (purple) and DAD/A boxes (Taken from Hassan & Noor, 2022*)* [11].

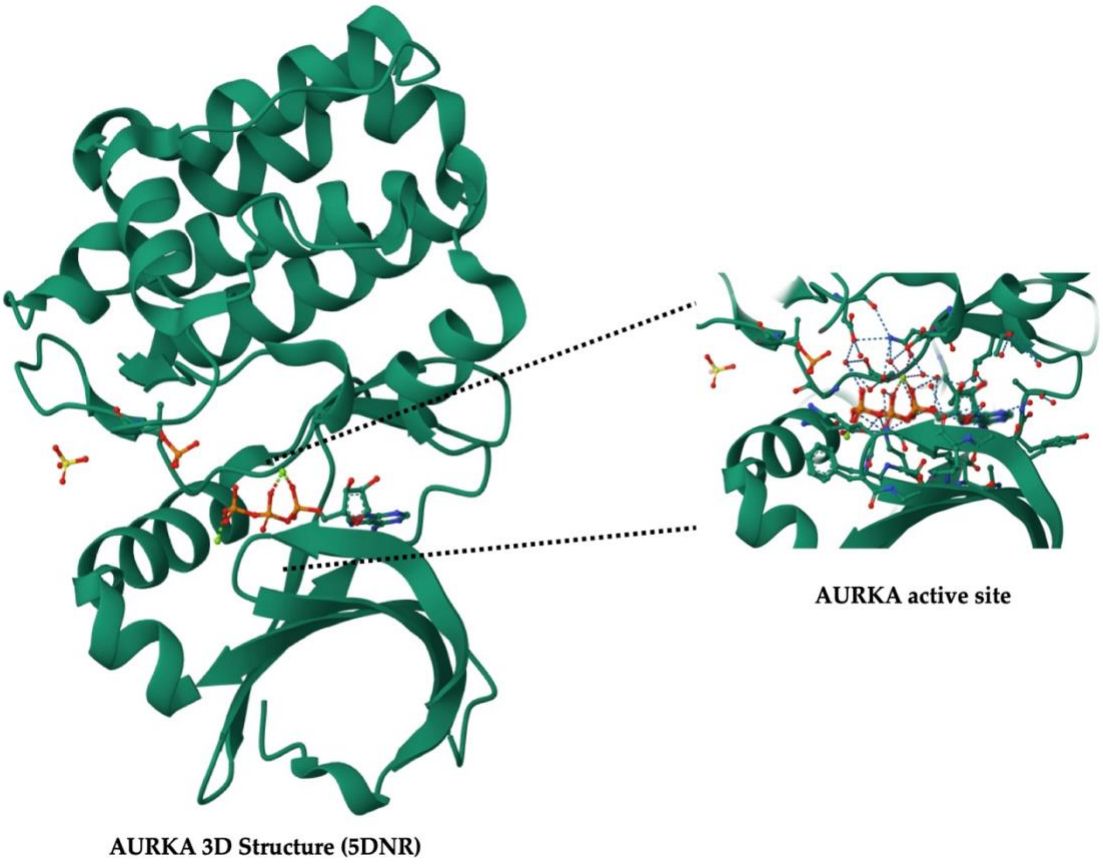

Figure 2. Aurora kinase A 3D Protein Structure. The crystal structure 5DNR from the Protein Data Bank (PDB) database (include the link) shows human AURKA structure in its open, ATP-bound configuration. Phosphorylation of the activation loop activates AURKA by inducing conformational changes that allow ATP and substrate binding (Taken from Janecek et al., 2016) [12].

1.2.2 Aurora kinase A: Physiological function and cell cycle role

Under normal conditions, AURKA serves as an indispensable regulator of the cell cycle, orchestrating multiple critical aspects of mitosis including G_2/M transition, centrosome maturation, mitotic entry, microtubule reorganization, spindle assembly, and the final cytokinetic division [14]. AURKA activity increases in the late stages of S and G_2 phases and peaks in mitosis. AURKA activation is mediated by phosphorylation by BORA Aurora Kinase A activator (BORA) and this triggers the Cyclin-dependent kinase (CDK1)-Cyclin B complex to unlock the G_2/M checkpoint, allowing mitosis to progress. Activated AURKA then localizes in the centrosome, where it phosphorylates

pericentriolar material proteins including Centrosomin, Large tumor suppressor 2 (LATS2), and Breast cancer type 1 (BRCA1). This promotes microtubule nucleation, a step required for mitotic spindle assembly. AURKA then interacts with TPX2 microtubule nucleation factor (TPX2) in the metaphase stage [12]. Furthermore, AURKA phosphorylates Heterochromatin protein 1 gamma (HP1γ) on Ser83, a key reader of histone H3K9 methylation, therefore facilitating AURKA's role in the epigenetic regulation of the cell cycle progression, thus inducing cell proliferation [17]. Moreover, mutations in *AURKA* gene causes disrupted spindle assembly, with the resulting abnormal spindles displaying an 'aurora'-like appearance [18,19]. Hence, the importance of AURKA regulation is underscored by the consequences of its dysfunction. These defects in spindle formation lead to chromosomal instability (CIN), aneuploidy, and ultimately contribute to the genomic instability—a well-recognized hallmark of cancer [20].

1.3. Beyond mitosis: Emerging non-canonical functions of AURKA

While AURKA's mitotic functions are well-established, mounting evidence suggests that AURKA exhibits functional plasticity extending beyond cell cycle regulation. Our unexpected finding of AURKA overexpression in the adjacent "non-tumoral" tissues led to the hypothesis that AURKA exhibits distinct regulatory functions depending on the pathological context. This functional versatility positions AURKA as a critical regulatory hub in liver pathogenesis, potentially in a context-dependent manner. Thus, this concept of context-dependent signaling represents a paradigm shift of cellular regulation. Rather than functioning as a simple "on/off" switch, AURKA appears to act as an integrator of multiple upstream and downstream signals in liver disease progression.

1.3.1. AURKA in chronic liver disease: Orchestrator of liver repair and regeneration

In CLD, AURKA's modulatory functions appear to center on tissue homeostasis, regenerative responses, and the coordination of complex

multicellular processes that are essential for liver repair and adaptation to chronic injury [21–23]. For example, the liver's remarkable regenerative capacity requires a sophisticated molecular machinery to coordinate hepatocyte proliferation, extracellular matrix remodeling, angiogenesis, and inflammatory responses [24]—processes that extend far beyond the canonical cell cycle regulation associated with AURKA.

AURKA mRNA expression in human liver samples exhibits a gradual upregulation throughout the progression of liver disease, progressing from normal liver tissue to CLD and ultimately HCC [25]. Dai and colleagues also demonstrated the significant upregulation of *AURKA* mRNA in human fibrotic and cirrhotic liver samples compared to normal livers, as well as in carbon tetrachloride (CCl_4)-induced and bile duct ligation murine fibrotic livers [22]. AURKA expression was notably observed in activated hepatic stellate cells (HSC), highlighting AURKA's role in promoting HSC activation during fibrosis [22].

The multifaceted role of AURKA in orchestrating liver repair and regeneration through hepatocyte proliferation control and HSC activation creates a biological framework that rationalizes its aberrant expression patterns observed in CLD development [21–23]. Despite this, only a few studies are available in investigating the role of AURKA in CLD. Liu et al., demonstrated how upregulated AURKA in alcohol-related condition functions as a pro-fibrotic factor by preventing HSC senescence. The study further demonstrated that CD73 directly interacts with AURKA and blocks its ubiquitination, thereby stabilizing AURKA protein levels and promoting fibrosis progression through suppression of the p53 signaling that normally induces HSC senescence [26]. AURKA knockdown in LX-2 cells, an immortalized primary human HSC cell line, led to the significant downregulation of Wingless-related integration site (WNT)/β-catenin (CTNNB1) pathway, characterized by marked increase in *GSK-3β*, and downregulated expression of *Wingless-related integration site 6*

(WNT6), *T cell factor 1 (TCF1)*, *Cyclin D1 (CCND1)*, *Matrix metallopeptidase 7 (MMP7)*. Further validation of increased GSK-3β and reduced CTNNB1protein expression following AURKA knockdown suggested that AURKA promotes HSC activation *via* WNT/β-catenin pathway [22].

1.3.2. *AURKA in other fibrotic conditions*

While AURKA's role in CLD remains surprisingly understudied with only two studies to date directly implicating AURKA in CLD progression, emerging evidence from other organ systems strongly supports its pro-fibrotic functions across multiple tissues. Jiang et al. demonstrated that AURKA was highly expressed in fibrotic kidneys from both chronic kidney disease (CKD) patients and mouse models with unilateral ureteral obstruction (UUO), establishing AURKA as a pro-fibrotic mediator in CKD [27]. Furthermore, treatment with MK-5108, an AURKA inhibitor, remarkably attenuated renal fibrosis by suppressing fibroblast proliferation and activation, thereby reducing inflammation [27]. *In vitro* data further confirmed that MK-5108 reduced levels of transforming growth factor-beta 1 (TGF-β1)-induced pro-fibrotic responses in renal cells, providing a proof-of-concept evidence that AURKA inhibition could represent a viable therapeutic node for fibrotic conditions [27]. These cross-organ studies are particularly important because they suggest that AURKA's pro-fibrotic roles may represent a conserved mechanism that operates across different tissue types and disease contexts.

1.4. The potential modulatory role of AURKA on Yes-associated protein 1 (YAP1) in CLD

Given the limited understanding of the underlying molecular mechanisms AURKA is involved in CLD progression as well as the emerging evidence of its pro-fibrotic roles in CLD and CKD, there remains a critical need to identify key downstream effectors through which AURKA exerts its pathological functions within the hepatic microenvironment. One particularly compelling candidate that warrants investigation

is the Yes-associated Protein 1 (YAP1), a transcriptional co-activator and the central effector of the Hippo signaling pathway that has emerged as a master regulator of liver homeostasis and disease progression [28].

YAP1 is a transcriptional co-activator and acts as the central regulator of the Hippo pathway that controls organ size, stem cell self-renewal, and tissue regeneration. In healthy tissues, Hippo kinases such as the Large Tumor Suppressor kinase 1 and 2 (LATS1/2) phosphorylate YAP1 at Serine 127, creating a docking site for 14-3-3 proteins that sequester YAP1 in the cytoplasm, thereby blunting its co-transcriptional activity [29]. LATS1/2 also phosphorylate YAP1 at Serine 397 in the cytoplasm, priming YAP1 for subsequent Casein Kinase 1 (CK1) phosphorylation and eventual proteasomal degradation of YAP1 [30,31]. This dual control of YAP1 activation and localization normally restrains YAP1 in the cytoplasm.

1.4.1. YAP1 dysregulation in liver disease

However, in liver diseases, Hippo attenuation lifts these brakes, allowing the nuclear translocation of YAP1 and elevates YAP1's transcriptional activity, with profound consequences for liver pathophysiology [32,33]. Increased YAP1 activation was previously observed in patients with alcoholic steatosis, hepatitis, and cirrhosis. Additionally, nuclear accumulation of YAP1 was observed in CCl_4-induced hepatocytes in murine models [34]. Moreover, YAP1 levels from patients with fibrosis and cirrhosis showed repetitively elevated expression compared to healthy livers and the extent of YAP1 activity is correlated with the severity of the disease [35,36]. YAP1 activity in hepatocytes promoted fibrosis by activating pro-fibrogenic proteins such as collagen type 1 alpha 1 chain (COL1A1), tissue inhibitor of metalloproteinase 1 (TIMP1), platelet-derived growth factor c (PDGFc), TGF-β2, as well as inflammatory proteins including tumor necrosis factor and interleukin-1β. Patients with non-alcoholic steatohepatitis exhibited a direct correlation between YAP1 and CYR61, a chemokine frequently upregulated during liver injury [37].

1.4.2. AURKA as a non-canonical YAP1 modulator in CLD

Despite the well-described significance of YAP1 expression in several chronic liver disease conditions, the upstream regulatory mechanisms that control YAP1 activity in CLD remain poorly understood. While canonical Hippo pathway regulation has been characterized, non-canonical regulators of YAP1, particularly kinase-mediated post-translational modifications that could be therapeutically exploited, represent a significant knowledge gap. Intriguingly, recent evidence from other fibrotic conditions such as pulmonary fibrosis revealed that AURKA may function as a novel upstream regulator of YAP1 activity, suggesting a potential mechanistic connection that remain unexplored in CLD contexts [38]. Furthermore, the mechanistic basis for AURKA's regulation of YAP1 has been demonstrated across multiple disease contexts, revealing a sophisticated regulatory relationship between AURKA and YAP1. In a triple-negative breast cancer study using MDA-MB-231 cells, AURKA directly phosphorylated YAP1 (Ser397) in the nucleus, increasing YAP1's activity [39]. This establishes a direct kinase-substrate relationship operating independently of the canonical Hippo regulation of YAP1 [39]. Another distinct mechanism of AURKA-mediated YAP1 modulation was demonstrated by Wang et al. in lung cancer (A549 cells) where AURKA activation increased YAP1 protein abundance by blocking autophagy-mediated degradation *via* the mTOR pathway, promoting YAP1 stability and prolonging its transcriptional activity [40]. This regulation required AURKA kinase activity and is independent of proteasomal degradation, Hippo/LATS signaling, and YAP1 Ser397 phosphorylation, as the kinase-dead S397A mutant did not prevent AURKA-driven YAP1 stabilization [40].

These studies collectively suggest that AURKA exhibits multiple mechanisms in maintaining elevated YAP1 activity, utilizing both direct post-translation modifications and protein stability mechanisms to ensure robust YAP1 function

in pathological contexts. Whether similar regulatory mechanisms operate in the liver during CLD progression remains completely unknown, representing a fundamental knowledge gap that requires further investigation to determine the specific molecular pathways through which AURKA might influence YAP1 activity in CLD.

1.5. Chronic liver disease: disease spectrum and etiological landscape

Chronic Liver Disease (CLD) comprises a heterogeneous group of hepatic diseases defined by sustained inflammation and progressive formation of scar tissues as a result of excessive deposition of extracellular matrix (ECM) protein, eventually culminating in cirrhosis [41]. The etiology of CLD is diverse with metabolic dysfunction-associated steatotic liver disease (MASLD) now considered as the most common cause of CLD and is the leading cause of liver-related morbidity and mortality especially in developed nations [42]. CLD can also arise from chronic viral hepatitis B or C infections, and alcoholic liver disease (ALD); other important causes – albeit less common – include certain autoimmune (i.e., primary sclerosing cholangitis, primary biliary cholangitis, and autoimmune hepatitis) and genetic disorders (i.e., hemochromatosis, Wilson's disease, alpha-1 antitrypsin deficiency and polycystic liver disease) [41]. Regardless of the initial cause, chronic liver injury triggers a cascade of cellular and molecular events that disrupt liver homeostasis and lead to fibrotic scarring [43].

1.6. Chronic liver disease: Cellular and molecular complexity

CLD progression follows a relatively consistent pattern at the cellular level: Initial hepatocyte injury triggers the release of damage-associated molecular patterns (DAMPs) and apoptotic bodies which then stimulate the activation of HSCs. Activated HSCs are principally involved in the increased ECM deposition, a key hallmark of fibrosis. Mutual stimulation also occurs between activated HSCs and Kupffer cells, thus recruiting immune cells eventually triggering inflammatory events that further aggravate the disease [44] (Figure 3). Persistent inflammation and fibrosis can

eventually lead to cirrhosis, characterized by disrupted liver architecture and impaired liver function, which significantly raises the risk of developing HCC [45].

The molecular mechanisms underlying CLD represent a complex interplay of HSC cellular activation [46], inflammatory signaling [47], and tissue remodeling processes [24]. The activation of HSCs represents a pivotal event in liver fibrosis pathogenesis. Under physiological conditions, HSCs exist in a quiescent state, serving as Vitamin A storage cells in the space of Disse. However, chronic liver damage triggers their activation into proliferative, contractile, and fibrogenic myofibroblasts [46]. The molecular machinery governing HSC activation involves multiple signaling pathways often originating from the ECM and stimuli from resident and infiltrating inflammatory cells [45]. Transforming growth factor-β (TGFβ) is generally considered as a master regulator of fibrogenesis through SMAD-dependent pathway modulation (Figure 3) [48]. TGF-β further triggers the mitogen-activated protein kinase (MAPK) cascades–including extracellular signal-regulated kinase (ERK/MAPK1), p38 MAPK, and c-JUN N-terminal kinase (JNK) – thereby driving HSC activation [49,50]. Additionally, platelet-derived growth factor (PDGF) which is a crucial mitogen and chemo-attractant in the liver also drives HSC activation and migration [51] (Figure 3). Other notable cytokines that promote HSC activation and proliferation include vascular endothelial growth factor (VEGF) [52], connective tissue growth factor (CTGF) [53], and interleukin-20 (IL-20) [54].

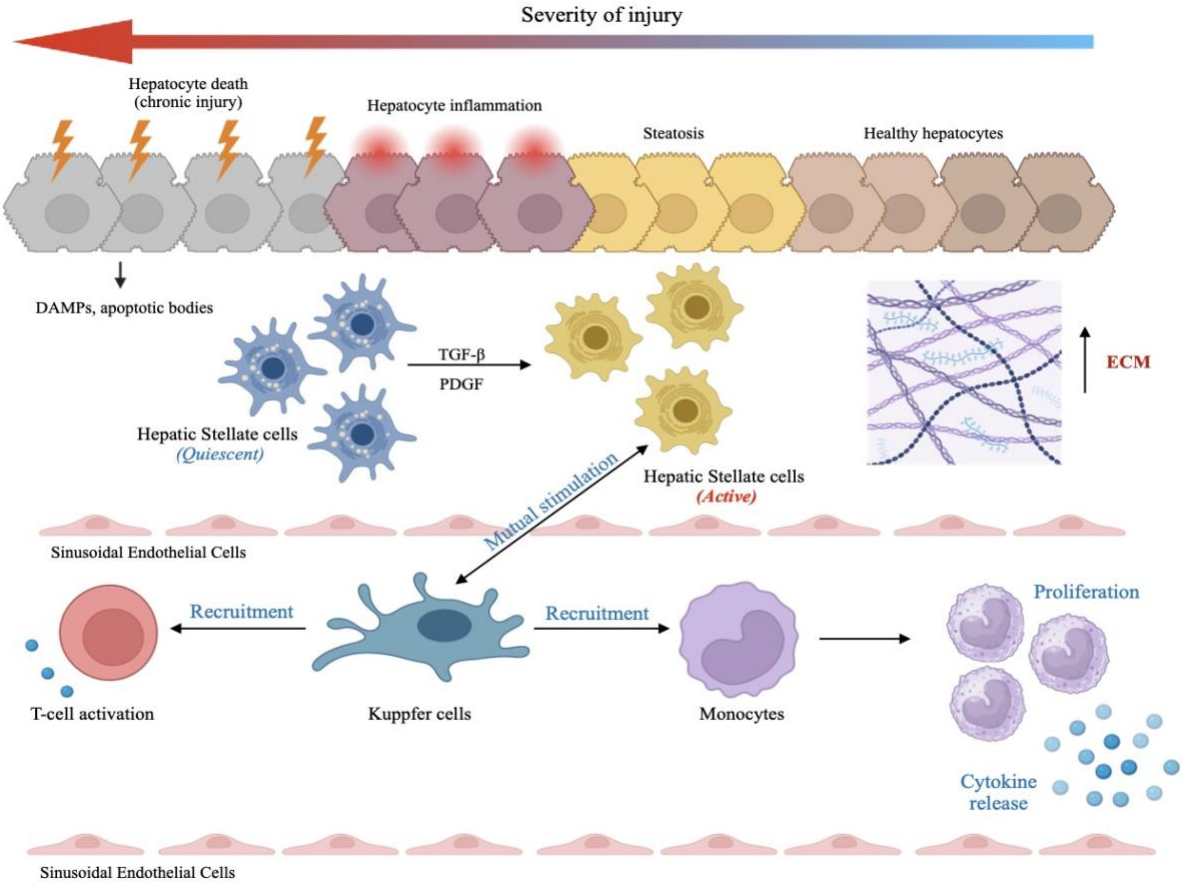

Figure 3. Mechanistic concept of key cellular events occurring in liver fibrosis as seen in chronic liver diseases. The pathogenesis of liver fibrosis primarily occurs due to chronic hepatocyte injury accompanied by inflammation that triggers the release of damage-related patterns and apoptotic bodies, which activate hepatic stellate cells (HSC) and recruit immune cells. Mutual stimulation also occurs between Kupffer cells and activated HSCs, leading to increased extracellular matrix deposition and inflammatory events. Abbreviations: DAMPs: Damage-associated patterns; TGF-b: Transforming Growth Factor Beta; PDGF: Platelet Derived Growth Factor; ECM: extracellular matrix. Created with BioRender.com

Inflammation represents a major feature in CLDs and plays a critical role in any stage of the multi-step fibrogenic cascade. Hepatocyte loss serves as an early, pivotal trigger for chronic inflammation [55]. Apoptotic bodies released from dying hepatocytes prompt macrophages to release pro-inflammatory and pro-fibrogenic cytokines and, *via* autophagy induction, directly promote HSC activation [56]. Apoptotic hepatocytes also shed various damage-associated molecular patterns (DAMPs) such as extracellular ATP, phormyl peptides, High Mobility Group Box 1 (HMGB1) as well as the cytokine IL-33. These signals activate HSCs either directly or indirectly; the latter occurs through IL-33-driven stimulation of group 2 innate lymphoid cells (ILC2),

which subsequently secrete the pro-fibrogenic cytokine IL-13. The simultaneous release of inflammatory mediators infiltrating immune cells exacerbate hepatocyte death, further aggravating liver injury [57].

As a compensatory mechanism, chronic liver injury triggers a maladaptive regenerative response encompassing three overlapping stages–initiation, proliferation, and termination–underlying progressive fibrosis and risk of neoplastic transformation [58]. In acute liver injury, liver regeneration is primarily driven by hepatocyte self-replication, characterized by high expression of Ki67, a marker of cell proliferation, indicating a robust cell division and effective regeneration [59]. Mild injuries, on the one hand, exhibit reduced capacity of mature hepatocytes to replicate. Hybrid Periportal Hepatocytes (HybHP) are specialized cells located near the portal areas that aid in liver regeneration in mild injuries [60]. However, as the chronic liver disease progresses both mature hepatocytes and HybHPs become senescent, paving the way for ductular proliferation since the main regenerative pathways are already exhausted. This process is less effective and is often linked with ongoing fibrosis and an already impaired liver function – although the underlying cause of poor hepatocyte proliferation or replicative senescence in cirrhosis remains poorly understood [61]. Accompanying these cellular responses is the activation of pro-fibrogenic signals (Nuclear Factor kappa-light-chain-enhancer of activated B cells (NF-κB)) [62], proliferative cues (Signal Transducer and Activator of Transcription 3 (STAT3) [63], Insulin-like Growth Factor (IGF) [64], PDGF [65]) and developmental pathways (Sonic Hedgehog (SHH) [66], TGF-β [48], Growth arrest-specific 6 (GAS6)/TYRO3,AXL, and MerTK (TAM) [67], and WNT/β-catenin (CTNNB1) [68,69]). Yet among these cascades, the Hippo pathway and its downstream effector YAP1 has now emerged as critical regulators of hepatocyte fate in physiological and disease contexts [30,32].

1.7. Hepatocellular carcinoma: From chronic liver disease to malignant transformation

The transition from CLD to HCC represents one of the most clinically significant progressions in gastroenterology and oncology. Recent epidemiological projections paint an increasingly concerning picture for the future burden of HCC. The evolving epidemiology of HCC reflects the changing risk factors globally. While viral hepatitis B (HBV) or C (HCV) remain a major driver in many regions including sub-Saharan Africa and Asia, the proportion of HCC patients with ALD and MASLD has increased from 13% to 18% and 5% to 6%, respectively [70,71]. The etiology and distribution of HCC are evolving globally, indicated by the noticeable shift from primarily viral origins to more cases linked to non-viral factors, particular those associated with chronic, excessive alcohol intake and MASLD especially in Europe and North America [72].

Chronic Liver Diseases such as cirrhosis remains one of the major risk factors for HCC since about 80-90% of HCC cases develop in a cirrhotic liver, highlighting the strong link between CLD and hepatocarcinogenesis [73]. The progression from CLD to HCC involves a complex interplay of genetic alterations [74], epigenetic modification [75], and dysregulating signaling cascades [5,41,45,57,72,76] that drive hepatocyte transformation and tumor development [8].

1.8. Molecular pathogenesis: From normal hepatocyte to malignant cell

At the molecular level, HCC arises from the sequential accumulation of somatic mutations and copy number variations targeting key driver genes [74]. Advances in high-throughput next-generation sequencing technologies have enabled profiling of cancer driver genes, revealing both oncogenic and tumor-suppressor mutations in HCC. Telomerase reactivation, predominantly due to mutations in the telomerase reverse transcriptase (TERT) promoter [77], integration of viral genomes [78], chromosomal rearrangements, or gene amplification [79]—alterations collectively present in roughly 80% of HCC cases [4]. On the one hand, hyperactivation of the

WNT/β-catenin (CTNNB1) signaling is typically attributed to the high mutation rate (37%) of catenin B1 (*CTNNB1*) and WNT/β-catenin signal-associated genes (54%). Additionally, loss-of-function mutations occur in tumor suppressor genes within the pathway, such as *AXIN1* and adenomatous polyposis coli (*APC*) [80,81]. Emerging evidence also suggests that hyperactivation of this pathway is linked to low T-cell infiltration in the tumor microenvironment, thus creating an immune-cold HCC tumor that is considered a major factor of resistance to immunotherapy [82].

1.9. Glycogen synthase kinase 3-beta (GSK-3β): a key regulator in HCC

The glycogen-synthase kinase 3-beta (GSK-3β) is a particularly intriguing member of the WNT pathway. GSK-3β is a key negative regulator of this pathway, phosphorylating CTNNB1 at specific serine and threonine residues (Ser33, Ser37, and Thr41) within the β-catenin (CTNNB1) destruction complex thereby targeting CTNNB1 for ubiquitin-mediated proteasomal degradation and maintaining low cytoplasmic CTNNB1 levels in the absence of WNT stimulation [83]. However, GSK-3β seems to have a paradoxical role in HCC. In its active state, GSK-3β phosphorylates CTNNB1 [83], along with other oncogenic substrates such as cyclin D1 (CCND1) [84], and SNAIL [85]—thereby restraining proliferation, epithelial-to-mesenchymal transition (EMT) and metastasis [86]. With its canonical tumor-suppressive role, it is therefore expected to exhibit a lower expression in HCC which was what Huang and colleagues observed in their study of 80 paired HCC tumors and adjacent tissue samples and 20 normal livers [87]. A similar study by Hu and colleagues was conducted, supporting the tumor-suppressive role of GSK-3β in HCC and further suggested that increased GSK-3β in HCC may serve as a good prognostic indicator [88]. Mechanistically, hepatitis B virus (HBx) and hepatitis C virus core/NS5A proteins, as well as tumor-intrinsic drivers such as N-myc downstream regulated gene 1 (NDRG1), RNA binding motif on the Y chromosome (RBMY), Matrilin-2 loss, and Sirtuin 2 (SIRT2) converge on extracellular signal-regulated kinase (ERK)- or

Phosphoinositide 3-kinase (PI3K)/ Protein Kinase B (AKT)-mediated phosphorylation of GSK-3β at Ser9 or Thr43, rendering it inactive [89–92].

1.10. The AURKA-GSK-3β -PD-L1 Axis: Linking cell cycle control to immune evasion

1.10.1. PD-L1: A critical regulator of immune evasion in HCC

PD-L1, also known as CD274 or B7-H1, functions as a key inhibitory checkpoint protein that fine-tunes T-cell responses, thereby safeguarding immune homeostasis required for the removal of pathogens as well as senescent or cancer cells. PD-L1 binds to the programmed cell death-1 (PD-1) receptor, initiating a negative-feedback loop that attenuates T-cell receptor signaling, causing an exhausted phenotype and averting excessive immune activation. Elevated PD-L1 expression suppresses cytotoxic T cells, permitting tumor cells to evade the immune cells [93]. PD-L1 expression in HCC is linked to a progenitor subtype, high tumor mutational burden (TMB), a positive correlation with markers of tumor aggressiveness, macrovascular invasion, and reduced overall survival [94,95]. Despite the transformative impact of PD-L1 targeting in HCC, its therapeutic efficacy remains limited. For instance, the combination of atezolizumab and bevacizumab—which targets PD-L1 and the vascular endothelial growth factor A (VEGF-A), respectively, and constitutes the current standard of care for advanced HCC—yields an objective response rate of only about 30%, even though it improved patient overall survival relative to sorafenib monotherapy [96]. Hence, current efforts focus on two key objectives: (1) identifying reliable biomarkers that can prospectively identify patients most likely to benefit from immune-checkpoint inhibitors (ICIs) and (2) elucidate the molecular circuitry modulating PD-L1 expression in HCC to guide rational combination or sequential therapies.

Multiple mechanistic studies have demonstrated how diverse oncogenic, inflammatory and epigenetic cues converge to induce PD-L1 expression in HCC [97]. Oncoproteins including the Human Leukocyte Antigen (HLA)-F

adjacent transcript 10 (FAT10) and the protein arginine methyltransferase 3 (PRMT3) induce PD-L1 expression in HCC *via* activating PI3K/AKT/mTOR and pyruvate dehydrogenase kinase 1 (PDHK1), respectively, thereby inducing PD-L1 expression in HCC [98,99]. Inflammatory cues within the tumor microenvironment also upregulate PD-L1. M1-polarized macrophages secrete interleukin-1β, which activates NF-κB/Interferon Regulatory Factor 1 (IRF1) signaling in neighboring cancer cells, robustly inducing PD-L1 transcription and surface expression. Immunohistochemical analyses of 90 HCC specimens exhibited high intratumoral M1 macrophage infiltration which positively correlated with PD-L1 expression, underscoring a clinical relevant link between inflammation and immune-checkpoint expression [100].

1.10.2. PD-L1 Glycosylation and GSK-3β-mediated Regulation

Beyond protein expression levels, PD-L1 function is controlled by certain post-translational modifications that alter its biological activity and response to therapeutic intervention. Among these modifications, N-linked glycosylation emerges as a critical determinant of PD-L1 stability, subcellular localization and immune checkpoint function [101]. PD-L1 undergoes extensive N-linked glycosylation at multiple asparagine residues, particularly N35, N192, N200, and N219, resulting in the formation of mature, complex glycoforms (~45 kDa) that exhibit significantly enhanced protein stability compared to their non-glycosylated counterparts (~33 kDa) [102]. This glycosylation process serves multiple functional purposes: mature complex N-glycans stabilize PD-L1 protein structure, thereby enhancing its binding affinity to PD-1 receptor, and critically, provide protection against degradation pathways [103].

This protective effect of glycosylation becomes particularly evident in the context of GSK-3β-mediated regulation of PD-L1 turnover. Catalytically active GSK-3β phosphorylates the non-glycosylated PD-L1 molecule, creating a phosphodegron that recruits E3 ligase beta-transducin repeat-containing

protein (β-TrCP). This leads to ubiquitination and rapid proteasomal clearance of the immature PD-L1 pool [102]. When GSK-3β is blocked either by upstream AKT phosphorylation at Ser9 or by oncogenic signaling, phosphorylation of PD-L1 is therefore inhibited, allowing newly synthesized PD-L1 to escape degradation, becoming fully glycosylated and accumulate into the plasma membrane [102,104].

In HCC, this axis is especially relevant given the observed overexpression of PD-L1 in this tumor type, often correlating with poor patient outcome [105]. However, GSK-3β has been reported to have dual-function in many cancers and, true enough, previous studies have supported this notion. Sun et al. specifically examined macrophage GSK-3β deficiency in tumor-associated macrophages (TAMs) and found that it inhibits HCC growth, proliferation, invasion and migration. It also enhances anti-PD-1 immunotherapy sensitivity where tumors with GSK-3β-deficient macrophages respond to PD-1 blockade. Lastly, their study found the GSK-3β expression in TAMs differed between anti-PD-1 treatment responsive and non-responsive HCC groups [106]. This study appears to contradict the earlier breast cancer study by Li and colleagues [102]. The key difference seems to be cell type specificity where Sun and colleagues focused on GSK-3β function in macrophages rather than tumor cells themselves highlighting that context matters tremendously in evaluating the role GSK-3β in PD-L1 regulation especially in HCC.

1.11. AURKA in hepatocellular carcinoma: Beyond cell cycle control

AURKA's oncogenic influence in HCC encompasses profound dysregulation that fundamentally alters its cellular functions from a tightly controlled cell cycle modulator to an oncogenic driver. This dysregulation manifests through multiple mechanisms including gene amplification, transcriptional upregulation, and post-transcriptional modifications that collectively contribute to AURKA hyperactivation and its subsequent oncogenic effects [9,25]. Clinically, AURKA expression patterns

demonstrate significant prognostic value in HCC. Elevated *AURKA* levels consistently correlate with aggressive tumor phenotypes, advanced pathological staging and poor clinical outcomes across diverse patient cohorts [107,108]. Furthermore, *AURKA* overexpression correlates with increased metastatic potential and therapeutic resistance, reinforcing its role as a driver of advanced HCC [109].

The molecular mechanisms underlying AURKA's oncogenic transformation in HCC encompass multiple cancer hallmarks. AURKA promotes uncontrolled cellular proliferation through direct interaction with *MYC* oncogene, where binding to MYC's nuclear hypersensitive elements enhances its transcriptional activity and drives aggressive tumor behavior [110]. AURKA also orchestrates critical metastatic processes by regulating EMT, chemoresistance and cancer stem cell properties through activation of the PI3K/AKT and p38/MAPK signaling cascades [111]. Under hypoxic conditions within the tumor microenvironment, AURKA enhances cancer cell survival and proliferation by regulating hypoxia-inducible factor 1α (HIF-1 α), further contributing to therapeutic resistance mechanisms [112]. AURKA also promotes the nuclear translocation of CTNNB1, thereby amplifying WNT/β-catenin signaling and promoting malignant transformation [8,113].

1.12. The Hunt for the missing link: AURKA-GSK-3β -PD-L1 regulatory network

Despite extensive documentation of AURKA's oncogenic functions in HCC, critical knowledge gap remains regarding its specific regulatory interactions with key downstream effectors. While AURKA's general influence on many oncogenic pathways is well-established, its precise regulatory function towards GSK-3β and PD-L1 represents an underexplored area of investigation. A study from a gastric cancer model suggested that AURKA negatively regulates GSK-3β *via* phosphorylation at Ser9, thereby blocking the activity of the latter [114]. A more recent study on a partial hepatectomy mouse model similarly suggested that AURKA plays a key role in liver regeneration through its regulatory role on GSK-3β through the same post-translational modification at Ser9 [21]. Importantly, GSK-3β inactivation through Ser9

phosphorylation has been linked to increased PD-L1 expression in melanoma [115], head and neck squamous cell carcinoma (HNSCC) [116], and HCC [117]. Mechanistically, GSK-3β normally functions as a negative regulator of PD-L1 through a phosphorylation-dependent proteasome degradation of PD-L1 in breast cancer [102]. Moreover, glycosylation of PD-L1 at N192, N200 and N219 further antagonizes GSK-3β binding on PD-L1, which further enhances PD-L1 stability [102].

However, the potential AURKA-GSK-3β-PD-L1 regulatory axis has not been investigated in HCC, despite the clinical significance of both GSK-3β dysregulation and PD-L1 overexpression in HCC pathogenesis. Given AURKA's demonstrated ability to inactivate GSK-3β through Ser9 phosphorylation and the established role of GSK-3β as a PD-L1 regulator, we hypothesize that AURKA may indirectly control PD-L1 expression in HCC through a GSK-3β-mediated mechanism. This proposed regulatory network would position AURKA as a dual coordinator of both oncogenic signaling and immune evasion, creating a convergence point where cell cycle dysregulation intersects with immune checkpoint modulation in HCC.

.

Chapter 2

Objectives of the Study

2.1. Study rationale and research objectives

HCC remains one of the most prevalent malignancies worldwide and ranks as the third leading cause of cancer-related mortalities. Despite notable advances in HCC management, this persistent high mortality rate is primarily attributed to many factors such as late-stage diagnoses, tumor heterogeneity, and limited therapeutic options. In advanced stages, the combination of targeted therapy and immunotherapy such as the bevacizumab (anti-angiogenic) and atezolizumab (anti—PD-L1) has become the standard of care therapy, demonstrating improved outcomes compared to previous monotherapies [118,119]. However, the modest improvements observed point to intricate variability and resistance mechanisms inherent to HCC. Consequently, there remains an urgent need to further understand and address the complex pathophysiology of HCC. It is therefore imperative to investigate the molecular mechanisms that drive HCC pathogenesis, to facilitate the identification of clinically relevant targets and therefore aid in the development of targeted drugs that may expand the therapeutic options for HCC patients.

AURKA has emerged as a key oncogene in HCC, participating in crucial functions in tumorigenic events such as proliferation, survival, and metastasis [8]. However, our initial data revealed an unexpected finding: AURKA protein expression was significantly overexpressed in paired, adjacent non-tumoral tissues compared to HCC tumor nodules themselves, challenging conventional tumor biology assumptions. This information suggests that AURKA may exhibit context-dependent regulatory functions across the liver disease spectrum, potentially orchestrating distinct pathways or effectors in CLD versus established malignancy.

Emerging evidence from other disease models such as renal and pulmonary fibroses suggest that AURKA positively influences fibrogenesis [27,38]. The role of Yes-associated protein 1 (YAP1), the central downstream effector of Hippo signaling,

particularly stood out based on several studies demonstrating AURKA's positive modulation of YAP1 in pulmonary fibrosis [38], lung [40], and breast cancer [39]. Importantly, these studies demonstrated different mechanisms by which AURKA positively regulate YAP1, leading us to hypothesize that AURKA may also have a distinct function within the chronically diseased liver. On the one hand, as the disease progresses to overt carcinoma, AURKA's regulatory role may shift towards immune evasion mechanisms and cell cycle progression. AURKA and PD-L1 demonstrate regulatory relationship across multiple cancer models, though the directional impact varies by context. For instance, AURKA inhibition promoted PD-L1 expression in non-small-cell lung cancer [120] and breast cancer, leading to immune suppression [121]. However, in a glioblastoma study, AURKA inhibition suppressed PD-L1 expression, enhancing natural killer cell cytotoxicity [122]. This relationship between AURKA and PD-L1 across different tumor types highlights the complex, context-dependent nature of their interaction and underscores why combination treatment targeting both pathways show promise in overcoming immune evasion mechanisms. However, the relationship between AURKA and PD-L1 in HCC remains unexplored. Broadly, this study aims to investigate the potential relationship between AURKA and PD-L1; and determine whether GSK-3β is a key mediator between AURKA and PD-L1.

Considering the limited information available on AURKA's context-dependent role in liver pathology, this project aims to comprehensively investigate the expression and regulatory functions of AURKA across the continuum from CLD to HCC. We seek to elucidate AURKA's distinct downstream networks, with particular focus on YAP1 regulation in CLD and the GSK-3β-PD-L1 axis in HCC.

2.2. Experimental framework and specific aims

A. Characterization of AURKA's Context-dependent expression patterns

   i. Evaluate AURKA expression and activation status *in vivo* (paired adjacent, non-tumoral *vs* tumor nodules from HCC patients)

ii. Establish correlations with key downstream effectors to define the foundation for context-specific regulatory relationships

B. Define the AURKA-YAP1 axis in CLD by investigating the clinical correlation between AURKA expression and YAP1 regulation in CLD context

i. Assess YAP1 protein levels and phosphorylation status (Ser397) *in vivo*

ii. Evaluate correlations between AURKA expression/activation and YAP1 expression and phosphorylation patterns

iii. Validate functional regulation through AURKA silencing experiments in cell models

C. Investigation of the AURKA- GSK-3β-PD-L1 axis in HCC

i. Assess the expression of GSK-3β and PD-L1 *in vivo* and correlate with AURKA expression patterns

ii. Determine the relationship between AURKA and PD-L1, and AURKA and GSK-3β *in vitro*

iii. Elucidate the tripartite regulatory axis linking AURKA to PD-L1 through GSK-3β-mediated control

D. Assessment of other downstream regulatory effectors of AURKA and GSK-3β in HCC

i. Determine whether AURKA and GSK-3β influences other downstream effectors through an exploratory screening strategy

This study aims to enhance our understanding of the intricate dynamics of AURKA and its context-dependent regulatory networks throughout liver disease progression. The knowledge gained could pave the way for the development of novel therapeutic approaches through rational combination strategies with AURKA blockade at its forefront.

Chapter 3

Materials and Methods

3.1. Human samples

A total of 56 patients with HCC, diagnosed according to the European Association for the Study of the Liver (EASL) criteria, were enrolled in the study. All patients underwent partial hepatectomy between December 2008 and January 2023 at the Department of Surgery, University Hospital, Trieste, Italy. Inclusion criteria were limited to adults with confirmed HCC. Exclusion criteria comprised primary hepatic malignancies or other active malignant diseases, as well as pediatric HCC. The study was approved by Comitato Etico Regionale Unico of Friuli Venezia Giulia, Prot. No. 18854. Informed consent was diligently obtained from each patient or their legal representative. Sensitive data were meticulously protected through anonymization. From each patient, multiple liver specimens were obtained, including tumor nodules and matched adjacent non-tumorous tissues. Sampling followed a standardized protocol specifying specimen size, tissue type, and storage conditions. Fresh tissues were preserved in RNAlater stabilization solution (M7021, Invitrogen, Waltham, MA, USA) or snap-frozen in liquid nitrogen and stored at -80ºC. Parallel portions were fixed in formalin, embedded in parafin, section serially, and subjected to comprehensive histopathological evaluation, including hematoxylin and eosin (H&E) staining, performed by Azienda Sanitaria Universitaria Giuliano Isontina (ASUGI), Trieste, Italy.

The cohort had a median age of 69.95 [62.33-74.48] and included 44 males and 12 women. Reported etiologies were 11% (5/56) hepatitis B virus (HBV), 30% (17/56) hepatitis C virus (HCV), 38% (21/56) metabolic dysfunction-associated liver disease (MASLD) and 9& (5/56) alcohol-associated liver disease (ALD) (Table 1).

Table 1. Pathological Variables and Characteristics of HCC patients.

Variables	HCC (N=56)
Etiology (HCV/HBV/MASLD and/or ALD/mix)	17/6/21/5
Fibrosis Score (F0-F4/F5-F6)	16/38
Child-Pugh Score (A/B/C)	53/3/0
BCLC Classes (0-A/B/C)	38/13/5
Cirrhosis (Y/N)	43/13
Grading (Well/Medium/Poor/Not diff.)	15/28/8/1

Categorical variables were represented by the number of patients. HCV, Hepatitis C Virus; HBV, Hepatitis C Virus; MASLD, Metabolic dysfunction-associated steatotic liver disease; ALD, Alcohol-associated liver disease; Y, Yes; N, No.

Thirteen (13) MASLD patients with a fibrosis score of F0-F4 were also recruited from a cohort of patients with severe obesity enrolled in a bariatric surgery program. Eligibility required adult age with a body mass index (BMI) ≥ 40 kg/m^2, or ≥ 35 kg/m^2 with obesity-related co-morbidities, acceptable operative risk, failure of non-surgical treatments, and agreement to lifelong medical follow-up. Exclusion criteria included any concurrent CLD including suspected or confirmed HCC, ALD (> 25 g/day alcohol intake), seropositivity for HBV, HCV, or HIV, and use of medications with potential hepatic effects. Liver biopsies were conducted at the time of the surgery. All enrolled patients in the study provided written consent and the local ethics committee approved the study under these protocols: bariatric cohort, study protocol No. 22979 (Comitato Etico Regionale Unico, Friuli Venezia Giulia, SSN, Italy). Fresh liver specimens were kept at 4ºC and processed within 1 hour.

The patient cohort included 9 males and 8 females, with a median age of 53.00 [39.00 – 58.00] years. Among the patients, 41% (7/17) exhibited metabolic dysfunction-

associated steatotic liver (MAFL), while 59% (10/17) had metabolic dysfunction-associated steatohepatitis (MASH) (Table 2).

Table 2. Pathological Variables and Characteristics of MASLD patients.

Variables	MASLD (N=13)
Steatosis (0/1/2/3)	0/0/010/6
Lobular inflammation (0/1/2/3)	3/11/3/0
Portal inflammation (0/1/2/3)	6/11/0/0
Ballooning (0/1/2/3)	6/9/2/0
MAFL/MASH	7/10
Fibrosis Score (F0/F1/F2/F3/F4)	9/0/0/6/2

Categorical variables were represented by the number of patients. MAFLD, Metabolic dysfunction-associated steatotic liver; MASH, Metabolic dysfunction-associated steatohepatitis; MASLD, Metabolic dysfunction-associated steatotic liver disease.

3.2. Cell culture models

Five different hepatocellular carcinoma cell lines were included in this study: JHH6 (JCRB1030), HuH7 (JCRB0403), HLE, HLF, and Hep3B. JHH6 and HuH7 were obtained from the Japan Health Science Research Resources Bank (HSRRB) in Tokyo, Japan; while HLE, HLF, and Hep3B were generously gifted by Dr. Giannelli of the National Institute of Gastroenterology S. de Bellis Research Hospital, Bari, Italy. JHH6 is a hepatocellular carcinoma cell line with poorly differentiated HCC primary tumor and considered to be of S1 lineage [123,124]. HuH7, on the one hand, is of S2 lineage and characterized by its well-differentiated hepatocellular carcinoma tumor that is positive to Hepatitis C virus [125]. Meanwhile, HLE and HLF were originally derived from the same undifferentiated primary HCC tumor characterized by their S1 tumor lineage. HLE has an epithelial-like morphology while HLF exhibits a spindle/rhombic

"fibroblast-like" morphology [126]. Lastly, Hep3B is an HBV positive tumor with an epithelial-like morphology of S2 lineage [127]. For routine cell maintenance, cells were detached using 0.5% Trypsin-EDTA (Gibco, Thermo Fisher Scientific, Scotland, UK). Table 2 summarizes the list of cell lines, their corresponding culture media, and seeding density for downstream cellular and molecular biology assays. All culture media were supplemented with 10% (v/v) fetal bovine serum (FBS), 1% L-glutamine 100X, and 1% penicillin/streptomycin (10,000 U/mL Penicillin and 10 mg/mL Streptomycin). The cells were incubated at 37ºC at 5% CO_2 humidity. The list of cell lines used in this study is summarized on Table 3.

Table 3. Culture media and seeding densities of hepatocellular carcinoma cell lines used in this study.

CELL LINE	CULTURE MEDIA	SEEDING DENSITY (CELLS PER CM^2)
JHH6	William's E (Gibco, Thermo Fisher, Waltham, MA, USA)	3,000
HUH7	Dulbecco's modified eagle medium (DMEM) (Gibco, Thermo Fisher, Waltham, MA, USA)	8,000
HLE		2,500
HLF		2,500
HEP3B	Minimum Essential medium (MEM) w/ Earle's Salts (Euroclone, Milan, Italy)	8,000

3.3 Chemical compounds and treatments

The pharmacological inhibition of AURKA was conducted using the highly selective inhibitor, AK-01 (LY3295668, CAS No. 1919888-06-4, ChemiTek, Indianapolis, IN, USA), dissolved in 100% dimethyl sulfoxide (DMSO) (Sigma-Aldrich, St. Louis, MO, USA). Our lab has previously established the working concentration for AK-01 at 1.00 μM for both JHH6 and HuH7 cell lines. Both cell lines were seeded accordingly and treated with AK-01 for 72 hours.

3.3.1. PD-L1 turnover experiment

Cycloheximide (Actidione®, CAS No. 66-81-9, SERVA, Heidelberg, Germany) was used to inhibit protein synthesis. Cycloheximide binds to the 60S ribosomal subunit, interfering with the translocation step of translation [128]. The compound was dissolved in DMSO and optimal working concentration was determined with MTT assay. 400nM cyloheximide was used for JHH6, while 100nM cycloheximide was used for all the other cell lines.

To evaluate the presence of proteasome-dependent mechanism of protein degradation the membrane permeable MG-132 inhibitor (CAS No. S2619, Selleck Chemicals, Houston, TX, USA) was used to blocks the proteolytic activity of the 26S proteasome complex [129]. MG132 was dissolved in DMSO and a working concentration of 250nM was used for JHH6 while 125nM was used for all the other cell lines.

Cells were seeded according to Table 3 and treated with cycloheximide and MG-132 (separately) 24h post-seeding in an antibiotic-free medium. Protein lysates were then harvested at 24h, 48h, 72h, and 96h post-treatment for downstream protein expression analyses.

3.3.2. AKT inhibition Experiment

MK-2206 (CAS No. HY-108232, MedChemExpress, Monmouth Junction, NJ, USA) is a highly specific allosteric AKT inhibitor with potential anti-neoplastic activity [130]. The compound was dissolved in DMSO and working concentration was established at 1μM for JHH6 and 0.50μM for HuH7 cells. JHH6 and HuH7 cells were treated with MK-2206 24h post-seeding in an antibiotic-free medium. Protein lysates were then harvested 72h post-treatment for downstream analyses.

3.4. AURKA, PD-L1, and GSK-3β gene silencing

Gene silencing of AURKA (siR-AURKA, Silencer Select siRNA s197, Invitrogen™, Waltham, MA, USA), PD-L1/CD274 (siR-PD-L1/siR-CD274, Silencer Pre-designed

siRNA AM16708, Thermo Fisher, Waltham, MA, USA) and GSK-3β (siR-GSK-3β, Silencer Select, s6241, Invitrogen™, Pleasanton, CA, USA) were performed using small interference RNA (siRNA) dissolved in nuclease-free water (R0581, Life Technologies, Austin, TX, USA). siLentFect™ Lipid Reagent (170-3362, Bio-Rad, Hercules, CA, USA) transfection reagent was used following manufacturer's instructions (0.1% dilution in the culture medium). JHH6 and HuH7 cells were seeded according to the established seeding density on Table 2. The culture media were then switched to fresh antibiotic-free medium 15 minutes prior to transfection. Then, mixture of siLenFect Lipid Reagent, siRNA, or siR-CTRL (scramble) was prepared in a supplement-free medium and this mixture was allowed to stand at room temperature for 25 to 30 minutes to allow for complex assembly. The mixture was then added to the cultured cells in a dropwise manner and incubated for 24 hours at 37ºC at 5% CO_2 humidity. After 24 hours, the culture medium was substituted with the corresponding complete maintenance medium and gene silencing was tested through RT-qPCR.

3.5. Cell viability estimation

Cell viability, intended as a measure of mitochondrial activity, was selected as the parameter to establish the working concentrations for each compound mentioned in section *3.1.3.* These concentrations were determined using the3-(4,5-dimethylthiazol-2-yl)-2,5-diphenyltetrazolium bromide MTT assay. Serial dilution strategy was employed to select the optimal concentration for each compound suitable for each experiment. Cell viability was evaluated for MK-2206 after 24 h, 48 h, and 72 h, while this time frame was extended to a 96-hour evaluation for cycloheximide and MG-132. After treatment, cells were incubated with the freshly prepared MTT solution (0.5% MTT in culture medium with 10% (v/v) Phosphate-Buffered saline (PBS; 137 mM NaCl, 10 mM phosphate, 2.7 mM KCl; pH 7.4) for 1 hour. The solution was replaced with DMSO for cell lysis and incubated on a rocking incubator for 5 minutes at room temperature to allow the dissolution of the formazan salts resulting from the cellular metabolic activity. Absorbance readings were recorded at 562 nm using the

Spectrophotometer EnSpire™ Multi-mode Plate Reader (Perkin Elmer Inc., Waltham, MA, USA). Absorbance values were normalized to vehicle control to calculate the percentage of viable cells for each experimental setup.

3.6. Total RNA extraction from frozen tissues and cell lines

Total RNA extraction from liver tissues was conducted using Tri Reagent® (Sigma-Aldrich, St. Louis, MO, USA). Tissues were homogenized using homogenizer beads (1.4 mm Ceramic Beads Bulk, with 625 mg *per* cryovial, Omni International, Kennesaw, GA, USA) using the Bead Ruptor 4 (Omni International, Kennesaw, GA, USA) at maximum speed for 60 seconds.

TriFast™ (EMR517100, Euroclone, S.P.A., Milan, Italy) was used to extract RNA from JHH6 and HuH7 cells. Cells were scraped from the 2D monolayer and RNA extraction was performed according to the manufacturer's instructions.

Briefly, phase separation for both the tissues and cell was done with the addition of chloroform, then precipitated with isopropanol, and washed twice with 75% ethanol. The RNA pellet was then dissolved in nuclease-free water and stored at -80ºC until further analysis.

RNA was quantified at 260 nm wavelength using the ONDA touch UV-31 scan UV/VIS Spectrophotometer (Vetrotechnica, Padova, IT) with a quartz cuvette MICRO-100μL, 10mm (ONDA) and Nanodrop™ 2000/2000c Spectrophotometer (S/N 0823, Thermo Scientific™, Wilmington, DE, USA). RNA purity was assessed according to the Minimum information for publication of quantitative Real-Time polymerase chain reaction (PCR) experiments (MIQE) guidelines by measuring the A_{260}/A_{280} ratio [131].

3.7. Reverse transcription and quantitative Real-time

cDNA was synthesized from 1 μg of purified RNA through reverse transcription using High-Capacity cDNA Reverse Transcription Kit (Applied Biosystems, Waltham, MA, USA). The kit components included 10X RT Buffer, 25X dNTP mix (100mM), 10X RT Random Primers, Reverse Transcriptase, and nuclease-free water. Reverse

transcription was performed according to manufacturer's protocol (25 minutes annealing at 25ºC, synthesis for 2 h at 37ºC, and enzyme activation for 5 minutes at 85ºC) using the T100 Thermal Cycler (Bio-Rad, Hercules, CA, USA) instrument. The resulting cDNA was stored at -20ºC until further use.

cDNA amplification was performed by qRT-PCR with each 25 µL reaction containing: 25 ng of cDNA, SYBR SSO advanced 1X master mix (Bio-Rad Laboratories, Hercules, CA, USA), and 250nM gene-specific forward and reverse primers. Reactions were run in duplicate in a 96-well plate under the following thermal profile: pre-incubation/activation (30 s, 95ºC), 50 cycles of denaturation (5 s, 95ºC), and annealing/extension (20 s, 60ºC). The melting curve step verified primer/product specificity, and standard curves for each target were used to calculate primer efficiencies.

C_T values were averaged across duplicates with the CFX Maestro v2.2 (Bio-Rad) and relative expression was calculated using the Pfaffl modification of the $\Delta\Delta C_T$ equation, while considering efficiency values of each target gene. The results were normalized to the housekeeping gene, *18S*. Expression levels are reported relative to the housekeeping gene. Primer sets were designed in Beacon Designer 7.9 (PREMIER Biosoft, Palo Alto, CA, USA) and are listed in Table 4.

Table 4. List of Primers used in RT-qPCR.

Gene	Accession number	Forward (5′ to 3′)	Reverse (5′ to 3′)
AURKA	NM_198433	GAGAATTGTGCTACTTATACTG	GGTACTAGGAAGGTTATTGC
YAP1	NM_006106.5	GTGAGTAGGTTCATAATGTG	ATAGAAGTAGGAGCAAGTC
GSK-3B	NM_002093.4	ATGCTCAGTCAAACCAAATCA	TCTATCAACGCCACTACCTT
CTNNB1	NM_001098210	CCTTTCCCATCATCGTGAGG	TTTAGCTCCTTCTTGATGTAATAAAAGGT
AXIN2	AF205888	GAATGAAGAAGAGGAGTG	TCTTGAAGGACCTGTATC

CCND1	NM_053056	AGAGGCGGAGGAGAACAAAC	AAGCGTGTGAGGCGGTAGTA
HIF1A	NM_001530	CAGCAGTTACTCATGGAATA	AACCATACAGCATTTAAGAATC
ACTA2	NM_001141945	TTGGCTTGGCTTGTCAGG	GCTTTAGGGTCGCTGGAG
COL1A1	NM_000088	CGGAGGAGAGTCAGGAAG	ACACAAGGAACAGAACAGTC
CDKN1A	NM_000389.5	GCGGAACAAGGAGTCAGACA	GAACCAGGACACATGGGAG
TGF-B1	NM_000660	AGGAGGCAGGACTTGG	AGGGACGCCGTGTAG
IL-6	NG_011640	ACAGATTTGAGAGTAGTGAGGAAC	GGCTGGCATTTGTGGTTGG
IL-1B	NM_000576	ACAGATGAAGTGCTCCTTCCA	GTCGGAGATTCGTAGCTGGAT
TNF-A	NM_000576	GTGAGGAGGACGAACATC	GAGCCAGAAGAGGTTGAG
GYS2	NM_021957.3	TGAAGTTGCTTGGGAAGTGAC	AGGTTCACACTGTTCCACCTG
GLUT1	NM_006516	AACTCTTCAGCCAGGGTCCAC	CACAGTGAAGATGATGAAGAC
PGK1	NM_000291.	CCACTGTGGCTTCTGGCATA	ATGAGAGCTTTGGTTCCCCG
PKM2	NM_001206796	CAGAGGCTGCCATCTACCAC	ACTGCAGCACTTGAAGGAGG
18S	NR_003286.2	CGTCTGCCCTATCAACTTTCG	GCCTGCTGCCTTCCTTGG

AURKA, Aurora Kinase A; YAP1, Yes-associated protein 1; GSK-3β, Glycogen synthase kinase-3 beta; CTNNB1, Catenin Beta 1; Axin2, Axin inhibition protein 2; CCND1, Cyclin D1; HIF1a, Hypoxia Inducible Factor 1 Subunit Alpha; ACTA2, Actin Alpha 2, Smooth Muscle; COL1A1, Collagen Type I Alpha 1 Chain; CDKN1A, Cyclin Dependent Kinase Inhibitor 1A; TGF-β1, Transforming Growth Factor Beta 1; IL-6, Interleukin 6; IL-1B, Interleukin 1 Beta;, TNF-A, Tumor Necrosis Factor Alpha; GYS2, Glycogen Synthase 2; GLUT1, Glucose Transporter Type 1; PGK1, Phosphoglycerate Kinase 1; PKM2, Pyruvate Kinase M/2

3.8. Tissue homogenization and protein extraction

Tissue disruption and protein extraction were carried out with protocols tailored to each sample type. Frozen human HCC tissues were homogenized in a sucrose-based homogenization buffer (0.25M sucrose, 0.98mM K2HPO4, 40.2mM KH2PO4, 1mM EDTA, 0.1mM DTT; pH 7.4) with the 650 mg of beads *per* cryovial. The tissues were then disrupted using the Bead Ruptor 4 operated at full speed for 1 minute. Fresh MASLD samples were ground in HNTG lysis buffer (50 mM HEPES, 150 mM NaCL, 10% glycerol, 1% Triton X-100; pH 7.5) supplemented with 100µM

phenylmethylsulfonyl fluoride (PMSF) and homogenized using Potter-Elvehjem glass grinders to minimum proteolysis. For cultured cells, protein extraction started with trypsinization, with the pellet rinsed twice with ice-cold PBS, and lysed on ice for 5 minutes with 1X RIPA buffer supplemented with 1X Halt protease inhibitor and 1X phosphatase inhibitor. The resulting lysates were sonicated briefly (one 15-s pulse at 10 W, UW3100) to shear nucleic acids, then cleared by centrifugation at 14,000 x g for 12 min at 4ºC. Protein lysates were quantified with the bicinchoninic acid (BCA) assay according to manufacturer's protocol, and all extracts were stored at -80ºC until further downstream assay use.

3.9. Western blot assay and analyses

Western Blot assay was performed to evaluate protein expression in tissues and cell treatment setups. Fifty to eighty μg of total protein were used according to the corresponding protein target being probed. Lysates were solubilized in 5X Laemmli buffer with 10% β-mercaptoethanol, heated to 95ºC for 5 min to denature the protein prior to loading onto the stacking gel of a 12% polyacrylamide sodium dodecyl sulfate-polyacrylamide gel electrophoresis (SDS-PAGE). A 20-minute pre-run at 80 V was done to concentrate the proteins in the stacking layer before continuing at 180 V for 90 minutes. The separated proteins were transferred to polyvinylidene difluoride (PVDF) membrane through electroblotting at 100V for 2 hours using a transfer buffer composed of 25mM Tris base, 190mM Glycine, and 20% methanol. PVDF membranes were blocked for 1 h with either 4% non-fat milk or 5% bovine serum albumin (BSA) prepared in PBS-0.1% Tween 20 or TBS-0.1% Tween 20, depending on the antibody used, to prevent non-specific antibody binding. The blocking solutions used in this study are listed on Table 5. Membranes were incubated overnight with primary antibodies against the following proteins AURKA (sc-398814, Santa Cruz, Biotechnology, Dallas, TX, USA), p-AURKA (Thr288) (MA5-14904, Invitrogen™, Waltham, MA, USA), PD-L1/CD274 (66248-1-1g, Proteintech, Rosemont, IL, USA), YAP1 (GTX637643, GeneTex, Irvine, CA, USA), p-YAP (Ser397) (PA5-110163,

Invitrogen™, Thermo Fisher, Waltham, MA, USA), GSK-3β (GTX635886, GeneTex, Irvine, CA, USA), p-GSK-3β (Ser9) (MA5-14873, Invitrogen™, Thermo Fisher, Waltham, MA, USA), β-catenin (CAT-5H10, Invitrogen™, Thermo Fisher, Waltham, MA, USA), β-actin (A5411, Sigma-Aldrich, St. Lous, MO, USA). Secondary antibodies included anti-mouse IgG horse radish peroxidase (HRP) (p0260, Dako A/S, Glostrup, Denmark) and anti-rabbit IgG HRP (p0448, Dako A/S, Glostrup, Denmark) depending on the primary antibody. Primary and secondary antibody dilutions are listed on Table 5.

Table 5. Dilution of antibodies and blocking solution used for Western Blot assays.

Targets	HCC tissues	Cell Lines
AURKA (SC-398814)	4% milk in PBS-T (0.1%) 1:1000 (primary) 1:2000 (anti-mouse)	4% milk in PBS-T (0.1%) 1:250 (primary) 1:500 (anti-mouse)
p-AURKA (Thr288) (MA5-14904)	5% BSA in TBS-T (0.1%) 1:300 (primary) 1:500 (anti-rabbit)	N/A
YAP1 (GTX637643)	4% milk in PBS-T (0.1%) 1:2500 (primary) 1:5000 (anti-rabbit)	4% milk in PBS-T (0.1%) 1:2000 (primary) 1:4000 (anti-rabbit)
p-YAP1 (Ser397) (PA5-110163)	5% BSA in TBS-T (0.1%) 1:300 (primary) 1:500 (anti-rabbit)	5% BSA in TBS-T (0.1%) 1:500 (primary) 1:1000 (anti-rabbit)
GSK-3β (GTX635886)	4% milk in PBS-T (0.1%) 1:2500 (primary) 1:5000 (anti-mouse)	N/A
p-GSK-3β (Ser9) (MA5-14873)	5% BSA in TBS-T (0.1%) 1:500 (primary) 1:500 (anti-rabbit)	5% BSA in TBS-T (0.1%) 1:1000 (primary) 1:2000 (anti-rabbit)
PD-L1/CD274 (66248-1-Ig)	5% BSA in PBS-T (0.1%) 1:1000 (primary)	5% BSA in PBS-T (0.1%) 1:1000 (primary)

	1:2000 (anti-mouse)	1:2000 (anti-mouse)
CTNNB1/β-catenin (CAT-5H10)	4% milk in PBS-T (0.1%) 1:3000 (primary) 1:5000 (anti-mouse)	4% milk in PBS-T (0.1%) 1:2000 (primary) 1:3000 (anti-mouse)
β-actin (A5411)	4% milk in PBS-T (0.1%) 1:3000 (primary) 1:4000 (anti-mouse)	% milk in PBS-T (0.1%) 1:3000 (primary) 1:4000 (anti-mouse)

3.10. Immunohistochemical (IHC) Assay

The expression and distribution of AURKA protein expression in paraffin-embedded sections from eight (8) pairs of HCC and adjacent, non-tumoral tissues were evaluated using IHC. Formalin-fixed sections were first cleared of paraffin in xylene and rehydrated with decreasing ethanol concentrations. Antigen retrieval was carried out in 10 mM sodium citrate buffer containing 0.05% Tween-20 (pH 6.0) and intrinsic peroxidase activity was quenched with 3% hydrogen peroxide. Immunostaining was conducted following manufacturer's instructions for the VECTASTAIN® Universal Quick HRP Kit (PK-8800, Vector Laboratories, Newark, CA, USA) and ImmPACT® DAB Substrate Kit (SK-4105, Vector Laboratories, Newark, CA, USA). Slices were then blocked for 1 h in 5% horse serum in PBS to saturate non-specific binding sites, followed by an overnight incubation with 1:500 AURKA primary antibody (sc-398814, Santa Cruz Biotechnology, Dallas, TX, USA) diluted in the blocking solution. The biotinylated pan-specific universal antibody was used as the secondary antibody, and slices were incubated in the Stretavidin/Peroxidase complex. The colorimetric DAB substrate was then added to produce a brown precipitate at sites of AURKA expression. Lastly, nuclei were counterstained with hematoxylin, and the slides were dehydrated by washing in increasing concentrations of ethanol and xylene.

3.11. Statistical analyses

Statistical analyses were performed using GraphPad Prism 10 for macOS Version 10.2.3 (GraphPad Software, San Diego, CA, USA). Initial normal distribution was

evaluated, and significance level set at 0.05 (*p<0.05, **p<0.01, ***p<0.001, ****p<0.0001).

Statistical significance between the paired HCC and adjacent, non-tumoral samples were calculated using Wilcoxon signed rank tests to examine differences between the two groups. Correlations were calculated using Spearman's rank correlation test. For *in vitro* analyses, each experiment was conducted in minimum of two independent trials. The results are presented as mean ± SEM. Unpaired t-tests were used to assess the statistical significance of the differences in mRNA and protein between two sample groups (treatment vs. vehicle/control).

Chapter 4

Results

4.1. AURKA expression in HCC samples

In a previous finding from our research group, *AURKA* mRNA levels were significantly higher in HCC tissues (n=54) compared to the adjacent non-tumoral tissues (median 0.09740 [IQR 0.02575 – 0.2214]; mean 0.8247 [95% CI -0.1599 – 1.809] *vs.* median 0.02750 [IQR 0.01270 – 0.08543]; mean 0.5631 [95% CI -0.2590 – 1.385], p <0.0001) (Figure 3A). This observation further validates what has already been reported in literature [8,79,110,132]. Furthermore, 76% of patients (41/54) exhibited higher *AURKA* levels in nodules compared to the adjacent portion of diseased liver (Figure 3B). However, AURKA protein abundance showed significant downregulation in the tumors (n=55) compared to the paired, adjacent non-tumoral tissues (median: 0.2869 [IQR 0.0959 – 0.4823]; mean 0.3811 [95% CI 0.2705 –0.4917] *vs.* median 0.7295 [IQR 0.4045 – 0.9803]; mean 0.7829 [95% CI 0.6283 – 0.9375], p < 0.0001) (Figure 3C and 3E), with only 19% (10/54) of patients showing higher AURKA protein levels in neoplastic lesions (Figure 3D). These findings contradict previous literature evidence demonstrating higher AURKA protein levels in HCC tumors.

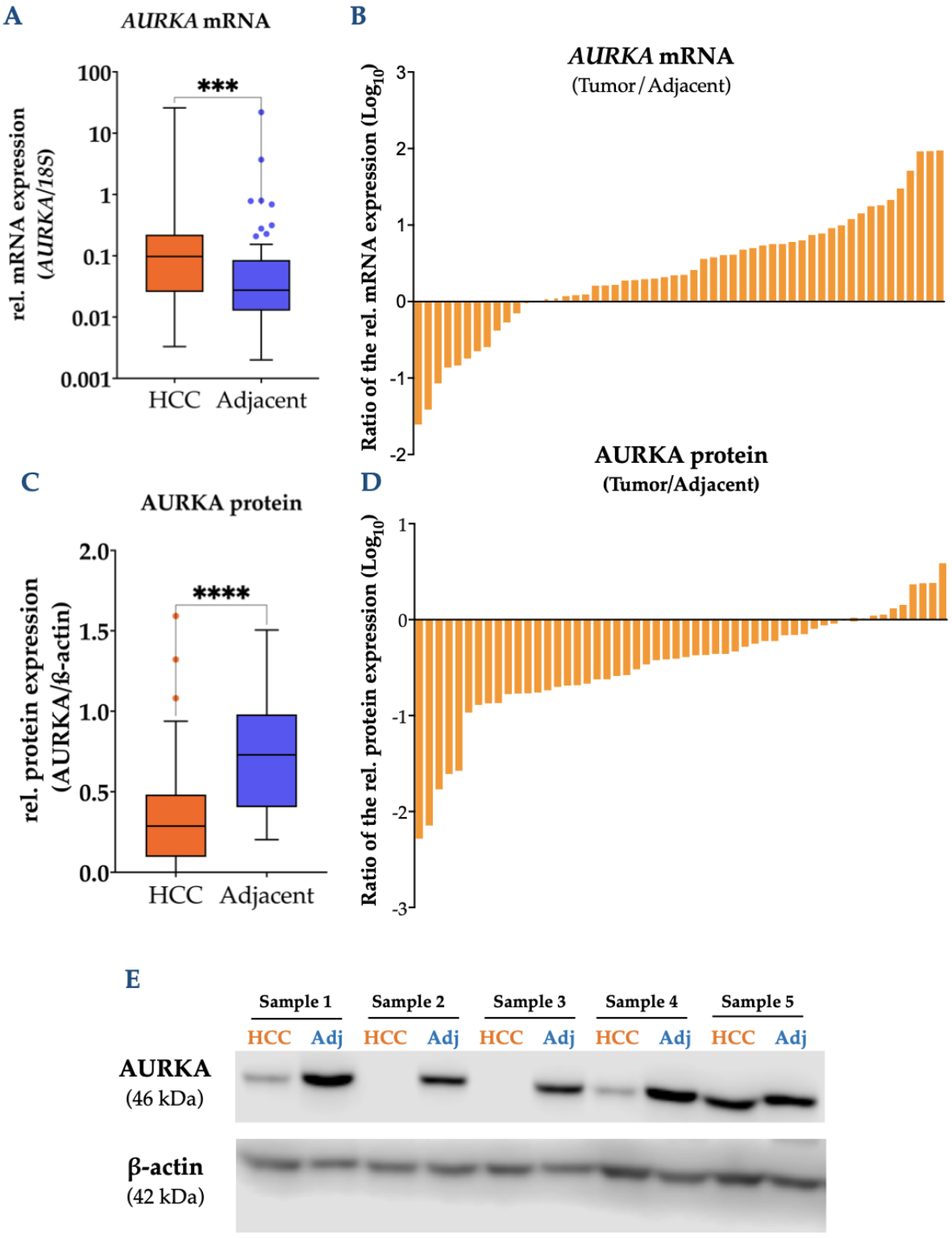

Figure 4. The mRNA and protein expression of AURKA in HCC and adjacent, non-tumoral tissues. (A) Relative ***AURKA*** mRNA levels in HCC tumor and paired adjacent non-tumoral tissues (n=54). (B) Ratio of the relative ***AURKA*** mRNA expression between HCC tumor and paired, adjacent non-tumoral tissues (n=54). (C) Relative AURKA protein abundance in HCC tumor and the paired adjacent, non-tumoral tissues (n=55). (D) Ratio of the relative AURKA protein abundance between HCC tumor and paired, adjacent non-tumoral tissues (n=55). (E) Representative western blot image for 6 paired HCC and adjacent tissue samples normalized to β-actin. *p< 0.05, **p<0.01, ***p< 0.001, ****p<0.0001.

AURKA protein upregulation in the adjacent tissues was further validated using immunohistochemistry (IHC) staining, revealing strong and prominent overexpression of AURKA, predominantly within the hepatocytes in the adjacent tissues, compared to the tumor nodules (Figure 4). Notably, AURKA expression remained strong in adjacent tissue samples with steatosis, suggesting a consistent role across various CLD etiologies and AURKA's possible involvement in hepatocyte regeneration or adaptation in response to chronic liver damage, regardless of the underlying cause. Histopathological examination of Sample 1 revealed poorly differentiated tumor characterized by a solid architectural pattern with prominent lymphocytic infiltration. The tumor displayed multinucleated syncytial giant cells distributed throughout the neoplastic tissues. IHC analysis demonstrated weak and focal AURKA expression with limited distribution across the tumor specimen. However, the paired adjacent tissue demonstrated robust and widespread AURKA expression throughout the tissue sample. Concurrent histopathological assessment revealed tissues have limited areas of early-stage cirrhosis as well (Figure 5A). HCC tumor from sample 2 exhibited a macro-trabecular growth pattern with positive AURKA expression in the subcapsular regions, while the central tumoral area which showed negative AURKA expression. On the one hand, microscopic evaluation of the adjacent tissue from sample 2 revealed markedly elevated AURKA expression through within a cirrhotic liver architecture attributed to underlying metabolic disease (Figure 5B). Lastly, HCC tumor from sample 3 demonstrated overall diminished AURKA expression. However, focal clusters of pre-apoptotic neoplastic hepatocytes exhibited AURKA immunoreactivity, potentially indicating a role for AURKA in the DNA damage response pathway. This expression pattern appeared to represent a transient phenomenon. Furthermore, these AURKA-positive hepatocytes were predominantly localized within the apoptotic foci characterized by dense lymphocytic infiltration. Histological examination of the corresponding adjacent tissue revealed macronodular cirrhosis, while IHC analyses demonstrated diffuse AURKA expression throughout the hepatic parenchyma (Figure 5C).

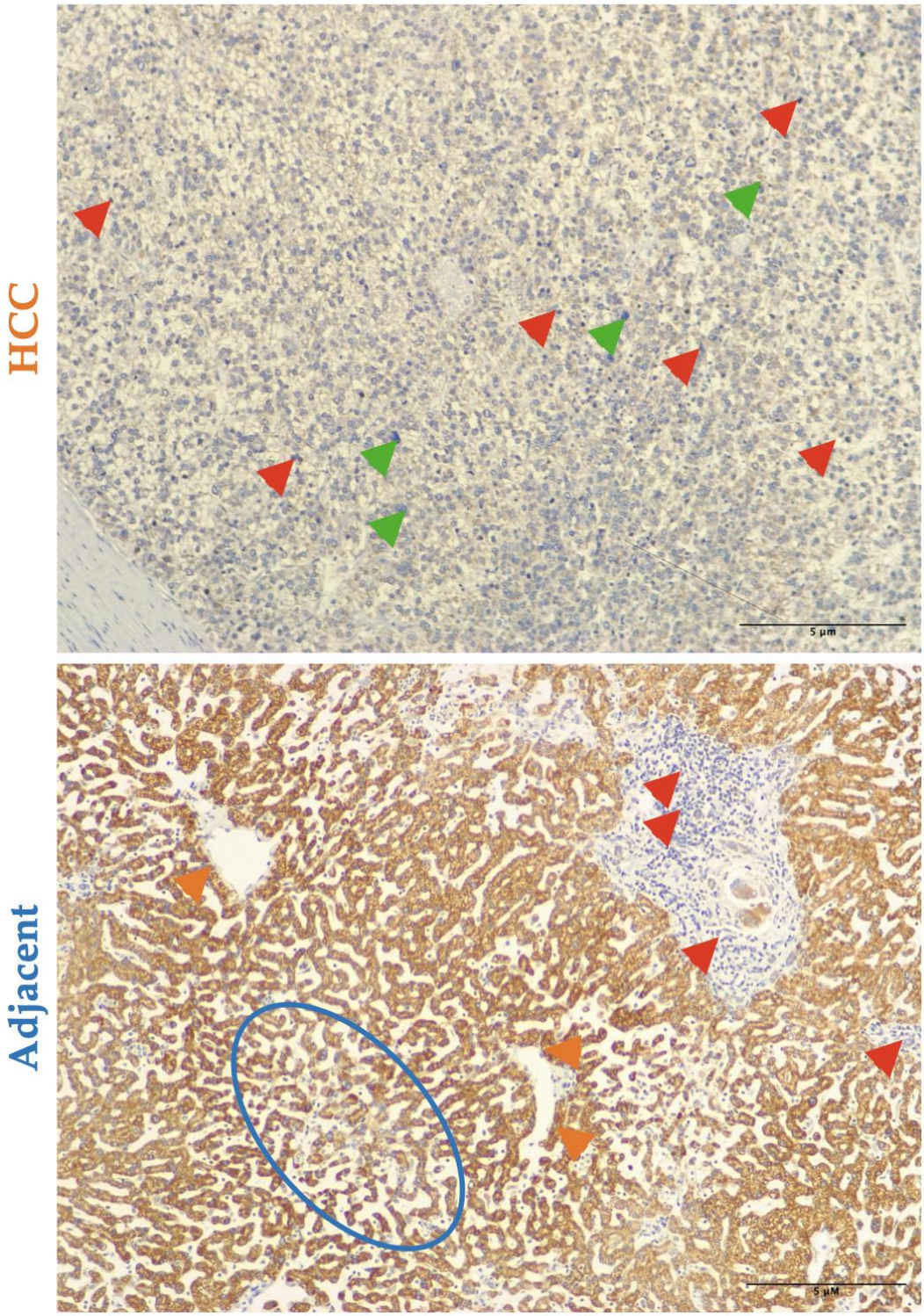

Figure 5A. Immunohistochemical staining of AURKA in the HCC and adjacent tissues of Sample 1. The top image corresponds to the HCC slice showing a weak overall expression of AURKA (brown staining). The poorly differentiated tumor is also characterized by a strong presence of lymphocytes (red arrowhead) with widespread distribution of multi-nucleated syncytial giant cells (green arrowhead). The adjacent tissues (bottom image) revealed a strong prominent AURKA expression (brown staining) especially adjacent to the portal vein (orange arrowhead) with lymphocytic infiltration (red arrowhead) and showed signs of early-stage cirrhosis (blue oval circle).

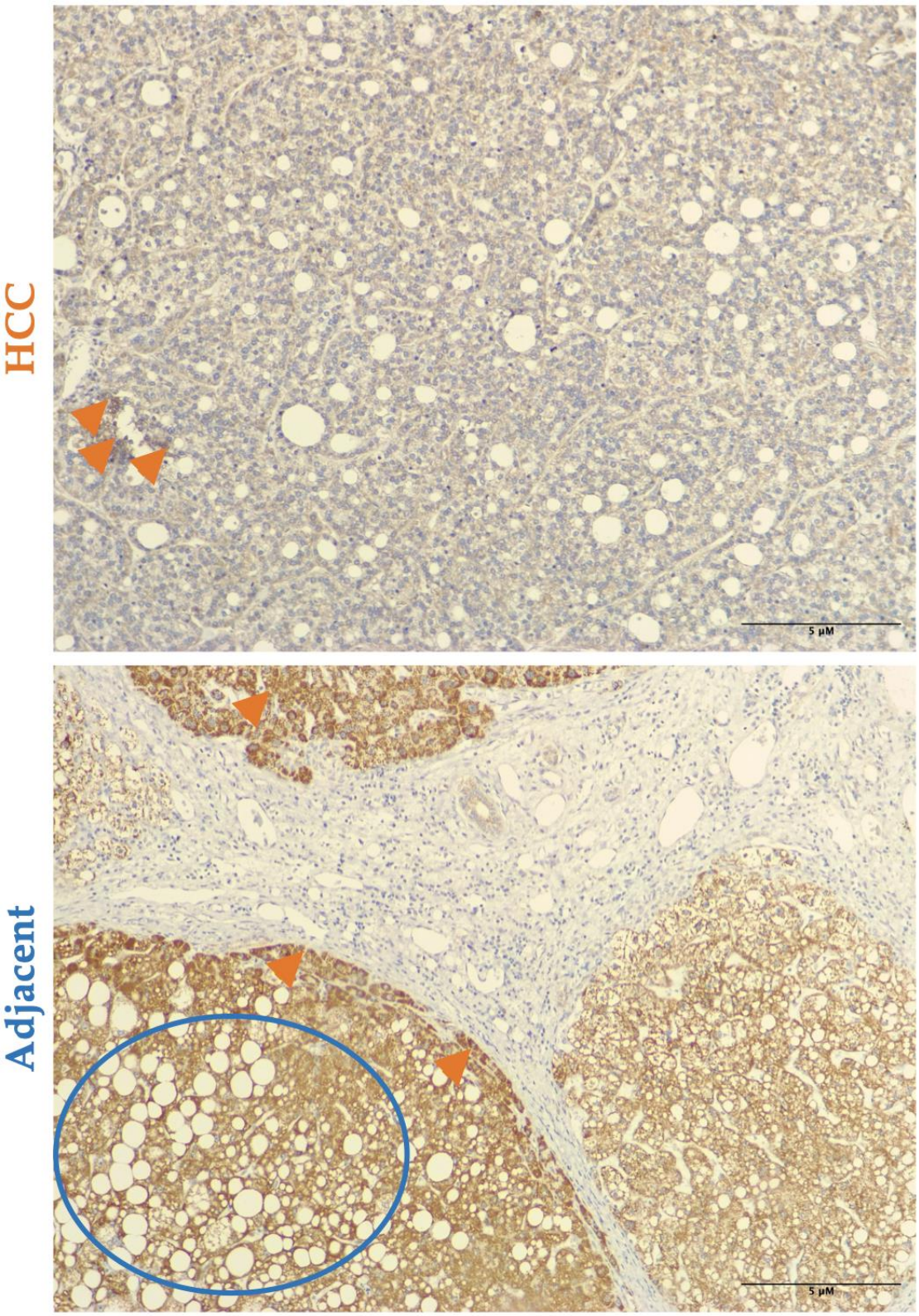

Figure 5B. Immunohistochemical staining of AURKA in the HCC and adjacent tissues of Sample 2. Top image represents HCC with macro-trabecular tumor growth characterized by sub-capsular AURKA positivity (orange arrowhead). The overall expression of AURKA is low within the entire slice. The bottom image represents the adjacent tissue with prominent AURKA expression adjacent to the portal tract (orange arrowhead). AURKA expression remains strong within the cirrhotic areas with steatosis (blue circle).

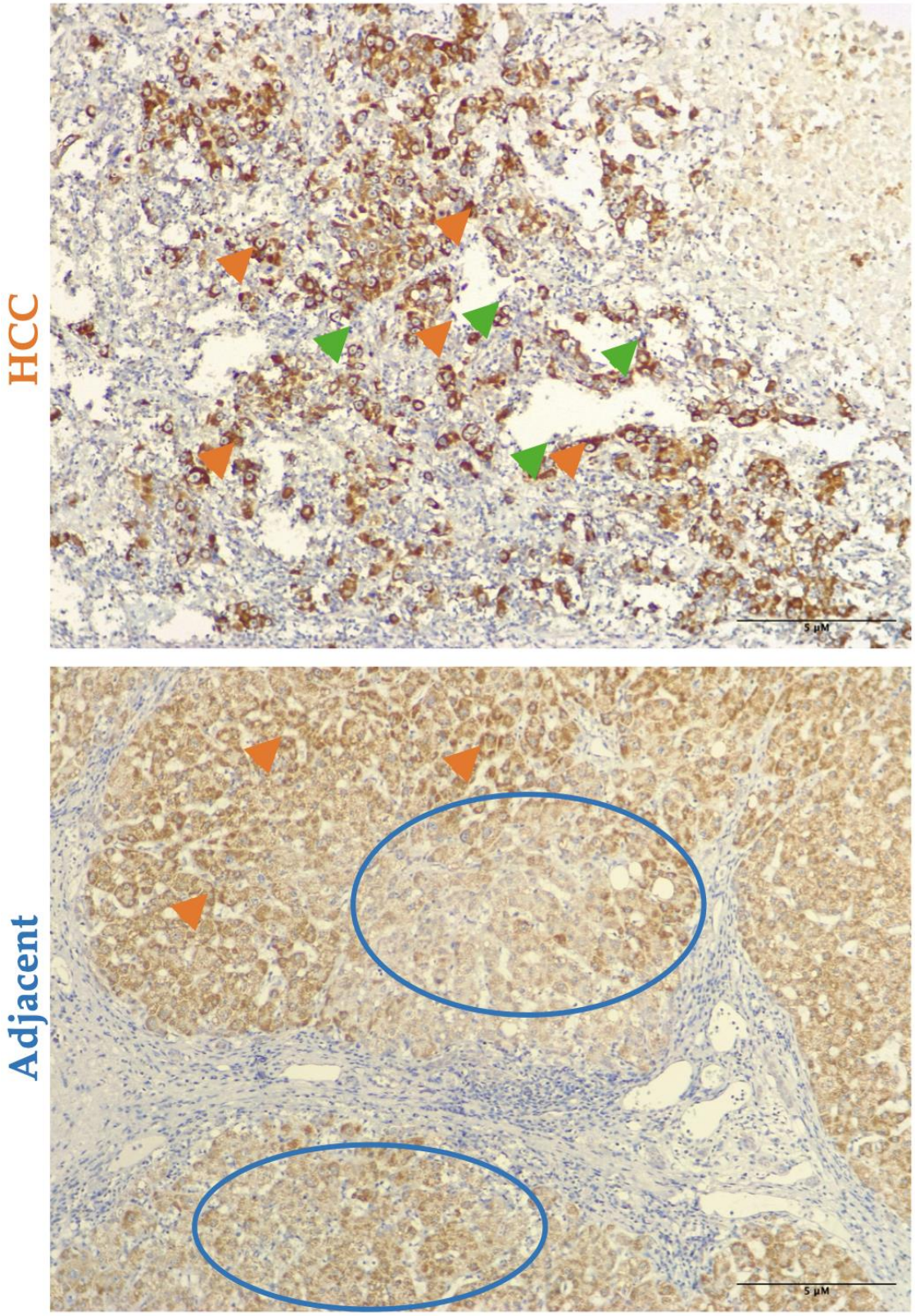

Figure 5C. Immunohistochemical staining of AURKA in the HCC and adjacent tissues of Sample 2. . Top image represents HCC with generally low AURKA expression predominantly in the group of neoplastic pre-apoptotic hepatocytes (orange arrowheads). The tissue also showed lymphocytic infiltration (green arrowheads). The bottom image represents the adjacent tissue with widespread AURKA expression in the parenchymal area (orange arrowheads). The tissue also exhibits macronodular cirrhosis (blue circle).

4.2. Phospho-AURKA (Thr288) is higher in tumors

Since AURKA activation is canonically mediated by Thr288 phosphorylation— a post-translational modification essential for increased kinase activity during spindle assembly and mitotic progression—we quantified the abundance of p-AURKA (Thr288) in HCC and adjacent tissue samples. Analyses interestingly revealed differences between tumors and adjacent non-tumoral tissues despite no statistically significant group-level difference in p-AURKA (Thr288) expression (tumor: median 0.0261 [IQR 0.00672 – 0.06873]; mean 0.04813 [95% CI 0.02544 – 0.07082] *vs.* adjacent: median 0.02791 [IQR 0.0121 – 0.07923]; mean 0.09191 [95% CI 0.01390 – 0.1699], p = 0.0595, ns) (Figure 6A).

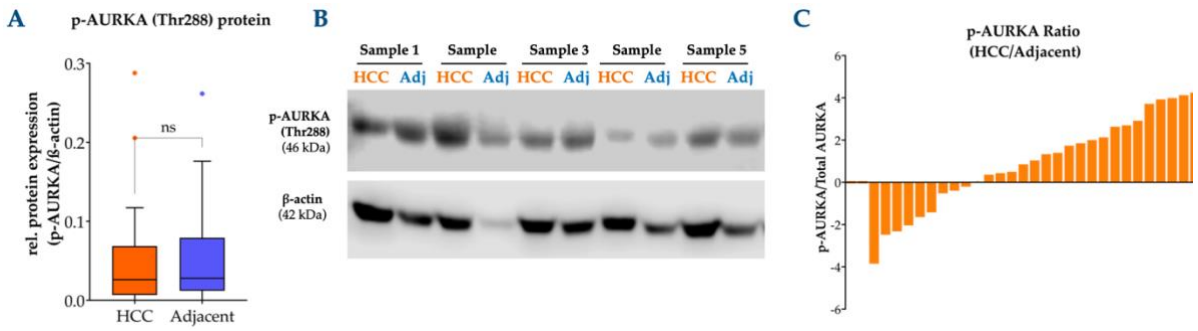

Figure 6. The protein expression and ratio of phospho-AURKA (Thr288) in HCC and adjacent tissues. (A) The relative protein expression of the p-AURKA (Thr288) in HCC and adjacent tissues normalized to β -actin (n=31). (B) Representative westerb blot image of HCC and adjacent tissue samples probed for p-AURKA (Thr288) and normalized to β-actin. (C) The ratio of p-AURKA expression between HCC and adjacent tissues (n=31). 61% of the samples exhibited higher tumoral p-AURKA compared to the adjacent tissues. *p< 0.05, **p<0.01, ***p< 0.001, ****p<0.0001.

Ratio analysis examining the proportion of p-AURKA (Thr288) relative to total AURKA protein showed that approximately 61% (17/31) of the tumor samples exhibited elevated p-AURKA ratio compared to their matched adjacent tissues (Figure 6C). These data indicate that HCC cells maintain a higher proportion of active AURKA compared to the adjacent tissues, possibly suggesting altered AURKA self-regulation either through autophosphorylation and TPX2-mediated activation linked to increased cell-cycle dependent activity of the protein rather than increased overall AURKA activation in the adjacent tissues.

4.3. *YAP1 mRNA* expression remains stable in HCC tumors and non-tumoral tissue samples

As AURKA has been demonstrated to regulate YAP1, a master transcriptional downstream effector of the Hippo pathway, either through direct phosphorylation and protein stabilization in other pathological contexts, we examined the potential modulatory role of AURKA on YAP1. The *YAP1* mRNA expression analysis comparing HCC tissues to adjacent non-tumor tissue (n=31) (Figure 7A) revealed no statistically significant difference between HCC and adjacent tissues (median 0.4620 [IQR 0.0894 – 0.9510]; mean 3.866 [95% CI -1.337 – 9.069] *vs*. median 0.1730 [IQR 0.0699 – 0.5593]; mean 4.076 [95% CI -2.843 – 10.99], p= 0.1110,), further supported by data from GEPIA database (369 tumor samples *vs*. 160 normal samples from LIHC cohort) (Figure 7B). This suggests that *YAP1* mRNA expression alone may not be a reliable marker for distinguishing malignant from non-malignant hepatic tissues in this context. However, since our study focuses on AURKA's regulatory role on YAP1 at the protein level, this mRNA result aligns with our hypothesis, as transcriptional regulation may not reflect the post-translational modifications and protein-level interactions that are central to our investigation.

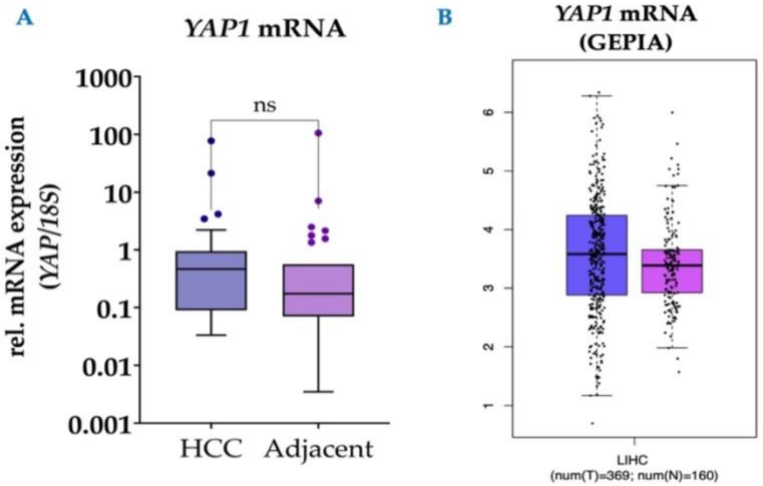

Figure 7. YAP1 mRNA expression in our cohort and data retrieved from the GEPIA database. (A) Relative mRNA expression of YAP1 normalized to *18S* in our cohort of patients (n=31). (B) *YAP1* mRNA levels in liver hepatocellular carcinoma (LIHC) tumor samples (T, n=369) compared to normal tissue samples (N, n=160) retrieved from The Cancer Genome Atlas (TCGA) database *via* GEPIA. *p< 0.05, **p<0.01, ***p< 0.001, ****p<0.0001. ns, not significant.

4.4. YAP1 and phospho-YAP1 (Ser397) protein levels are upregulated in the adjacent, non-tumoral tissues.

Consistent with the AURKA protein expression pattern, YAP1 protein showed significantly lower expression in tumors compared to the adjacent non-tumoral tissues (median 0.02252 [IQR 0.000145 – 0.1374]; mean 0.1016 [95% CI 0.04134 – 0.1619] *vs.* median 0.1469 [IQR 0.03786 – 0.3603]; mean 0.2183 [95% CI 0.1398 – 0.2969], $p < 0.01$) (Figure 8A). Furthermore, a significant correlation observed between AURKA and YAP1 in the adjacent, non-tumoral tissues (r=0.4412 [95% CI 0.08511 – 0.6973], $p<0.05$), whereas no significant correlation was observed between the two total proteins in HCC (Figure 9). Interestingly YAP1 protein is also significantly elevated in MASLD samples, reinforcing its potential role in CLD as MASLD remains the most common cause of CLD [42] (Figure 8A). Interestingly, even though p-YAP1 (Ser397) level was higher in the adjacent tissues (Figure 8B) the p-YAP1 (Ser397) / total YAP1 ratio revealed that about 63% (17/27) had a higher p-YAP1 (Ser397) expression in the tumors (Figure 8C). It is important to note that Serine 397 phosphorylation of YAP1, under canonical Hippo regulation, subjects the protein to proteasomal degradation, restricting YAP1's transcriptional activity.

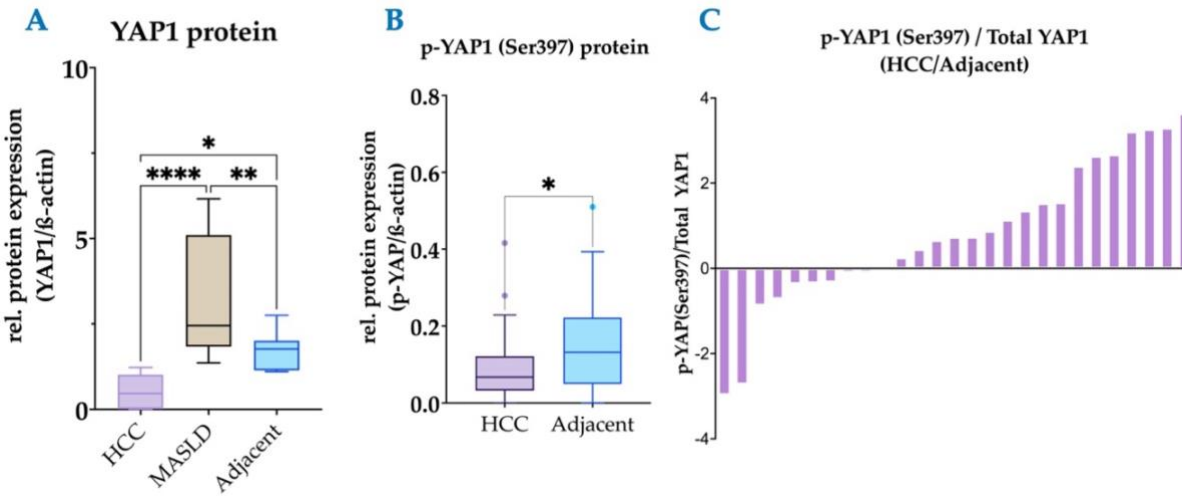

Figure 8. YAP1 and phospho-YAP1 protein expression in HCC and adjacent tissues. (A) Relative protein expression of total YAP1 in HCC (n=30), adjacent tissues (n=30), and MASLD tissues (n=13). (B) Relative phospho-YAP1 (Ser397) levels in HCC and adjacent tissues (n=35). (C) The ratio between p-YAP1 (Ser397) and Total YAP1 in HCC evaluated in 27 tissue samples. *p< 0.05, **p<0.01, ***p< 0.001, ****p<0.0001.

4.5. Context-dependent AURKA-YAP1 Protein Correlations

Correlation analyses revealed distinct patterns between AURKA and YAP1 across tissue types and phosphorylation states. No significant correlation was observed between AURKA and YAP1 protein expression in HCC tissues (r = 0.08441, [95% CI -0.2947 – 0.4406] p=0.6574) (Figure 9A). In contrast, adjacent tissues showed a significant positive correlation between AURKA and YAP1 protein levels (r=0.4412, [95% CI 0.08511 – 0.6973], p <0.05) (Figure 9B). Meanwhile, p-AURKA (Thr288) and p-YAP1 (Ser397), demonstrated significant positive correlations in both HCC (r=0.3939, [95% CI -0.0043 – 0.6843] p < 0.05) and adjacent tissues (r=0.5003, [95% CI 0.1451 – 0.7413] p <0.01). These findings indicate that the relationship between AURKA and YAP1 may be context-dependent with stronger associations in adjacent tissues and at the phosphorylated protein level across both tissue types.

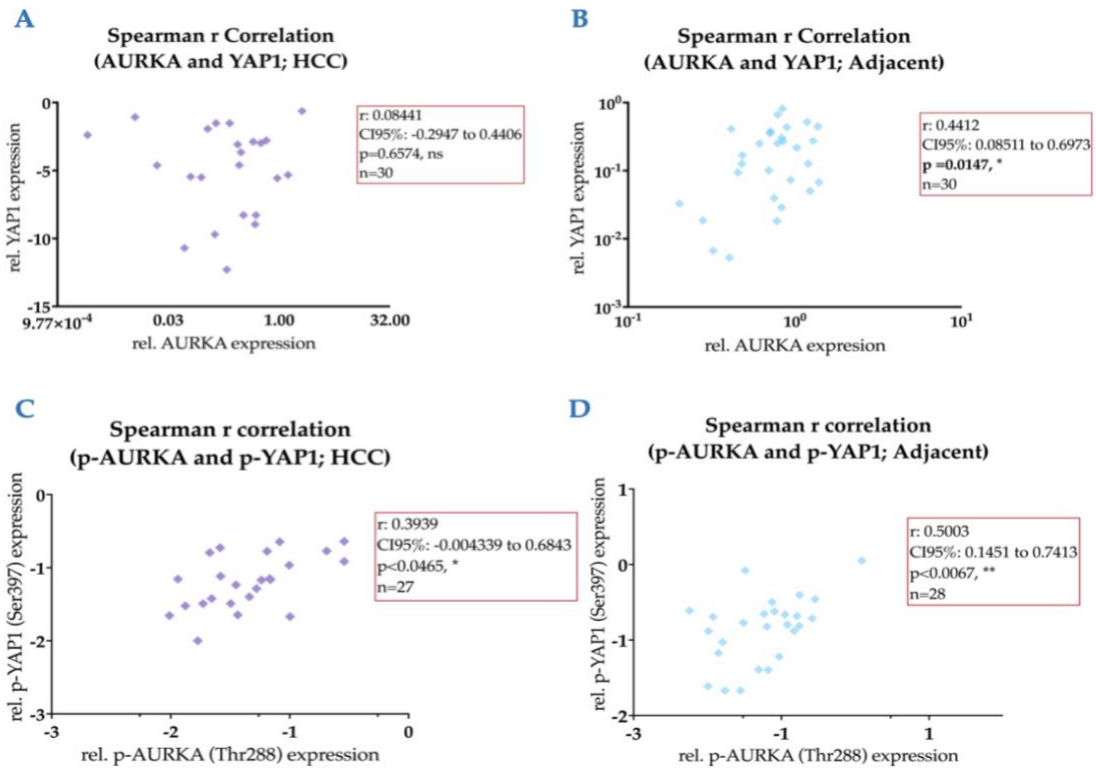

Figure 9. Relative protein expression correlation between AURKA and YAP1 and their phosphorylated forms in HCC and adjacent tissues. (A) No correlation was found between AURKA and YAP1 in HCC tissues (B) AURKA and YAP1 protein expression are significantly correlated in the adjacent tissues. (C-D) p-AURKA (Thr288) and p-YAP1 (Ser397) in HCC and adjacent tissues are significantly correlated, with stronger positive correlation evident in adjacent samples. Spearman's rank correlation test was used to detect correlation (*p<0.05, **p<0.01, ***p<0.001).

4.6. AURKA silencing significantly downregulated *YAP1* mRNA and protein, with modest effects on phospho-YAP1 (Ser397) in JHH6 cells

YAP1 mRNA levels were significantly downregulated following a 72-h knockdown with siR-AURKA (Figure 10A). Similarly, total YAP1 protein was significantly downregulated under the same conditions, with protein expression dropping by approximately 50% compared to the scrambled control (Figure 10B). In contrast, p-YAP1 (Ser397) was only modestly affected, decreasing by around 10% under the same conditions (Figure 10D). This pronounced disparity suggests that AURKA may exert its primary regulatory effects on the overall abundance or stability of YAP1 protein rather than on its phosphorylation at Ser397, which was further confirmed by almost four-fold increase in the ratio of p-YAP1 (Ser397)/total YAP1. These results align with the study conducted by Wang and colleagues wherein AURKA positively regulated YAP1 stability by blocking autophagy [40]. However, a better *in vitro* model system of fibrosis or CLD is necessary to confirm these findings since JHH6 is an HCC cell line model.

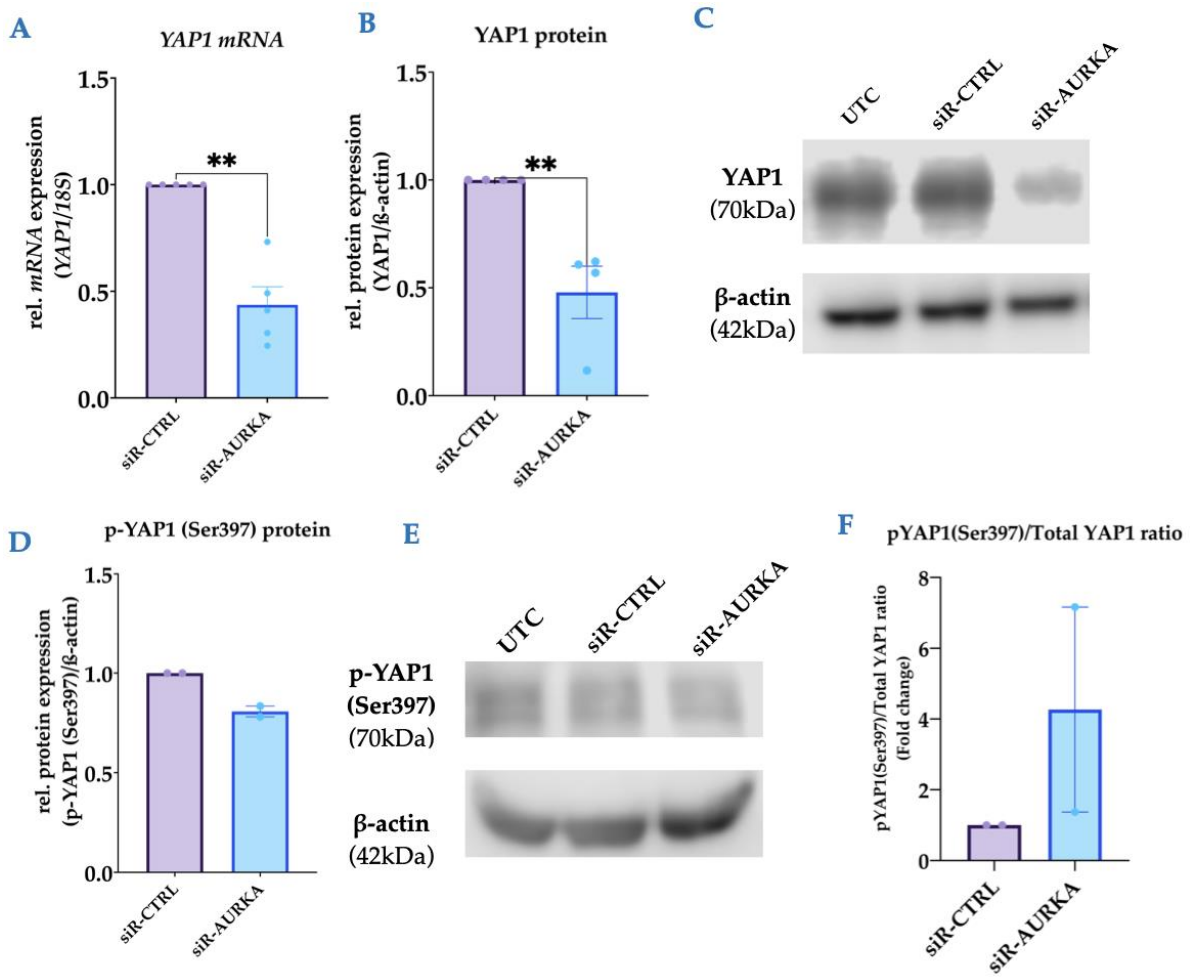

Figure 10. Relative protein expression of Total YAP1 and phospho-YAP1 (Ser397) following AURKA silencing at 72 h. (A) *YAP1 mRNA* expression was significantly reduced 72 h post-silencing with siR-AURKA (n=5). (B) Significant reduction in the relative expression Total YAP1 protein 72 h post-silencing with siR-AURKA (n=4). (C) Representative western blot image of Total YAP1 after AURKA silencing. (D) Modest reduction in relative protein expression of p-YAP1 (Ser397) 72 h post-silencing with siR-AURKA (n=2). (E) Representative western blot image of p-YAP1 (Ser397) after AURKA silencing. (F) p-YAP1 (Ser397)/total YAP1 ratio increased four-fold following AURKA silencing (n=2). Data presented as mean±SEM. *p< 0.05, **p<0.01, ***p< 0.001, ****p<0.0001.

4.7. The limited *in vivo* evidence of AURKA regulation of GSK-3β in CLD

Building upon the well-established role of AURKA in modulating key signaling pathways, we also sought to investigate its potential regulatory function with GSK-3β within the context of CLD. A prior liver regeneration study in mice demonstrated that AURKA negatively regulates GSK-3β activity through Ser9 phosphorylation, resulting to the latter's inactivation. To explore this, we analyzed protein expression levels of AURKA and GSK-3β, including its phosphorylated form at Ser9, in both

tumor and adjacent, non-tumoral liver tissues. In HCC, GSK-3β protein was higher (median: 0.1561 [IQR 0.05115 – 0.3018]; mean 0.1981 [95% CI 0.1407 – 0.2555]) *vs*. median: 0.03198 [IQR 0.005436 – 0.07608]; mean 0.05316 [95% CI 0.03469 – 0.07162], p<0.0001) (Figure 11A), while p-GSK-3β (Ser9) expression were similar between the paired HCC and adjacent non-tumoral tissues (median: 0.09442 [IQR 0.03533 – 0.1342]; mean 0.0.09412 [95% CI 0.0.06566 – 0.1226) *vs*. median: 0.06852 [IQR 0.01501 – 0.1448]; mean 0.0.08311 [95% CI 0.04954 – 0.1167], p=8028) (Figure 11B). Indeed, *in vitro* silencing of AURKA in JHH6 cells showed no effects on the Ser9 phosphorylation levels of GSK-3β (Figure 11C) and correlation analyses between AURKA and p-GSK-3β (Ser9) levels yielded no significant correlation in either tissue types (Figure 11D and 11E).

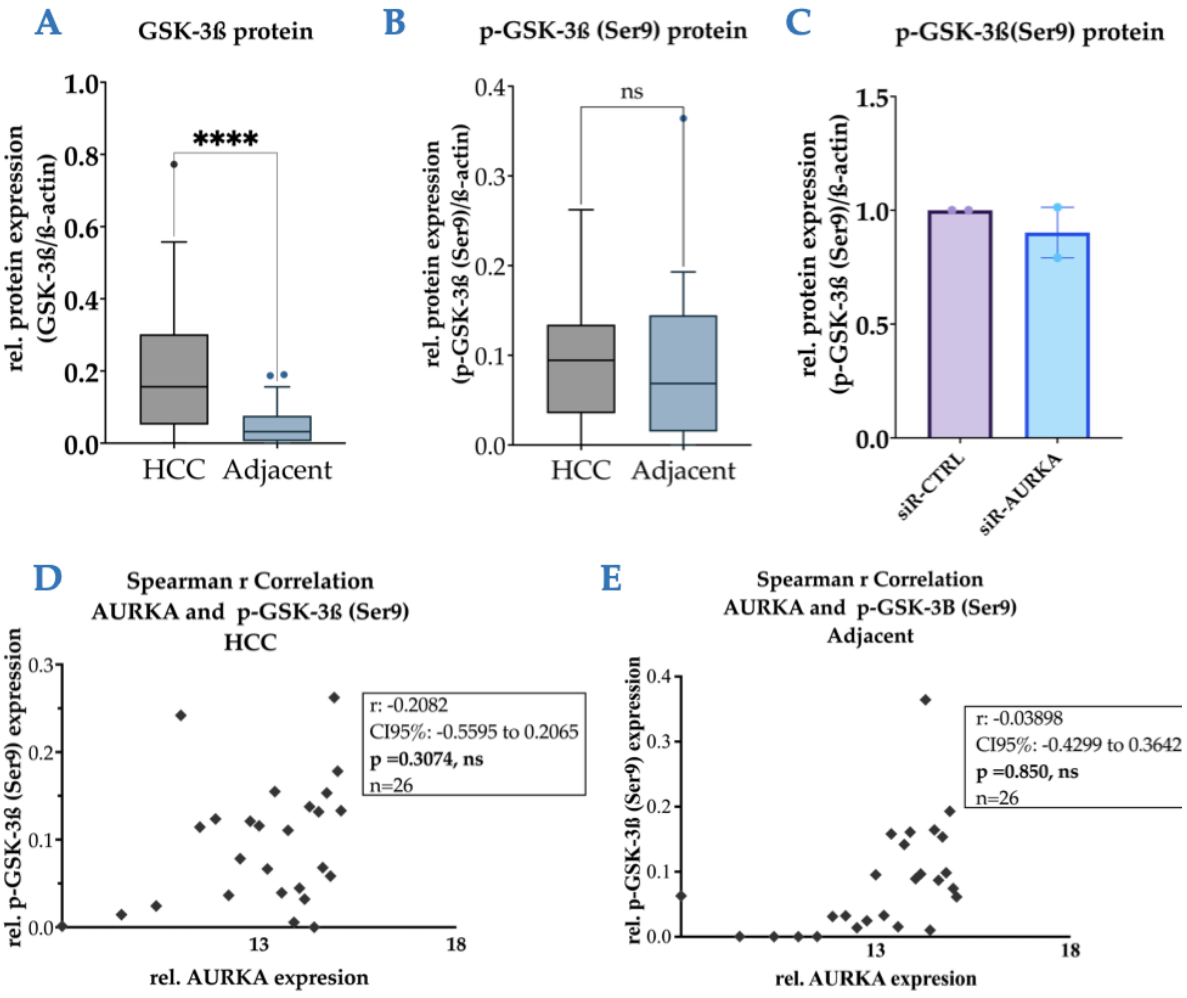

Figure 11. The relative protein expression of GSK-3β and p-GSK-3β (Ser9) and correlation analyses between AURKA and GSK-3β *in vivo* (A) Total GSK-3β protein was significantly elevated in HCC compared to adjacent

tissues (n=37). **(B)** p-GSK-3β (Ser9) levels remained stable between HCC and adjacent tissues (n=27). **(C)** No marked reduction of p-GSK-3β (Ser9) levels was observed following AURKA silencing in JHH6 for 72h (n=2). **(D-E)** No significant correlation was observed between AURKA and p-GSK-3β expression in either tissue types. Data presented as mean±SEM. *p< 0.05, **p<0.01, ***p< 0.001, ****p<0.0001.

Since GSK-3β functions as a regulator of CTNNB1 stability through phosphorylation-dependent mechanism, we next examined whether the observed alterations in GSK-3β expression and phosphorylation status would affect downstream CTNNB1 mRNA and protein levels. *CTNNB1* mRNA was higher in HCC compared to the adjacent tissues (median: 0.6490 [IQR 0.2520 – 1.291]; mean 0.8939 [95% CI 0.6086 – 1.179], *vs*. median: 0.1265 [IQR 0.04525 – 0.2463]; mean 0.1624 [95% CI 0.1164 – 0.2084], p<0.0001) (Figure 12A), revealing a statistically significant fold change of 5.5X in tumors. CTNNB1 protein was also significantly overexpressed in HCC (median: 0.0.04890 [IQR 0.01771 – 0.3149]; mean 0.1893 [95% CI 0.06147 – 0.3172] *vs*. median: 0.0.006770 [IQR 0.0005 – 0.01043]; mean 0.0095 [95% CI 0.0009624 – 0.01801], p<0.01) (Figure 12B), corresponding to about 20X (p <0.01) fold-change in tumors compared to the adjacent tissues. Despite the lower total GSK-3β expression in adjacent non-tumoral tissues, approximately 63% (17/27) of GSK-3β is present in its inactive, phosphorylated form in contrast to only about 15% (4/27) GSK-3β inactivation in the tumors (Figure 12C and 12D).

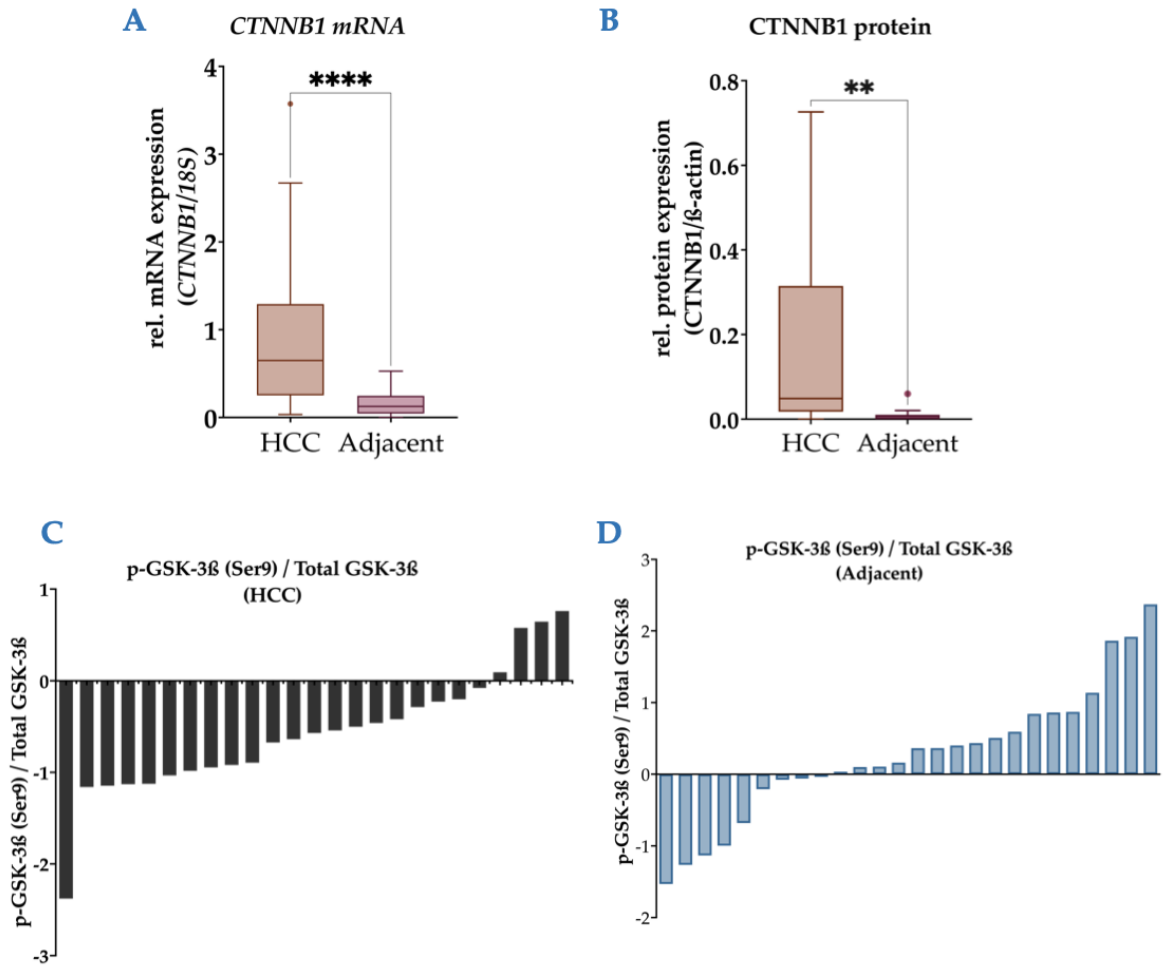

Figure 12. The relative mRNA and protein expression CTNNB1 *in vivo*. (A) *CTNNB1* mRNA expression was significantly higher in HCC (n=36). **(G)** CTNNB1 protein was significantly overexpressed in HCC (n=15). **(C)** 15% of HCC tumor samples exhibited 15% (4/27) GSK-3β inactivation. **(D)** Approximately 63% (17/27) of GSK-3β is inactivated in the adjacent tissues. *p< 0.05, **p<0.01, ***p< 0.001, ****p<0.0001.

4.8. Gene expression profiling revealed distinct downstream networks for GSK-3β in Hepatocellular Carcinoma cell lines

Since only ~15% of GSK-3β is phosphorylated in tumors, this limited inactivation does not adequately explain the elevated CTNNB1 levels at the mRNA and protein levels observed. Active GSK-3β (non-phosphorylated at Ser9) should promote CTNNB1 degradation through the canonical destruction complex, which requires sequential phosphorylation by CK1α and GSK-3β followed by recognition by APC and AXIN, and ultimately ubiquitination and proteasomal degradation of CTNNB1 [133]. However, in tumors, GSK3β can be sequestered or repurposed into alternative signaling pathways—including proliferation, fibrosis, inflammation, and glucose

metabolism—thereby reducing its availability for CTNNB1 regulation [134–138]. Thus, we explored the changes in representative genes of each pathway following GSK3β silencing to assess its downstream effects (Figure 13).

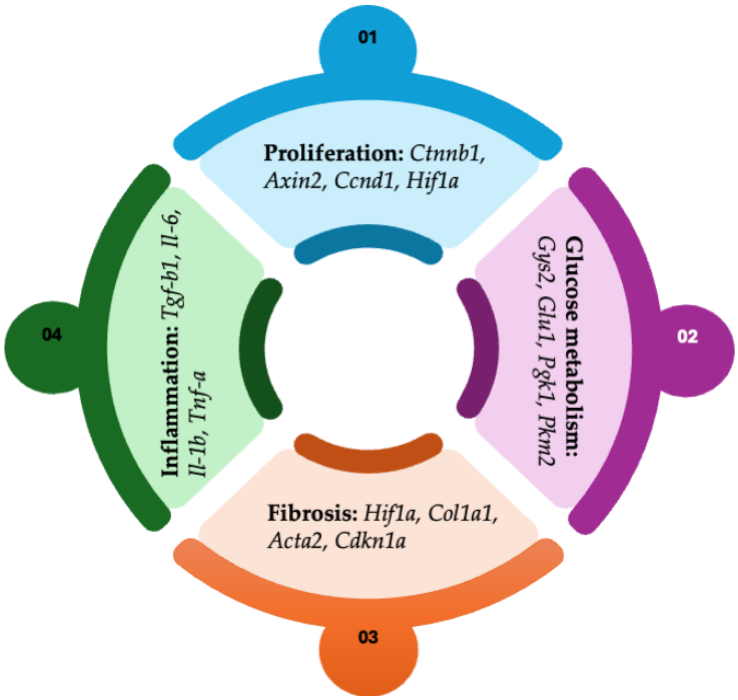

Figure 13. Schematic illustration of distinct downstream networks regulated by GSK-3β in cancer. *The diagram illustrates four major biological process categories affected by GSK-3β in several cancers. (01) Proliferation: genes involved in cell cycle regulation and growth signaling (CTNNB1, AXIN2, CCND1, HIF1A; (02) Glucose metabolism: genes involved in glucose metabolic networks (GYS2, GLUT1, PGK1, PKM2); (3) Fibrosis: genes involved in ECM and fibrotic responses (HIF1A, COL1A1, ACTA2, and CDKN1A); (4) Inflammation: genes involved in cytokine production and inflammatory responses (TGF-B1, IL-6, IL-1B, and TNF-A)*

Using siRNA-mediated knockdown of GSK-3β in JHH6 and HuH7 cell lines, we identified distinct regulatory pathways that might reveal functional involvement of GSK-3β in HCC. The analyses revealed pronounced cell line-specific differences in gene regulation patterns. In JHH6, an S1-type tumor with a more proliferative phenotype, *GSK-3β* knockdown commonly downregulated proliferation-associated genes including *CTNNB1* and *CDKN1A* along with the glutamine transporter, *GLUT1*; While *IL-1B* was upregulated (Figure 14A). In contrast, HuH7 cells which are more differentiated revealed a distinct regulatory pattern as well with *GSK-3β* knockdown preferentially modulating fibrotic and inflammatory-associated genes such as *ACTA2*, *IL-6*, and TNF-A. (Figure 14B).

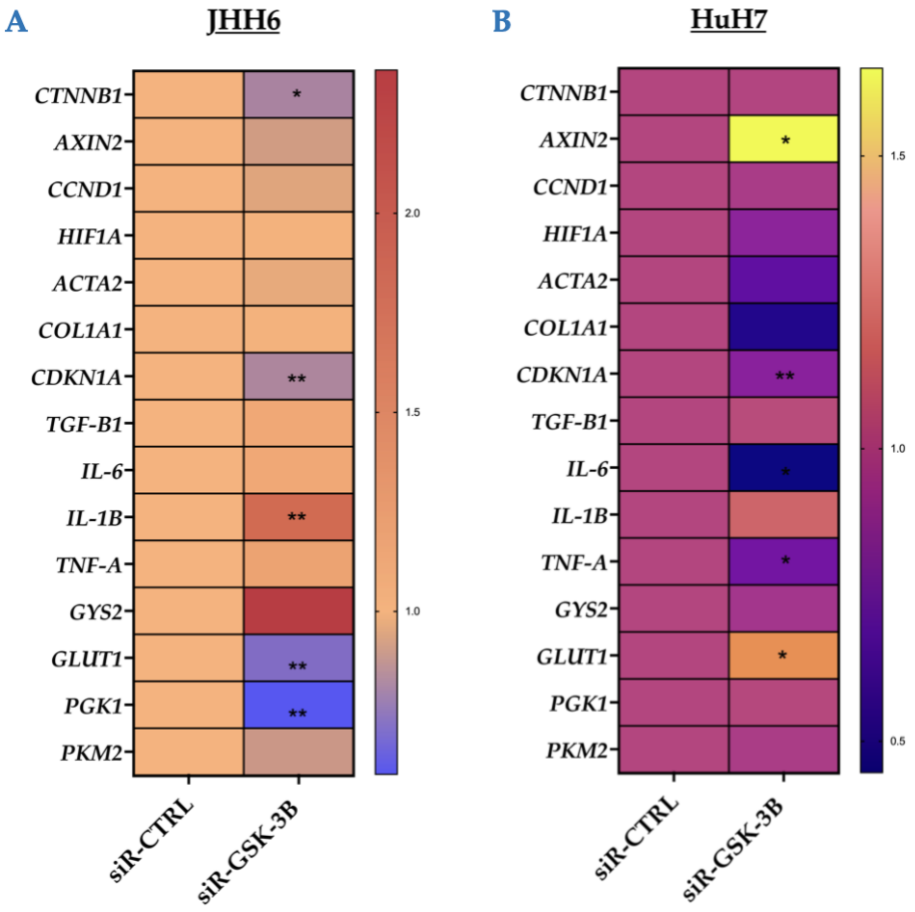

Figure 14. **Cell line-specific gene expression profiles revealed distinct regulatory networks downstream of GSK-3B in hepatocellular carcinoma.** JHH6 and HuH7 cells were transfected with siR-CTRL (scramble) or *siR-GSK-3β,* and gene expression changes of target genes were analyzed by RT-qPCR. **(A)** GSK-3β knockdown in JHH6 cells led to decreased *CTNNB1*, *CDKN1A*, *GLUT1*, and *PGK1*, with specific upregulation of *IL-1B*. (B) *GSK-3β* knockdown in HuH7 downregulated *CDKN1A* and *TNF-A*; and upregulated *AXIN2* and *GLUT1*. *p< 0.05, **p<0.01, ***p< 0.001, ****p<0.0001.

4.9. AURKA inhibition reduced PD-L1 in JHH6 and HuH7 cells

We then explored the possible role of AURKA in immune evasion by evaluating PD-L1 levels following AURKA inhibition in HCC (JHH6 and HuH7 cell models) with either AK-01 or siRNA. AURKA inhibition with AK-01 significantly reduced PD-L1 protein expression in JHH6 (Figure 15A) and HuH7 (Figure 15D) cells at 72h, while siRNA-mediated knockdown of AURKA in JHH6 required 144h to achieve comparable reduction (Figure 15A). Immunoblotting revealed a heterogeneous PD-L1 banding pattern with multiple bands in both JHH6 (Figure 15C) and HuH7 (Figure 15F), consistent with the extensive post-translational modification reported in literature. Previous studies demonstrated that PD-L1 undergoes extensive

glycosylation, primarily through N-linked glycosylation, which is critical for protein stability and immune checkpoint function [102,104]. Since the PD-L1 banding profile has not been comprehensively characterized in literature, we treated cell lysates with peptide-N-glycosidase (PNGase F) which cleaves N-linked glycans thus allows for the better characterization of PD-L1 banding/glycosylation pattern in our models.

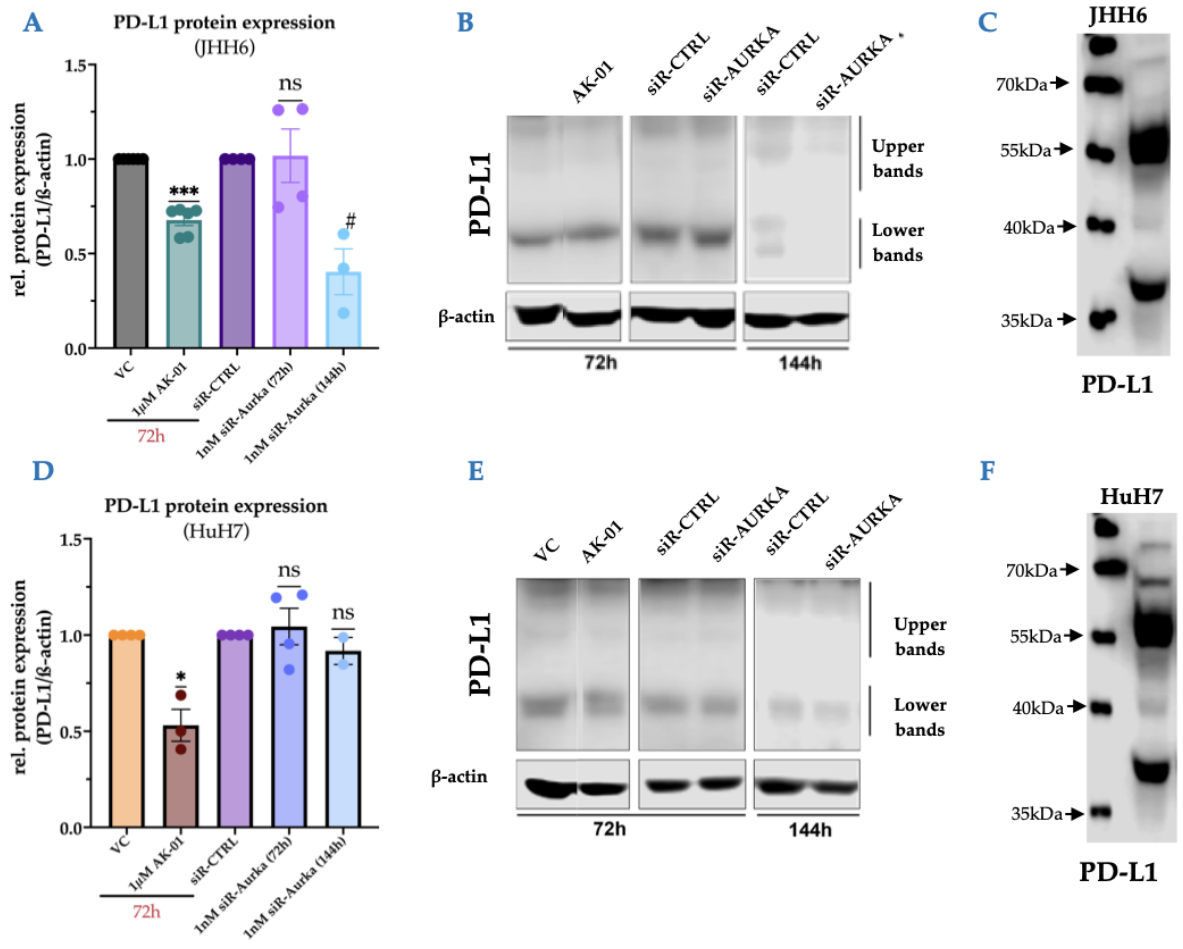

Figure 15. The relative PD-L1 protein expression following AURKA inhibition and the heterogeneous PD-L1 banding profiles in JHH6 and HuH7. (A) AURKA inhibition with AK-01 and siR-AURKA (at 144h) significantly decreased PD-L1 protein in JHH6. (B) Representative immunoblot of AK-01 and siR-AURKA treatment in JHH6. **(C)** Representative PD-L1 immunoblots of untreated JHH6 depicting the heterogeneous PD-L1 banding profile consistent with heavy glycosylation of PD-L1. (D) AURKA inhibition with AK-01 significantly reduced PD-L1 in HuH7 at 72h, with no observable effects with siR-AURKA setups. (E) Representative immunoblot of AK-01 and siR-AURKA treatment in HuH7. (F) Representative PD-L1 immunoblots of untreated HuH7 depicting heterogeneous banding of PD-L1 consistent with heavy glycosylation. *p< 0.05, **p<0.01, ***p< 0.001, ****p<0.0001. Data presented as mean±SEM. N=3. VC, vehicle control.

4.10. PNGase F confirms N-glycosylation of PD-L1 in Hepatocellular Carcinoma cells

Using the endoglycosidase PNGase F enzyme, PD-L1 N-glycans were enzymatically removed in matched protein lysates from JHH6 and HuH7 to collapse the heterogeneous glycoforms into the core species. In untreated samples, PD-L1 resolved as a broad upper band below 50 kDa consistent with the mature glycosylated forms, with a visibly stronger glycosylated signal in JHH6 than HuH7, indicating a higher steady-state burden of glycosylated PD-L1 in JHH6. PNGase F shifted PD-L1 to a lower ~33-37 kDa core band in both lines, confirming N-linked glycosylation as the source of the mobility heterogeneity and providing consistent basis for total PD-L1 comparison across cell lines (Figrue 16A). Further analyses showed that glycosylated PD-L1 exceeded the non-glycosylated forms in both models, with the N-glycosylation-dominant pattern more pronounced in JHH6 (Figure 16B), supporting the interpretation that glycosylation-stabilized pools may constitute the bulk of PD-L1 in these HCC cells.

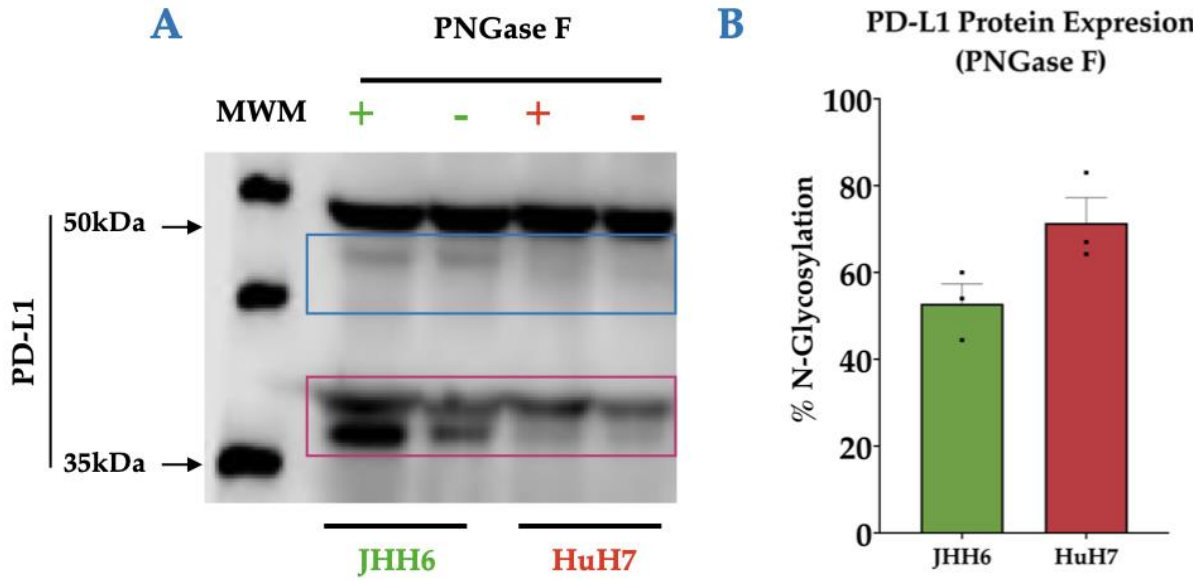

Figure 16. PD-L1 glycosylation profile in JHH6 and HuH7 cells. (A) Representative immunoblot image of PD-L1 expression following PNGase F treatment in JHH6 and HuH7 cell. The blue box represents the mature, glycosylated PD-L1, while the pink box represents the immature, less- or non-glycosylated PD-L1. **(B)** % N-glycosylation following PNGase F treatment on JHH6 and HuH7 (n=3). Data presented as mean±SEM. N=3.

4.11. Comparative PD-L1 abundance in a panel of HCC cell lines

Across six hepatocellular carcinoma cell lines categorized as either S1 (JHH6, HLE, and HLF) or S2 (HuH7 and Hep3B) tumors, PD-L1 resolved as a dominant glycosylated band profile, below 50 kDa accompanied by a weaker ~35 kDa less-glycosylated or non-glycosylated species, with β-actin used for lane-to-lane normalization to control for loading variability (Figure 17A). The mature, glycosylated PD-L1 showed the highest levels in JHH6 and HLF, intermediate in HLE and HuH7, and consistently lowest in Hep3B (Figure 17B). Focusing on this band isolates the complex N-glycosylated form that localizes in the plasma membrane and mediates PD-1 engagement, making it the most informative pool for immune-evasion relevant comparisons among cell lines.

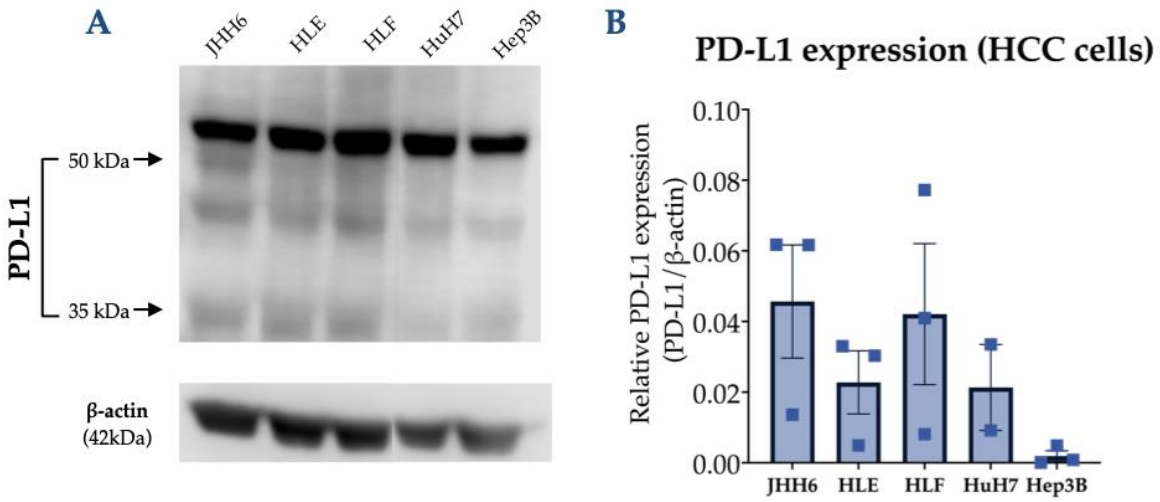

Figure 17. Comparative analyses of PD-L1 protein expression in Hepatocellular Carcinoma cell lines. (A) Representative western blot image of PD-L1 expression in JHH6, HLE, HLF, HuH7, and Hep3B cells. (B) Different PD-L1 expression profile was observed with JHH6 and HLF exhibiting the highest expression, while Hep3B the lowest (n=3). Data presented as mean±SEM. N=3.

4.12. siRNA validation of PD-L1 bands in JHH6 and HuH7

To further confirm the identities of immunoblot bands attributed to PD-L1, cells were transfected with 5nM siR-PD-L1 and protein lysates harvested 72 hours post-transfection alongside controls (siR-CTRL, scramble). In JHH6, siR-PD-L1 markedly

reduced the glycosylated PD-L1 as well as the ~35 kDa species, considered as PD-L1 immature forms. Interestingly, in JHH6 cells, a faint band of approximately 40 kDa was detected, which likely represents PD-L1, as it was reduced upon PD-L1 silencing (Figure 18A). (Figure 18B and 18C). This siRNA validation is consistent with transcript-level depletion that reduces the levels of precursor (immature) PD-L1 and, consequently, the membrane-bound mature, glycosylated form.

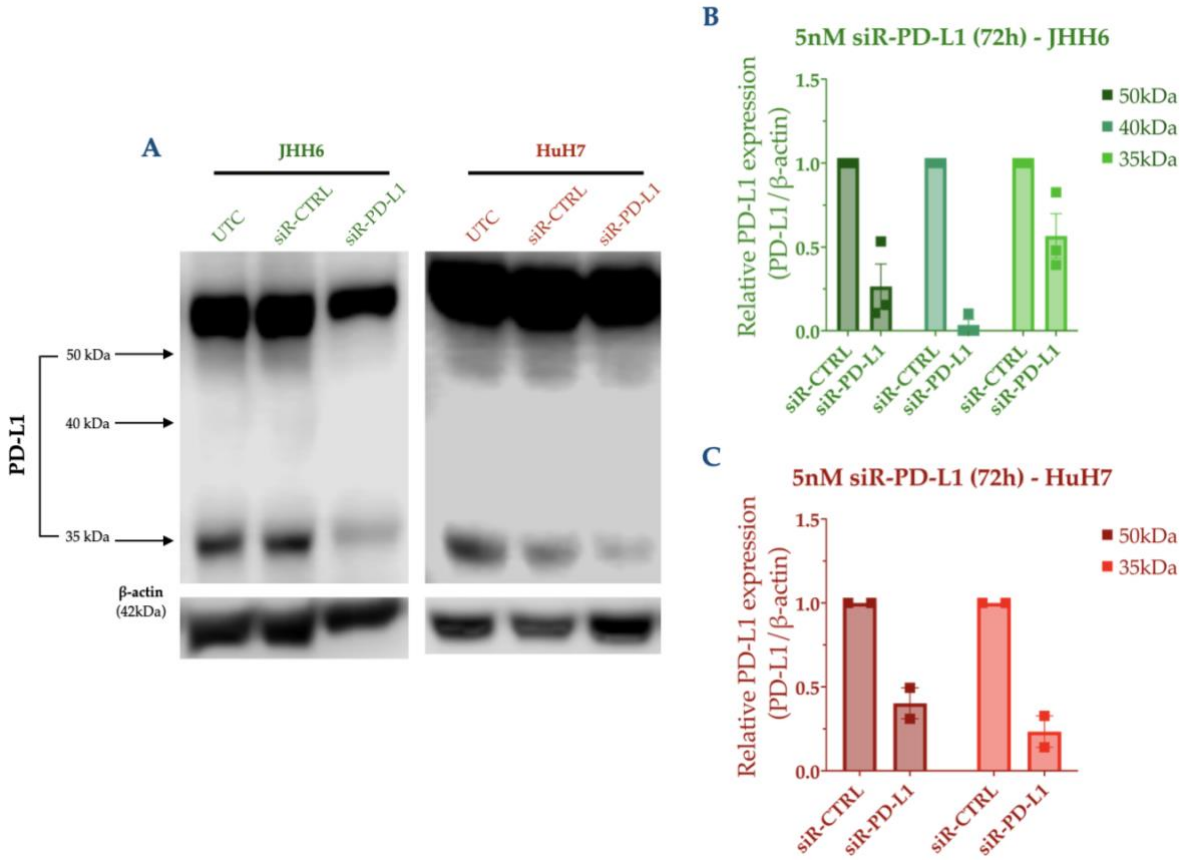

Figure 18. Evaluation and identification of PD-L1 bands following silencing in JHH6 and HuH7 cells for 72 hours. (A) Representative western blot image of PD-L1 protein after a 72-hour siRNA silencing of PD-L1 in JHH6 and HuH7 cells. (B) Marked downregulation of 50 kDa, 40 kDa, and 35 kDa PD-L1 bands was observed in JHH6 cells (n=3) (C) Marked reduction of the 50 kDa and 35 kDa PD-L1 bands was observed in HuH7 (n=-2). UTC, Untreated control; siR-CTRL, scramble. Data presented as mean±SEM.

4.13. Differential PD-L1 turnover rates across HCC Cell lines

Cycloheximide treatment in HCC cell lines demonstrated a clear stability hierarchy across the five cell lines tested. In JHH6, PD-L1 declined slowly despite the higher 400nM cycloheximide dose, with a visible drop only on the extended chase at 96 h, indicating a long effective half-life and strong buffering from the mature pool. This is

consistent with prior observations that JHH6 carries high baseline glycosylated PD-L1. In HuH7, total PD-L1 showed an early drop at 24 h, followed by a gradual rebound through 96 h, yielding a biphasic profile rather than a simple monotonic decay. HLF exhibited an intermediate profile with appreciable PD-L1 loss at 48 to 72 h. Fast PD-L1 decay was observed in both HLE and Hep3B, with about 50% loss at 24 h with just 100nM of cycloheximide compared to JHH6's 400nM dose, suggesting a short half-life of PD-L1 in these cell lines (Figure 19).

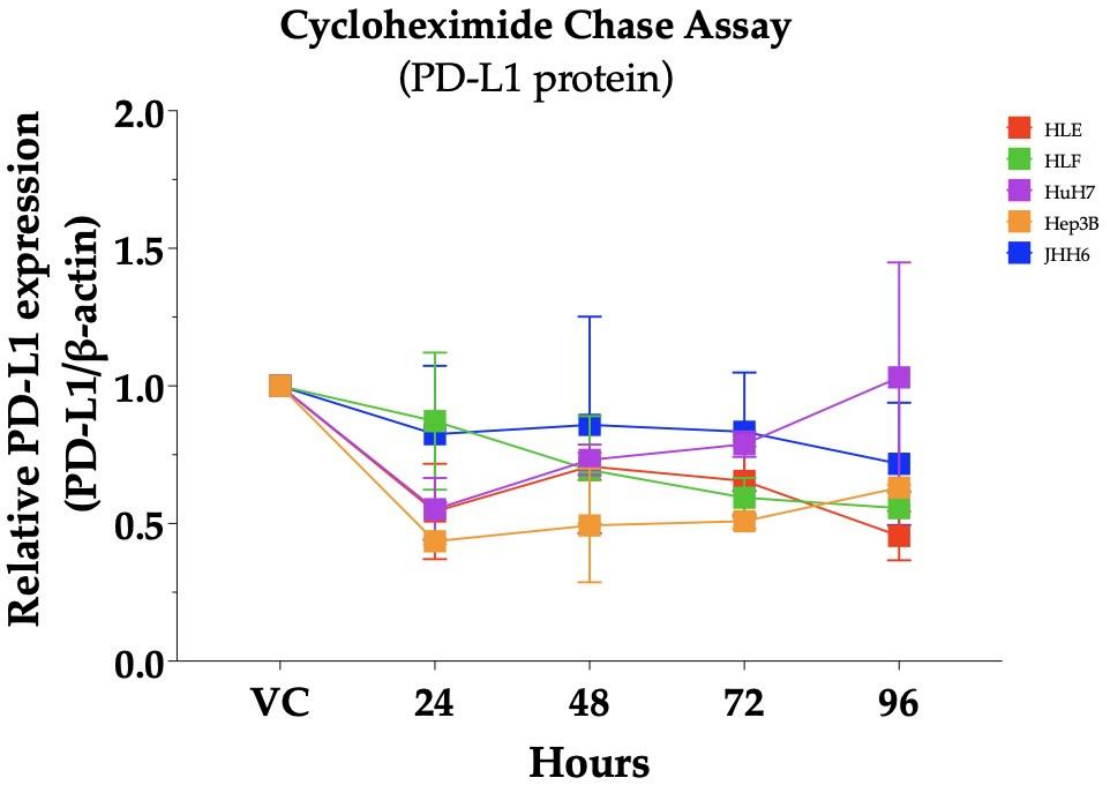

Figure 19. PD-L1 protein stability varies across HCC cell lines. HCC cell lines were treated with 100nM cycloheximide except for JHH6 which was treated with 400nM. PD-L1 levels were measured by Western Blot at indicated time points. PD-L1 expression was normalized to beta-actin and presented relative to vehicle control (VC). JHH6 exhibits the longest PD-L1 half-life with minimal decline over 96 hours, while HLE and Hep3B showed rapid PD-L1 loss. HuH7 displays a biphasic pattern with initial decline followed by partial recovery. HLF shows intermediate stability. Data presented mean ± SEM from independent experiments. VC, vehicle control.

Previous studies have described the proteasome pathway as one of the primary mechanisms of PD-L1 degradation [115,117,139]. MG-132, a proteasome inhibitor, was used to determine whether PD-L1 undergoes proteasome degradation in HCC. In JHH6, total PD-L1 showed only modest rescue primarily due to the increased mature of glycosylated PD-L1 pool in this cell line. On the one hand, treatment with 125nM

MG-132 in HuH7 resulted in a reduction of PD-L1 protein expression. This finding contrasts with the expected protein stabilization observed in JHH6 and is typically observed with proteasome inhibitors. HLF showed partial rescue, consistent with mixed control where both proteasomal turnover of non-glycosylated forms and supply/trafficking of the glycosylated form shape total PD-L1 abundance. Lastly, HLE and Hep3B, exhibited the highest accumulation of PD-L1, indicating the rapid loss in these cell lines is strongly proteasome-driven (Figure 20).

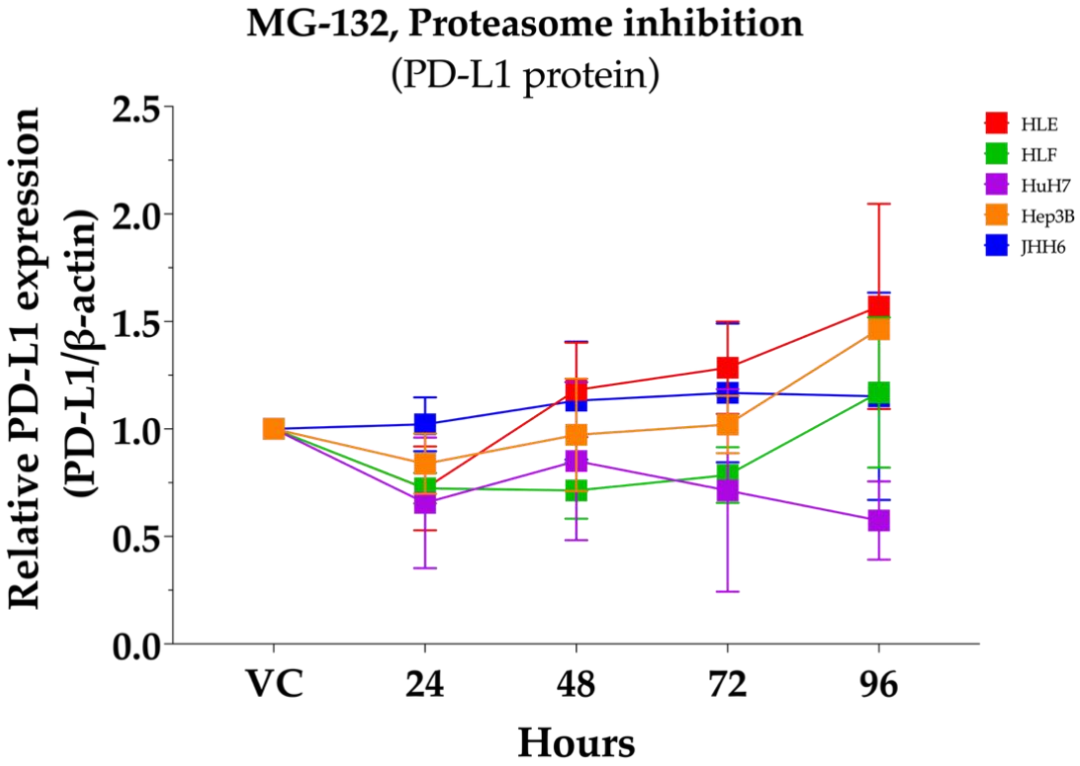

Figure 20. Proteasome inhibition revealed differential PD-L1 degradation rates across HCC cells. HCC cells were treated with 125nM MG-132 except for JHH6 which was treated with 250nM MG-132. PD-L1 protein levels were assessed by Western blot at indicated time points. PD-L1 expression was normalized to beta-actin and presented relative to vehicle control (VC). HLE and Hep3B demonstrated rapid and significant PD-L1 accumulation. HLF showed partial and intermediate rate of rescue consistent with the PD-L1 half-life. JHH6 exhibited slow and modest rescue. HuH7 unexpectedly showed PD-L1 reduction contrasting with the typical protein stabilization expected from proteasome inhibitors. Data presented as mean ± SEM from independent experiments. VC, vehicle control.

4.14. AURKA regulates PD-L1 in a GSK-3β -independent manner in JHH6

Literature evidence demonstrated that AURKA can negatively regulate GSK-3β in gastric carcinoma [114] and liver regeneration [140] and that GSK-3β is a negative regulator of PD-L1 stability through β-TrCP-dependent ubiquitination in a breast

cancer [102] and HNSCC [116] models . Under this model, AURKA activation would lead to GSK-3β inactivation, resulting to PD-L1 stabilization and enhanced immune checkpoint signaling that facilitates tumor immune evasion. However, as previously demonstrated, AURKA silencing does not alter GSK-3β phosphorylation at Ser9; nevertheless, PD-L1 expression was reduced upon AURKA inhibition.

In our JHH6 model, combined treatment with the AURKA inhibitor, AK-01, and the proteasome inhibitor, MG-132, for 72 h led to an increase in total PD-L1 protein levels compared to single-agent treatments and vehicle control (Figure 21A). Interestingly, the phosphorylation levels of GSK-3β at Ser9 did not decrease as anticipated with AK-01 treatment alone and even showed a slight increase with the AK-01+MG-132 setup, suggesting GSK-3β-independent regulatory role of AURKA on PD-L1 (Figure 21B).

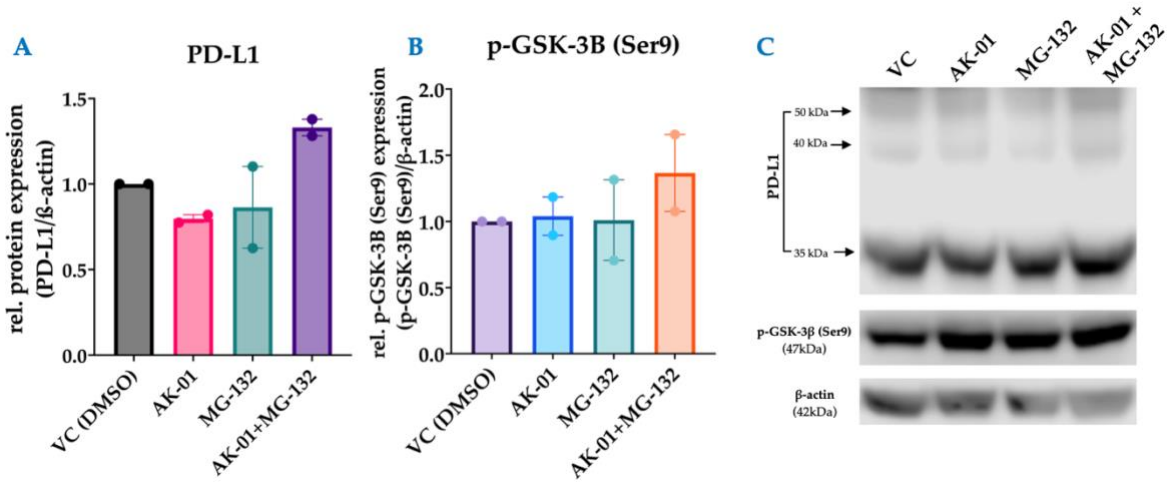

Figure 21. AURKA regulates PD-L1 independently of GSK-3β phosphorylation at Ser9. A) Relative PD-L1 protein expression showed elevated levels with combined AK-01 and MG-132 treatments compared to stand-alone treatment and vehicle control (VC) (n=2). **(B)** Relative p-GSK-3β (Ser9) expression remained stable following the same treatment conditions (n=2). **(C)** Representative immunoblot analyses of PD-L1 and p-GSK-3β (Ser9) normalized to b-actin under indicated treatment conditions.

To further validate this GSK-3β-independent mechanism, we performed additional combination experiments using siR-mediated knockdown of GSK-3β and AURKA inhibition (either with siRNA or AK-01). At 144h post-treatment, we evaluated p-GSK-3β and CTNNB1 protein expression across five conditions: (1) control (CTRL,

scramble), (2) siR-GSK-3β alone, (3) simultaneous siR-GSK-3β + siR- AURKA, (4) sequential siR-GSK-3β followed by siR-AURKA inhibition at 72h, and (5) sequential siR-GSK-3β followed by AK-01 at 72h. Consistent with our previous observations, none of the AURKA perturbation setups increased p-GSK-3β (Ser9) levels compared to the control, suggesting that AURKA does not affect Ser9 phosphorylation of GSK-3β in this model (Figure 22A). Furthermore, we examined CTNNB1 protein expression under the same treatment conditions, as CTNNB1 is a well-established downstream substrate of GSK-3β. Indeed, siR-GSK-3β alone increased CTNNB1 levels by about 20%, consistent with its known role as a negative regulator of CTNNB1. When AURKA was silenced simultaneously with GSK-3β knockdown (siR-GSK-3β + siR-AURKA sim), CTNNB1 level was reduced by approximately 30% compared to siR-GSK-3β treatment alone. Similarly, siR-GSK-3β followed by AK-01 treatment at 72h decreased CTNNB1 to almost the same level, indicating that AURKA inhibition can override the stabilizing effect of GSK-3β depletion. Interestingly, CTNNB1 expression increased by about 40% (*vs*. the control) when siR-AURKA was added 72h after siR-GSK-3β treatment, the highest level observed across all setups (Figure 22B). Furthermore, independent validation showed that siR-mediated knockdown of AURKA alone markedly reduced CTNNB1 protein in JHH6 cells at 72h, confirming direct AURKA-dependent positive regulation of CTNNB1 (Figure 22C).

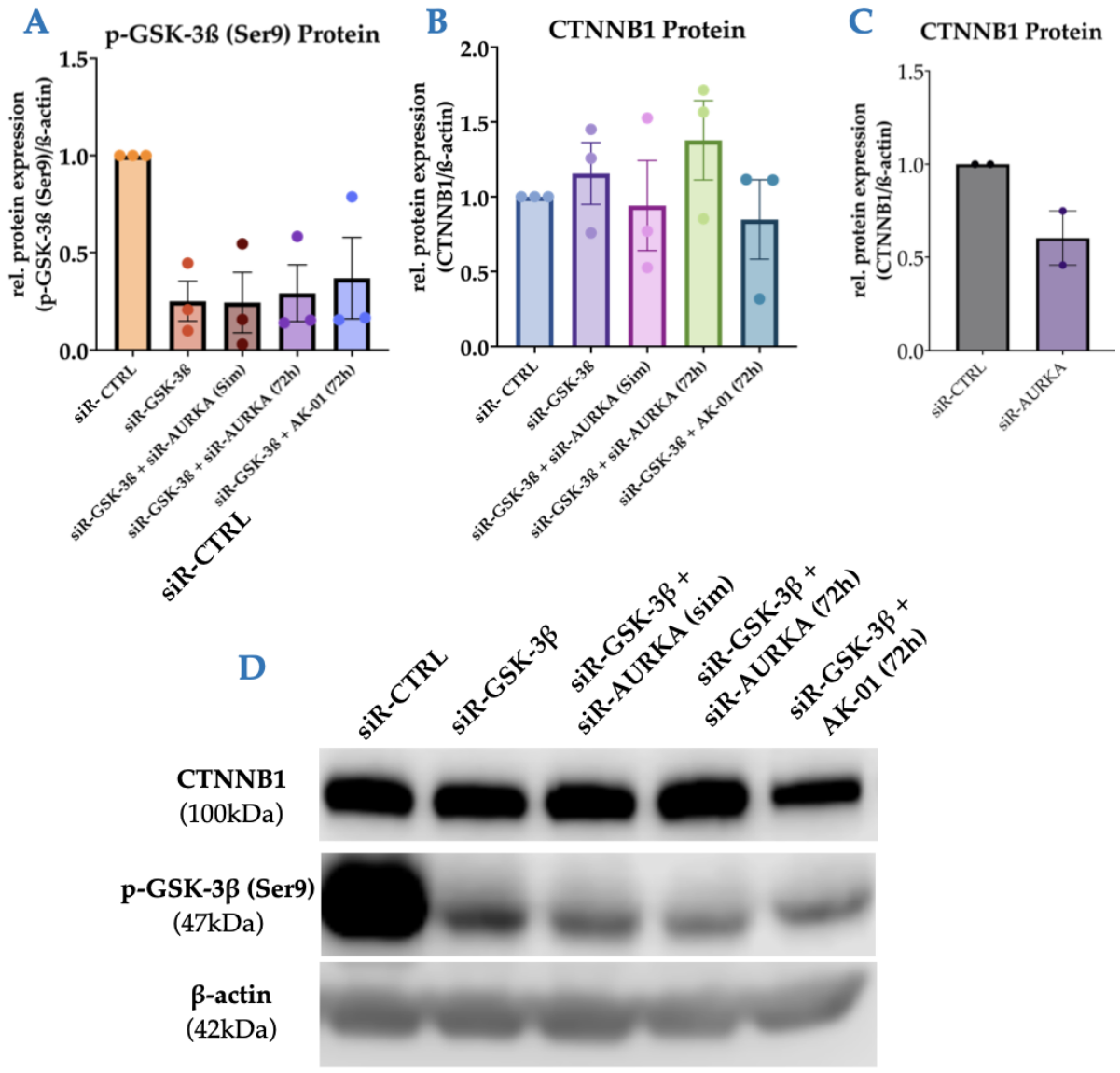

Figure 22. AURKA regulates CTNNB1 in JHH6 cells. (A-B) Relative p-GSK-3β (Ser9) and CTNNB1 expression following silencing with GSK-3β , either combined with siR-AURKA or AK-01 (n=3). **(C)** Relative expression of CTNNB1 following AURKA knockdown at 72h in JHH6 cells (n=2). (D) Representative immunoblot analyses of p-GSK-3β (Ser9) and CTNNB1 normalized to β-actin under indicated treatment conditions. Data presented as mean ± SEM from independent experiments. sim, simultaneous treatment; 72h, treatment added 72h post-GSK-3β silencing.

4.15. GSK-3β Knockdown and AKT inhibition revealed alternative PD-L1 regulatory mechanisms in HCC cells

To further delineate the potential role of GSK-3β on PD-L1 regulation, we directly assessed the impact of GSK-3β knockdown on PD-L1 expression in HCC cells. Additionally, since alternative mechanisms involve AKT as principal regulator

responsible for the GSK-3β Ser9 phosphorylation [141], we examined whether AKT inhibition with MK-2206 could modulate PD-L1 expression through this pathway. To test this, we performed a siRNA-mediated knockdown of GSK-3β and AKT inhibition experiments. GSK-3β knockdown (siRNA) reduced both the total and p-GSK-3β (Ser9) protein levels without marked effects on PD-L1 protein abundance in JHH6 cells (Figure 23A). In HuH7, even though similar reduction of total GSK-3β and p-GSK-3β (Ser9) levels was observed, PD-L1 protein expression decreased by ~30% (Figure 23B).

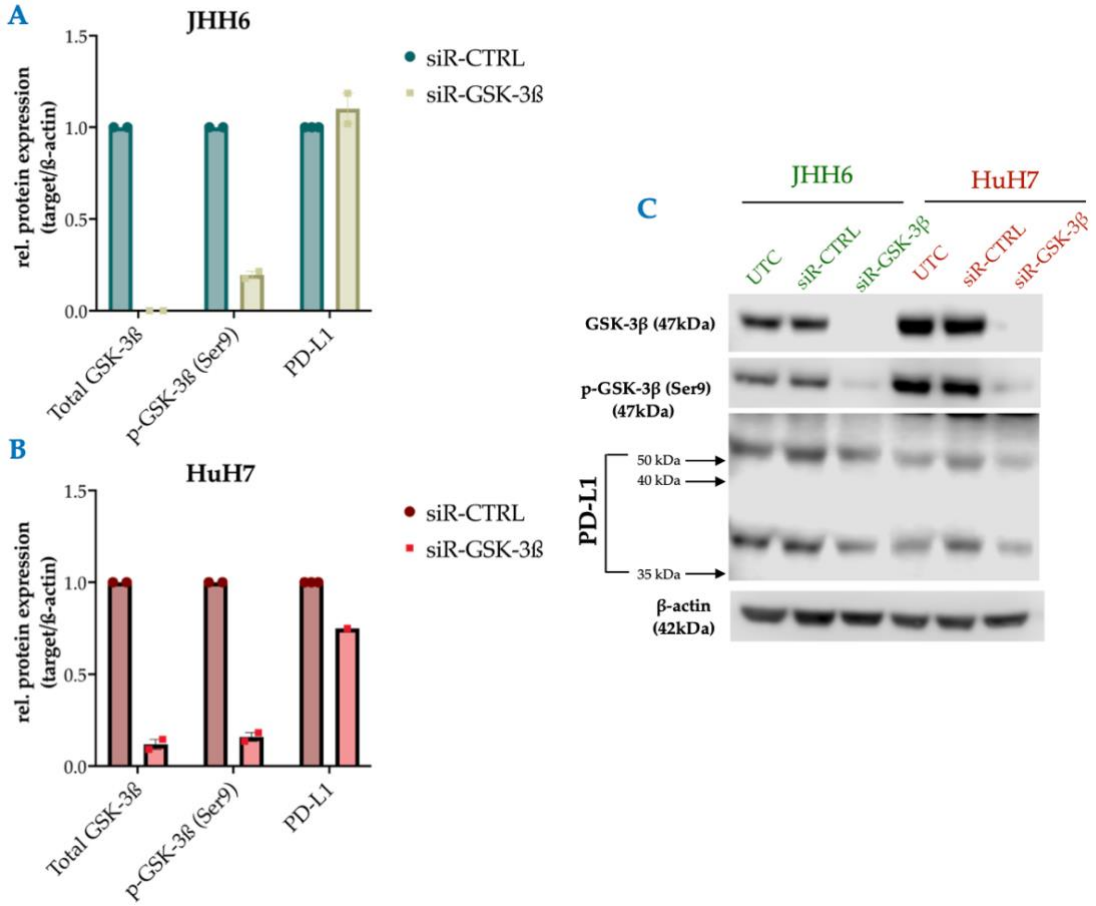

Figure 23. GSK-3β knockdown does not affect PD-L1 protein levels in HCC cells. (A) Relative protein levels of Total GSK-3β and p-GSK-3β (Ser9) were markedly reduced, while relative PD-L1 protein levels remained unchanged following a 72h siRNA-mediated knockdown of GSK-3β in JHH6 cells. **(B)** Relative protein expression of Total GSK-3β and p-GSK-3β (Ser9) were markedly reduced, with concurrent reduction of ~30% of PD-L1 protein in HuH7 following a 72h siRNA-mediated knockdown of GSK-3β in HuH7 cells. **(C)** Representative immunoblot of siRNA-mediated knockdown of GSK-3β in JHH6 and HuH7 cells probed for GSK-3β, p-GSK-3β (Ser9), and PD-L1. Protein expression of the targets was normalized against β-actin. Data presented as mean ± SEM from independent experiments, n=2.

Additionally, treatment with the AKT inhibitor, MK-2206, showed minimal effects or no observable reduction on p-GSK-3β (Ser9) levels in both cell lines (Figure 24A and 24B), suggesting that AKT inhibition does not substantially alter GSK-3β phosphorylation status in these HCC cell lines. On the one hand, PD-L1 levels displayed cell line-specific responses to MK-2206. While JHH6 cells showed no observable changes, PD-L1 expression in HuH7 increased by ~40% following MK-2206 treatment. (Figure 24C and 24D).

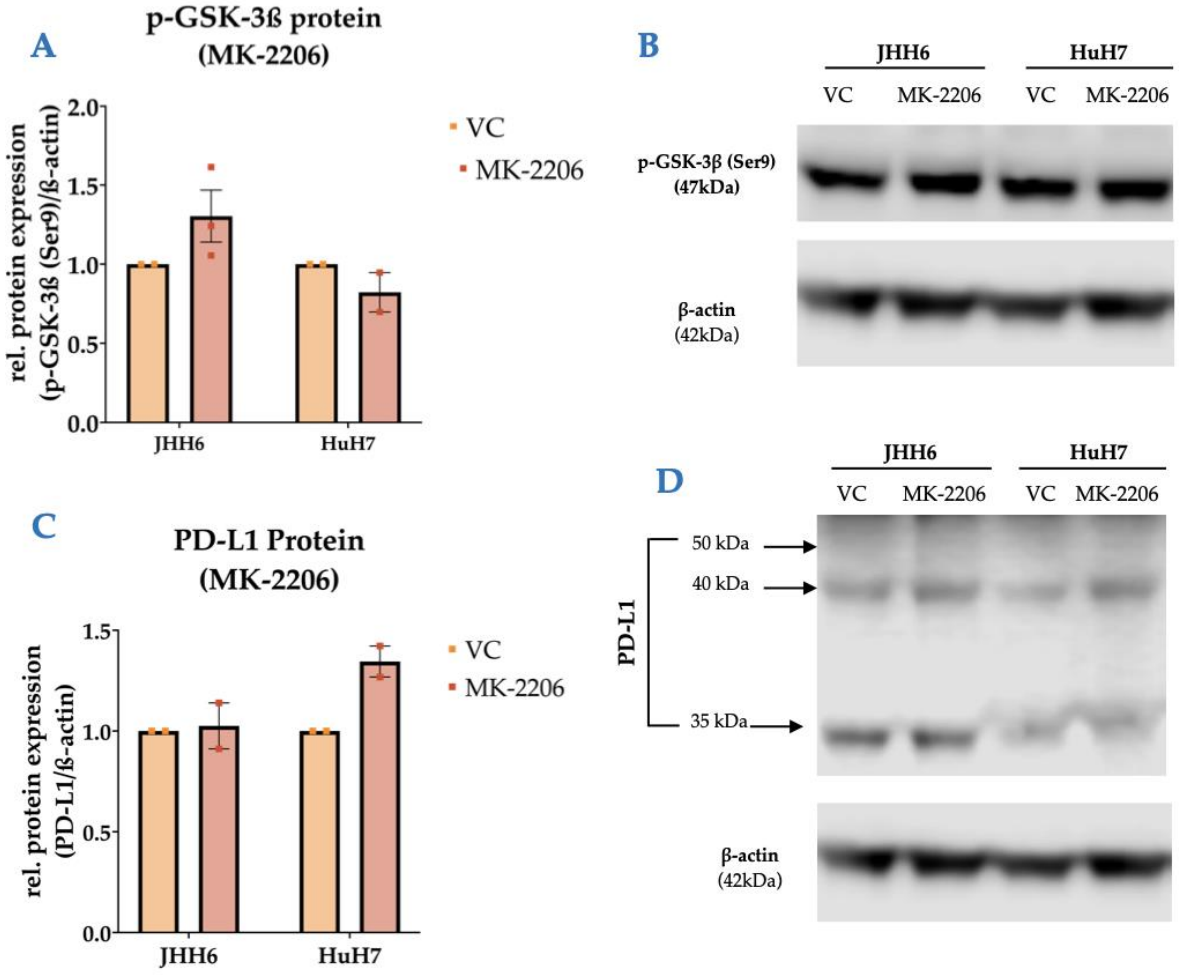

Figure 24. AKT inhibition demonstrated GSK-3β -independent regulation of PD-L1 in HCC cells. (A) Quantification of p-GSK-3B (Ser9) levels showed modest increase in JHH6 and slight reduction in HuH7 cells. **(B)** Representative western blot analysis of p-GSK-3B (Ser9) in both cell lines under treatment setups. **(C)** Quantification of PD-L1 levels demonstrating no observable changes in JHH6 but an obvious PD-L1 increase in HuH7 cells. **(D)** Representative western blot analyses of PD-L1 protein showed differential responses between cell lines. Protein expression of the targets are normalized against β-actin. Data presented as mean ± SEM from independent experiments, N=2.

These observations reveal an unexpected regulatory pattern in HuH7 cells, where both AURKA [25,122] and AKT [142,143] influence PD-L1 levels through GSK3β-independent mechanisms, challenging prior models of PD-L1 stabilization [102,116], further highlighting cell context-dependent regulation of immune checkpoint proteins in HCC.

4.16. Comparative gene expression profiling revealed distinct downstream networks of Aurora Kinase A in Hepatocellular Carcinoma cell lines

Since in our HCC samples, we observed that only about 25% of GSK-3β was inactivated at Ser9, implying that majority of GSK-3β remains catalytically active; paradoxically, CTNNB1 was overexpressed in our HCC samples. Under canonical expectations, a predominantly active GSK-3β pool should favor CTNNB1 turnover and reduced signaling, yet evidence says that tumors frequently rewire or repurpose GSK-3β's role, uncoupling this kinase from its classic destruction complex function. Thus, we undertook an exploratory analysis centered on AURKA. siRNA-mediated knockdown of AURKA in JHH6 and HuH7 cells was performed to profile pathway-level readouts across proliferation, fibrosis, inflammation, and glucose metabolism to partially define AURKA-dependent pathways or effectors that could account for the observed CTNNB1 expression/behavior independent of GSK-3β in HCC.

Interestingly, *CTNNB1* mRNA expression was only significantly downregulated in JHH6 cells but not in HuH7 upon AURKA knockdown. In JHH6, siR-AURKA also significantly reduced *AXIN2*, *CDKN1A*, *GLUT1*, and *PKM2*, with *IL-6* was significantly overexpressed (Figure 25A). In contrast, HuH7 exhibited a broader signature. AURKA knockdown significantly downregulated *CCND1*, *HIF1A*, *COL1A1*, *CDKN1A*, *GYS2*, *GLUT1*, *PGK1*, *PKM2*, and *IL-1B*; and significantly increased *IL-6* and *TNF-A* (Figure 25B). Together, these data revealed a JHH6-restricted repression of CTNNB1 transcription and drives broader metabolic and cytokine remodeling in HuH7 cells, underscoring cell context-dependent AURKA wiring in HCC.

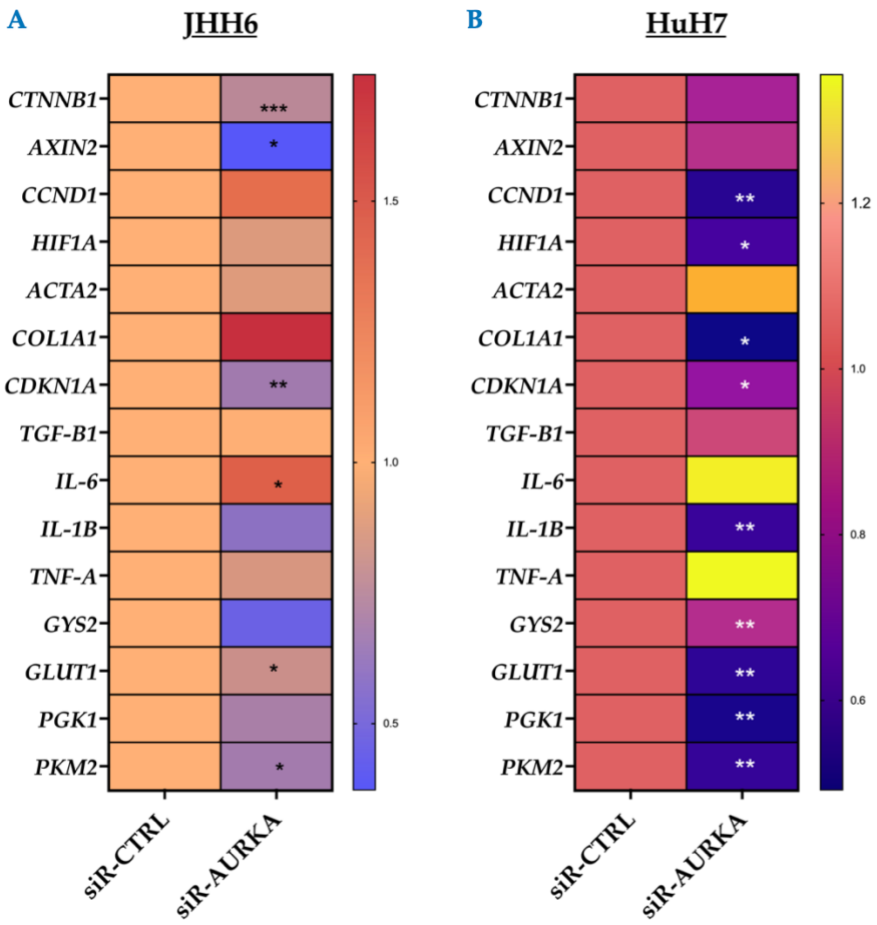

Figure 25. Differential gene expression following AURKA knockdown in JHH6 and HuH7 cells. Heatmaps show significantly dysregulated genes after siR-AURKA for 72h. **(A)** In JHH6, *CTNNB1*, *AXIN2*, *CDKN1A*, *GLUT1* and *PKM2* decreased, while *IL-6* increased. **(B)** In HuH7, *CCND1*, *HIF1A*, *COL1A1*, *CDKN1A*, *GYS2*, *GLUT1*, *PGK1*, *PKM2*, and *IL-1B* decreased, whereas *IL-6* and *TNF-A* increased. *p< 0.05, **p<0.01, ***p< 0.001, ****p<0.0001. N=3.

Chapter 5

Discussion

Hepatocellular carcinoma (HCC)—the malignant endpoint of most chronic liver diseases (CLD)—has become one of the world's leading public health and economic challenge. HCC is the third leading cause of cancer-related mortalities worldwide and despite on-going hepatitis-B vaccination and antiviral programs, both incidence and mortality are still expected to climb by 50-55% before 2050 [1]. Furthermore, these numbers are driven largely by the rising prevalence of metabolic dysfunction-associated steatotic liver diseases (MASLD) and alcohol-related cirrhosis [71,72]. Because majority of HCC cases develop in a chronically diseased liver, the progression of CLD represents a substantial reservoir of future cases [55,75]. These epidemiologic trends underscore an urgent need to understand the molecular crosstalk—including the AURKA-centered networks described here—that links chronic hepatic injury and malignant transformation.

Late-stage diagnoses remain the principal barrier for good prognosis in HCC. The potentially curative liver transplantation or anatomical resection is feasible only for solitary tumors or those with less than three lesions, leaving the majority of patients to rely on systemic treatments with historically modest survival benefits [119,144]. Recent combinatorial regimens such as the Atezolizumab plus Bevacizumab that couple targeted kinase inhibition with immune-checkpoint blockade have the benefits of extending overall survival by simultaneously attacking tumor-intrinsic pathways and alleviating immunosuppression [96,145]. This has driven current clinical trials toward multi-target strategies, underscoring the urgent need to identify and validate novel therapeutic nodes that can intervene effectively across the spectrum of CLD to HCC.

Th role of Aurora Kinase A (AURKA) across the liver disease spectrum remains underexplored. However, our data has unveiled a paradigm-shifting understanding

of kinase biology that fundamentally challenges the conventional oncogenic function of AURKA. Rather than functioning as a simple binary oncogenic switch, AURKA emerges as a potential molecular driver whose functions are dynamically shaped by cellular context, tissue microenvironment, and disease stage. This context-dependent functionally represents an interesting deviation from the conventional tumor-suppressor/oncogene classification toward a more nuanced understanding of how AURKA exerts its function in response to certain pathophysiological demands [132,146]. The clinical significance of exploring AURKA's role in CLD and HCC could pave the way for a more precise targeting in these disease contexts, where precision medicine increasingly drives therapeutic decision-making, understanding the functional plasticity of key regulatory molecules such as AURKA becomes essential for developing effective, targeted interventions. The unexpected pattern of AURKA upregulation in chronically injured liver tissues, contrasted with its complex regulation in established tumors, suggests that therapeutic strategies must be carefully calibrated to disease stage and molecular context to achieve optimal efficacy while minimizing adverse effects [147].

This study synthesizes findings across multiple methodological approaches—from clinical tissue analyses to cellular mechanistic studies—to establish a unified model of AURKA function that accounts for its potentially distinct roles in CLD and HCC. The implications of these findings extend beyond HCC to inform our broader understanding of kinase biology, tissue homeostasis, and therapeutic targeting strategies across multiple liver disease contexts.

The pronounced discordance between *AURKA* mRNA and AURKA protein expression patterns in HCC revealed an unexpected finding in this study. While tumors consistently demonstrated elevated mRNA expression—validating decades of literature demonstrating *AURKA* transcriptional upregulation in cancer [109–111,114,120,132]—the protein expression revealed an entirely opposite pattern, with significant downregulation in HCC tissues compared to the paired, adjacent

chronically injured liver tissues. This discordance between transcriptional and translational output represents a crucial gap in our understanding of AURKA regulation that may have relevant biological and clinical significance. Post-transcriptional regulatory mechanisms has emerged as a major determinant of protein abundance, with studies suggesting that mRNA levels explain only up to 40% of protein expression variability in many systems [148]. This may have important implications especially since a number of previous studies relied primarily on transcriptional expression measurement of AURKA in many disease models [149–152]. However, if protein levels are predominantly controlled by post-transcriptional mechanisms, mRNA-based stratification strategies may fail to identify patients most likely to benefit from AURKA-targeted therapies. Future biomarker development must therefore incorporate protein-level analyses to achieve accurate therapeutic predictions.

The extensive alternative splicing of AURKA—provides mechanistic framework for understanding this discordance [153]. Alternative splicing generates multiple AURKA transcript isoforms with distinct coding sequences and 5′/3′ UTRs that can differentially influence translation efficiency, localization, and protein stability, and may explain why total mRNA abundance often fails to predict protein levels. Different AURKA isoforms can produce truncated or modified proteins (or non-coding/poorly translated RNAs), meaning summed transcript measurements mask isoform-specific protein output and can therefore create mRNA-protein discordance [154].

The chronic liver disease microenvironment may favor specific AURKA isoforms that are efficiently translated despite potential negative regulatory mechanisms that suppress AURKA protein in established tumors. Under chronic hepatocyte injury and regenerative stress, cells prioritize shift toward survival and repair programs that may selectively enhance translation of tissue repair-associated proteins while suppressing those linked to uncontrolled proliferation [155]. Beyond its mitotic functions, AURKA attenuates homologous recombination (HR) by blocking RAD51 homolog 1 (RAD51)

binding at DNA double-stranded breaks (DSBs), steering repair mechanisms toward lower-fidelity pathways such as non-homologous end joining (NHEJ) [156,157]. AURKA also enhances mitochondrial ATP production in certain disease contexts, favoring disease progression by promoting metabolic reprogramming and oxidative stress [158,159], features that are commonly linked to many chronic liver diseases [160]. Moreover, AURKA potentiates the anti-apoptotic function of p27 in the cytoplasm to restrain BAX cleavage and apoptosis, [161], suggesting an anti-apoptotic AURKA-P27 axis that could, by analogy, support hepatocyte survival under CLD stress. This would explain the high AURKA protein expression observed in the adjacent, non-tumoral tissues, where cells prioritize tissue homeostasis over malignant transformation prevention.

The identification of a significant correlation between AURKA and YAP1 protein expression specifically in the adjacent, non-tumoral tissues represents a critical understanding on how AURKA may coordinate tissue repair and homeostatic response in CLD, especially considering previous evidence demonstrating that AURKA modulates YAP1 expression at the transcriptional level [40,162], supported by our silencing experiments showing a significant reduction in *YAP1* expression upon *AURKA* knockdown. YAP1, as the central effector of the Hippo pathway, serves as a master regulator of organ size, tissue regeneration, and cellular fate decisions, making it an ideal downstream target for AURKA's context-dependent regulatory functions [30]. The mechanistic basis for AURKA-YAP1 interaction encompasses several mechanisms that extend beyond the conventional and simple kinase-driven phosphorylation activation. Canonically, phosphorylation at Ser397 marks YAP1 for β-TrCP-mediated proteasomal degradation, a hallmark of Hippo pathway activation [28,30,163]. Interestingly, a recent study showed that direct phosphorylation of YAP1 by AURKA at Serine 397 in the nucleus can promote YAP1 activity in breast cancer [39]. However, the preliminary data in this study suggest that AURKA may positively regulate YAP1 by influencing YAP1 expression rather than phosphorylation-

dependent activation, supporting a context-dependent regulatory role of AURKA. Notably, silencing AURKA led to about 50% reduction in total YAP1 levels with only ~10% reduction in p-YAP1 (Ser397) expression, while we observed a four-fold increase in p-YAP1 (Ser397)/Total YAP1 ratio. This disproportionate effect indicates that AURKA knockdown preferentially regulates the non-phosphorylated, transcriptionally active YAP1 pool, with the residual YAP1 predominantly Ser397-phosphorylated destined for degradation. Interestingly, these findings align with what Wang and colleagues demonstrated in their lung cancer model where AURKA positively regulates YAP1 abundance and stability by blocking autophagy *via* mTOR activation, thereby preventing lysosome-dependent degradation of YAP1 and increasing YAP1 protein half-life [40]. Wang et al. showed that chloroquine treatment or *Beclin-1* knockdown rescued YAP1 protein when AURKA was depleted, whereas rapamycin, an mTOR inhibitor, abrogated AURKA-driven YAP1 accumulation, supporting an autophagy-dependent mechanism. This tissue-specific regulation suggests AURKA may exert distinct mechanisms depending on cellular context and pathological state, with both pathways ultimately enhancing YAP1 transcriptional activity to promote cellular responses appropriate to the microenvironmental demands [40].

The progressive reduction of YAP1 protein abundance from MASLD to HCC samples, the higher proportion of phosphorylated YAP1 (Ser397) in neoplastic tissues, and the lack of correlation between YAP1 and AURKA in HCC, are patterns consistent with Hippo-driven repression of YAP1 and that AURKA may not be sufficient to maintain YAP1 activity globally, possibly because it is switched to other pathways. Additionally, the higher Thr288-phosphorylated fraction of AURKA (the mitotically active pool), suggests that tumor cells may rely more on dysregulated mitotic checkpoint control rather than continuous YAP1-driven proliferation [164–167]. Indeed, a positive correlation between p-YAP1 (Ser397) and p-AURKA (Thr288) exists in tumors, indicating a shift towards increased mitotic AURKA activity.

Table 6. Summary of AURKA and YAP1 expression and activation in our experimental model.

	HCC	ADJACENT TISSUES
TOTAL YAP1	↓	↑
P-YAP (SER397)	↑ (more phosphorylated, cytoplasmically retained/degraded)	↓ (less phosphorylated, nuclear translocation)
TOTAL AURKA	↓	↑
P-AURKA (THR288) / TOTAL AURKA) RATIO	↑ (higher activation proportion)	↓ (less activated)
BIOLOGICAL IMPLICATION	Active Hippo pathway → YAP1 inactivation and degradation	Inactive Hippo pathway → increased co-transcriptional activity

Interestingly, recent evidence in other cancers such as clear cell renal cell carcinoma (ccRCC) [168,169], colorectal cancer (CRC) [170], and hematological malignancies [171], offer a possible explanation for alternative and seemingly multifaceted role of YAP1, highlighting its possible tumor-suppressive function.

Many discoveries over the past decade have made it clear that it is no longer possible to categorize a protein strictly as a tumor suppressor or as an oncogenic promoter. Given the complexity of eukaryotic cellular systems—particularly in cancer—it is reasonable to assume that a protein's function largely depends on temporal, cell type–specific, disease-specific, and microenvironment-dependent factors.

Indeed, while YAP1 is reduced and targeted for degradation in neoplastic tissue, it is increased in adjacent tissues and MASLD samples, highlighting the complex and context-dependent dual nature of YAP1 signaling. YAP1 activation may represent both an essential adaptive response that helps promote hepatocyte survival and regeneration under chronic liver injury and may also represent a potential pathological driver that can promote excessive fibrosis and, ultimately, malignant transformation. In early stages of CLD, YAP1 activation likely serves predominantly beneficial functions by promoting hepatocyte proliferation, coordinating angiogenic responses, and activating stem cell compartments to support tissue regeneration. However, sustained YAP1 activation over a long period can drive pathological changes including hepatic stellate cell activation, collagen deposition, enhanced inflammatory responses, and conditions favorable for HCC development. Furthermore, the absence of correlation between AURKA and YAP1 in HCC tissues, contrasted by the strong correlation in adjacent tissues, where the-modulatory activity of AURKA toward YAP1 may predominate, revealing fundamental differences in how these networks function across different pathological contexts.

Building upon the well-established role of AURKA in modulating multiple signaling pathways, we also sought to investigate its potential regulatory interaction with GSK-3β within the context of chronic liver disease (CLD). A previous study on liver regeneration in mice demonstrated that AURKA negatively regulates GSK-3β activity through Ser9 phosphorylation, leading to its inactivation [172]. To explore whether a similar mechanism occurs in human liver pathology, we analyzed the protein expression levels of AURKA and GSK-3β, including its phosphorylated form at Ser9, in both tumor and adjacent non-tumoral liver tissues.

Functional assays using AURKA silencing or pharmacological inhibition revealed no detectable effects on GSK-3β Ser9 phosphorylation. Consistently, correlation analyses showed no significant association between AURKA and GSK-3β protein levels in either tissue type. The relatively stable levels of p-GSK-3β (Ser9) observed in both

tumor and adjacent tissues, together with the higher p-GSK-3β/total GSK-3β ratio in adjacent tissues, suggests a limited role for GSK-3β activity in CLD. Additionally, the 15% p-GSK-3β (Ser9) level detected in tumors does not supports the high CTNNB1 accumulation, indicating that CTNNB1 stabilization in HCC arises *via* mechanisms other than GSK-3β Ser9 inactivation [173–175]. Indeed, evidence showed that in disease settings GSK-3β can be repurposed or sequestered into specialized subcellular pools that dissociate its function for CTNNB1 control, redirecting its function to alternative pathways [176]. We acknowledge the limitation that GSK-3β localization was not assessed; however, transcript data from our HCC cell models suggest that GSK-3β may contribute to sustaining proliferation, glucose metabolism, and inflammatory signaling. Indeed, GSK-3β silencing reduced *CTNNB1* and *CDKN1A* expression, consistent with its role in regulating transcription factors such as NF-κB [177], CREB [178], and c-MYC [136]. Moreover, GSK-3β is known to modulate metabolic genes such as *GLUT1 [179],* which we observed dysregulated following GSK-3β knockdown in our cell models. Moreover, GSK-3β serves as a co-activator of the NF-κB pathway [180,181], highlighting its role in inflammatory signaling, supported by the downregulation of *IL-6* and TNF-*α* in HuH7 following knockdown, while paradoxically upregulating IL-1β in JHH6 cells contrasting existing literature evidence that GSK-3β positively regulates IL-1β in other disease models [182,183]. Taken together, these observations align with broader evidence pointing to the context-dependent and—occasionally divergent—roles of GSK-3β across distinct liver disease etiologies consistent with the review by Emma et al. [184].

In line with our findings, we also investigated the potential role of GSK-3β as the key mediator of the effects of AURKA on PD-L1, which is an important ligand for PD-1 that suppresses T-cell activity and enables immune escape, and has become a cornerstone of immunotherapy research in recent years. Even though its exact mechanistic role in HCC remains poorly characterized, clinical benefits to anti-PD-L1 drugs have shown promising results. However, patient outcomes remain

heterogeneous and patient-dependent, highlighting the need to map upstream drivers and stability mechanisms that determine PD-L1 expression in HCC.

Our data revealed a heterogeneous pattern of PD-L1 expression possibly reflecting the intrinsic molecular diversity of HCC, where different cellular subtypes may represent distinct adaptation mechanisms with varying immune evasion strategies and therefore therapeutic vulnerabilities. The half-life analyses established a clear stability hierarchy—with JHH6 cells exhibiting the longest PD-L1 half-life and highest PD-L1 abundance, while HLE and Hep3B demonstrated rapid proteasome-dependent turnover—provides critical insights into the molecular mechanisms controlling PD-L1 abundance and function. The correlation between baseline PD-L1 expression across HCC cells and protein stability experiment with cycloheximide supports the protective role of N-linked glycosylation in preventing PD-L1 degradation. Glycosylation at N192, N200, and N219 residues sterically blocks access to the proteasome-dependent degradation machinery to the protein core while enhancing binding affinity to PD-1 receptors and promoting preferential localization to plasma membrane rafts where PD-1/PD-L1 interaction occur to facilitate tumor immune evasion [102,104]. JHH6 cells, with their high baseline glycosylated PD-L1 context and extended protein half-life, likely represent a highly immunosuppressive phenotype that would particularly be more resistant to immune checkpoint blockade treatments. The stable, functional PD-L1 expression in these cells would maintain persistent T-cell suppression even under therapeutic pressure. Conversely, HLE and Hep3B, with their rapid PD-L1 turnover and lower glycosylated content, might be more vulnerable to therapies that further destabilize PD-L1 or enhance its degradation rate. On the one hand, the biphasic response observed in HuH7 cell during cycloheximide chase experiments—characterized by initial decline followed by a partial recovery despite continued protein synthesis inhibition—represents a particularly intriguing pattern that likely reflects activation of cellular stress response pathways. Under conditions of global protein synthesis inhibition, cells activate integrated stress response pathways

that selectively maintain translation of specific mRNAs encoding stress response proteins and regulatory molecules [185,186]. PD-L1 mRNA contains multiple regulatory elements that could render it susceptible to stress-induced translational activation, potentially representing an adaptive mechanism that maintains immune checkpoint expression under therapeutic pressure [187,188].

The observed heterogeneity in PD-L1 stability and proteasome-dependent degradation rates across HCC cell lines can have a profound impact on patient stratification and therapeutic strategy development. Current approaches to immune checkpoint inhibitors rely primarily on PD-L1 expression levels as determined by immunohistochemistry, but these static measurements fail to capture the dynamic regulation of PD-L1 that ultimately determines therapeutic efficacy [189,190]. Tumors with high baseline glycosylated PD-L1 content and extended protein half-life would maintain persistent immune suppression even under therapeutic pressure from PD-L1 antibodies, requiring combination approaches that simultaneously target PD-L1 function and the cellular mechanisms responsible for PD-L1 stabilization or expression.

Given this heterogeneity in PD-L1 stability and expression, identifying upstream modulators becomes critical for developing rational combination therapies. Our study revealed that AURKA functions as a positive regulator of PD-L1 expression in HCC, with pharmacological inhibition (AK-01) and genetic knockdown of AURKA significantly reducing PD-L1 protein in HCC cells. This finding positions AURKA as a promising therapeutic target that could be leveraged alongside PD-L1 checkpoint blockade to overcome resistance mechanisms. Simultaneous targeting of PD-L1 and AURKA serve as a promising strategy to achieve a more durable immune response by both blocking PD-L1 function and preventing its upstream stabilization. Hence, the evidence of AURKA regulating PD-L1 in our HCC model directed our research toward understanding the mechanistic basis of AURKA-mediated PD-L1 regulation,

leading us to hypothesize that the glycogen synthase kinase-3 beta (GSK-3β) might serve as a critical intermediate in this regulatory axis.

Focusing on GSK-3β was motivated by previous evidence from other cancer models demonstrating its critical role in PD-L1 regulation. GSK-3β phosphorylates the non-glycosylated PD-L1, promoting its ubiquitination by β-TrCP and subsequent proteasomal degradation [102]. Moreover, previous reports also suggested that AURKA negatively regulates GSK-3β in gastric cancer [114] and liver regeneration process [21]. We then hypothesized that AURKA might indirectly stabilize PD-L1 by suppressing GSK-3β activity—creating an attractive regulatory axis linking cell cycle control with immune evasion.

However, our investigation revealed that AURKA regulates PD-L1 expression through mechanisms independent of GSK-3β Serine 9 phosphorylation. This finding represents a fundamental departure from the working hypothesis and necessitated a reconceptualization of how AURKA influences immune checkpoint regulation in HCC. Multiple lines of evidence from our experiments support GSK-3β-independent mechanisms: (1) absence of changes in GSK-3β Ser9 phosphorylation following AURKA inhibition or knockdown. Despite previous evidence supporting the negative modulatory effects of AURKA *via* GSK-3β (Ser9) inactivation, neither the selective AURKA inhibitor, AK-01, nor genetic knockdown of AURKA altered GSK-3β (Ser9) phosphorylation levels in our JHH6 model. This directly contradicts the expected mechanism whereby AURKA would inactivate GSK-3β to prevent PD-L1 degradation. While a recent proteogenomic analysis of HCC biopsies reported inverse correlation between AURKA and GSK-3β activity based on dysregulated phosphorylation levels [191], our direct functional experiments demonstrated GSK-3β (Ser9) phosphorylation-independent regulation of PD-L1 by AURKA. This apparent discrepancy likely reflects the difference between population-level correlations in heterogeneous tumor samples *vs* mechanistic relationships within defined cellular contexts such as ours. Our cell line-specific findings revealed that within individual

HCC subtypes, AURKA regulates PD-L1 through alternative mechanisms, emphasizing the relevance of context-specific experimental validation of inferred relationships from correlative proteogenomic data.

Moreover, we observed the (2) lack of PD-L1 changes following direct GSK-3β depletion. Direct siRNA-mediated knockdown of GSK-3β, which effectively reduced both total and phosphorylated GSK-3β protein levels, produced minimal changes in PD-L1 expression. If GSK-3β were the critical intermediate linking AURKA to PD-L1 regulation, its depletion should have the opposite effect of AURKA inhibition on PD-L1 levels. Lastly, the differential responses to AKT inhibition did not align with predicted GSK-3β-mediated effects. Treatment with the AKT inhibitor, MK-2206, resulted to a differential and contradictory effects across cell lines. No effect was observed in JHH6 cells, but a slight 30% increase was observed in HuH7 cells. Since AKT functions as a negative regulator of GSK-3β *via* phosphorylation at Ser9 [141,192], AKT inhibition should restore GSK-3β activity and promote PD-L1 degradation. Collectively, these findings demonstrate that the AURKA-GSK-3β-PD-L1 axis specifically through GSK-3β (Ser9)-phosphorylation described in other cancer types, does not operate in HCC. Furthermore, the lack of PD-L1 upregulation upon AKT inhibition reflects GSK-3β-independent regulatory network for PD-L1 in our model. Although AKT normally phosphorylates GSK-3β on Serine 9, treatment with MK-2206 showed little to no change in PD-L1 levels, proving that AKT-GSK-3β signaling is not the dominant PD-L1 control mechanism in this context.

Given our conclusion that AURKA does not regulate GSK-3β *via* Ser9 phosphorylation, several alternative mechanisms warrant further consideration for AURKA-mediated PD-L1 regulation. AURKA's role outside mitosis is now increasingly being recognized. For instance, nuclear AURKA can interact with multiple transcription factors that promote transcription of oncogenes including *C-MYC [193]*, *FOXM1 [194]*, and *CTNNB1 [195]*. These oncogenes have been implicated in immune checkpoint regulation of PD-L1 [196–198], and AURKA-mediated

enhancement of their activity could indirectly promote PD-L1 expression as well. CTNNB1 pathway represents a particularly attractive candidate mechanism given AURKA's demonstrated ability to promote CTNNB1 nuclear translocation and transcriptional activity. In esophageal squamous cell carcinoma (ESCC), AURKA directly interacts with CTNNB1 and phosphorylates it at Ser552 and Ser675, stabilizing CTNNB1 by inhibiting its ubiquitin-mediated proteasome degradation. This promotes CTNNB1's dissociation from cell-cell contacts and facilitates its nuclear translocation. Importantly, this regulation occurs through a WNT-independent mechanism, since AURKA overexpression did not affect GSK-3β levels or the formation of AXIN/GSK-3β/APC degradation complex [199].

Given the molecular diversity present and the pleiotropic roles of AURKA in HCC, we further profiled transcripts in JHH6 and HuH7 to identify convergent and possibly subtype-specific downstream targets, an approach similar to our exploratory analyses for GSK-3β. True enough, AURKA knockdown produced a subtype-specific transcriptional rewiring in HCC. In JHH6, *CTNNB1* was downregulated further validating that AURKA influences CTNNB1 both at the transcriptional and translational level. *AXIN2* and glycolytic genes (*GLUT1* and *PKM2*) were also downregulated, consistent with the role of AURKA in WNT pathway and metabolic control. In HuH7, AURKA knockdown broadly downregulated glycolytic markers, HIF1A, COL1A1, and CCND1, indicating a wider impact on several hallmarks such as hypoxia, ECM, and cell-cycle machinery. Inflammatory markers showed diverse expression underscoring context dependence. These observations highlight a wide AURKA signaling footprint and motivate focused mechanistic and patient-oriented studies to characterize its functions in hepatic diseases.

Chapter 6

Conclusions and Future Directions

Across the CLD-HCC spectrum in our cohort, AURKA displayed a context-dependent profile characterized by elevated tumoral mRNA expression yet higher protein abundance in adjacent, non-tumoral tissues, alongside a greater p-AURKA (Thr288) expression in tumors, indicating distinct regulation of expression versus activation across disease stages. In adjacent tissues, AURKA is significantly correlated with YAP1 levels, while *AURKA* silencing predominantly reduced total YAP1 rather than p-YAP1 (Ser397) supporting a stability-centric rather than phosphorylation-centric mode of YAP1 control. However, these findings need to be confirmed in a model of chronic liver disease since JHH6 is a hepatocellular carcinoma cell line even though the rationale behind using this cell line over LX-2 cells was because of the predominantly hepatocytic expression of AURKA in our immunohistochemistry findings. It is therefore imperative to dissect AURKA-YAP1 regulation in CLD in models such as primary hepatocytes, liver organoids, as well as CCl_4-induced mice models of fibrosis/cirrhosis, parsing autophagy/mTOR-dependent stabilization *versus* direct YAP1 Ser397 phosphorylation. In HCC, AURKA inhibition or knockdown consistently reduced PD-L1 protein expression. Furthermore, we confirmed that PD-L1 is heavily glycosylated as well in hepatocellular carcinoma cells. PD-L1 glycosylation has immense consequences on its stability and function *in vivo*. Hence, we wanted to determine PD-L1 turnover across HCC cell lines to capture its dynamic stability or abundance and pinpoint specific its degradation mechanism. Cycloheximide chase experiments revealed a stability hierarchy across cell lines, notably a long-lived highly glycosylated PD-L1 pool in JHH6 *versus* the rapid turnover observed in HLE and Hep3B. We also confirmed that PD-L1 is degraded *via* the proteasome pathway through our MG-132 experiments which also revealed differential PD-L1 accumulation across HCC cells consistent with their half-lives. Mechanistically, AURKA's positive regulation of PD-L1 occurred independently of GSK-3β (Ser9)

phosphorylation, as neither AURKA's perturbation altered p-GSK-3β (Ser9) nor did GSK-3β knockdown recapitulated PD-L1 accumulation. AKT inhibition, on the one hand, produced cell-specific, non-canonical effects, while transcript screening indicated that AURKA and GSK-3β operate largely in distinct networks for PD-L1 control in HCC. Hence, it is necessary to define other routes by which AURKA modulates PD-L1 independent of GSK-3β.

A forward-looking close: Collectively, these findings position AURKA as a clinically actionable, context-aware biomarker and therapeutic node within the liver disease spectrum, supporting rational combinations with immune-checkpoint blockade to deliver more precise and durable responses. Near-term priorities—prospective longitudinal cohorts to further refine patient selection and timing, paired with rigorous experimental validation (orthogonal assays, functional perturbation and rescue, glycoform-aware quantification, and disease-relevant models)—will accelerate translation by confirming mechanism and on-target activity while de-risking trials. Embedding validated AURKA networks and context-dependent regulation (e.g., YAP1 stability and non-canonical routes to PD-L1) into therapeutic decision frameworks can streamline study design and potentially shorten the path from discovery to actual clinical utility, paving the way for tailored treatment regimens in CLD and HCC.

References

1 Bray F, Laversanne M, Sung H, Ferlay J, Siegel RL, Soerjomataram I, et al. Global cancer statistics 2022: GLOBOCAN estimates of incidence and mortality worldwide for 36 cancers in 185 countries. CA A Cancer J Clinicians. 2024 May;74(3):229–63.

2 Li Q, Ding C, Cao M, Yang F, Yan X, He S, et al. Global epidemiology of liver cancer 2022: An emphasis on geographic disparities. Chin Med J (Engl). 2024 Oct;137(19):2334–42.

3 Rumgay H, Arnold M, Ferlay J, Lesi O, Cabasag CJ, Vignat J, et al. Global burden of primary liver cancer in 2020 and predictions to 2040. Journal of Hepatology. 2022 Dec;77(6):1598–606.

4 Llovet JM, Kelley RK, Villanueva A, Singal AG, Pikarsky E, Roayaie S, et al. Hepatocellular carcinoma. Nat Rev Dis Primers. 2021 Jan;7(1):6.

5 Yang Y, Kim S, Seki E. Inflammation and Liver Cancer: Molecular Mechanisms and Therapeutic Targets. Semin Liver Dis. 2019 Feb;39(01):026–42.

6 Huang X, Stern DF, Zhao H. Transcriptional Profiles from Paired Normal Samples Offer Complementary Information on Cancer Patient Survival – Evidence from TCGA Pan-Cancer Data. Sci Rep. 2016 Feb;6(1):20567.

7 Pan Q, Qin F, Yuan H, He B, Yang N, Zhang Y, et al. Normal tissue adjacent to tumor expression profile analysis developed and validated a prognostic model based on Hippo-related genes in hepatocellular carcinoma. Cancer Medicine. 2021 May;10(9):3139–52.

8 Grisetti L, Garcia CJC, Saponaro AA, Tiribelli C, Pascut D. The role of Aurora kinase A in hepatocellular carcinoma: Unveiling the intriguing functions of a key but still underexplored factor in liver cancer. Cell Proliferation. 2024 Apr;e13641.

9 Mou PK, Yang EJ, Shi C, Ren G, Tao S, Shim JS. Aurora kinase A, a synthetic lethal target for precision cancer medicine. Exp Mol Med. 2021 May;53(5):835–47.

10 Willems E, Dedobbeleer M, Digregorio M, Lombard A, Lumapat PN, Rogister B. The functional diversity of Aurora kinases: a comprehensive review. Cell Div. 2018;13:7.

11 Hassan I, Noor S, EBSCOhost, editors. Protein kinase inhibitors: from discovery to therapeutics. London, UK: Academic Press; 2022.

12 Janeček M, Rossmann M, Sharma P, Emery A, Huggins DJ, Stockwell SR, et al. Allosteric modulation of AURKA kinase activity by a small-molecule inhibitor of its protein-protein interaction with TPX2. Sci Rep. 2016 June;6(1):28528.

13 Tavernier N, Sicheri F, Pintard L. Aurora A kinase activation: Different means to different ends. Journal of Cell Biology. 2021 Sept;220(9):e202106128.

14 Nikonova AS, Astsaturov I, Serebriiskii IG, Dunbrack RL, Golemis EA. Aurora A kinase (AURKA) in normal and pathological cell division. Cell Mol Life Sci. 2013 Feb;70(4):661–87.

15 Castro A, Arlot-Bonnemains Y, Vigneron S, Labbé J, Prigent C, Lorca T. APC/Fizzy-Related targets Aurora-A kinase for proteolysis. EMBO Reports. 2002 May;3(5):457–62.

16 Grzenda A, Leonard P, Seo S, Mathison AJ, Urrutia G, Calvo E, et al. Functional impact of Aurora A-mediated phosphorylation of HP1γ at serine 83 during cell cycle progression. Epigenetics Chromatin. 2013 July;6(1):21.

17 Grzenda A, Leonard P, Seo S, Mathison AJ, Urrutia G, Calvo E, et al. Functional impact of Aurora A-mediated phosphorylation of HP1γ at serine 83 during cell cycle progression. Epigenetics Chromatin. 2013 July;6(1):21.

18 Glover DM, Alphey L, Axton JM, Cheshire A, Dalby B, Freeman M, et al. Mitosis in Drosophila development. J Cell Sci Suppl. 1989;12:277–91.

19 Glover DM, Leibowitz MH, McLean DA, Parry H. Mutations in aurora prevent centrosome separation leading to the formation of monopolar spindles. Cell. 1995 Apr;81(1):95–105.

20 Du R, Huang C, Liu K, Li X, Dong Z. Targeting AURKA in Cancer: molecular mechanisms and opportunities for Cancer therapy. Mol Cancer. 2021 Dec;20(1):15.

21 Yin Y, Kong D, He K, Xia Q. Aurora kinase A regulates liver regeneration through macrophages polarization and Wnt/β-catenin signalling. Liver International. 2022 Feb;42(2):468–78.

22 Dai G, Lin J, Jiang Y, Liu X, Chen P, Zhang Y, et al. Aurora kinase A promotes hepatic stellate cell activation and liver fibrosis through the Wnt/β-catenin pathway. Front Oncol. 2025 Jan;14. DOI: 10.3389/fonc.2024.1517226

23 Wang J, Li P, Li Y, Wang C, Xilizhati K, Ye J. Exploring the mechanism and drug candidates of alveolar echinococcosis affecting liver fibrosis through analysis of existing microarray data. Acta Tropica. 2025 Mar;263:107532.

24 Hora S, Wuestefeld T. Liver Injury and Regeneration: Current Understanding, New Approaches, and Future Perspectives. Cells. 2023 Aug;12(17):2129.

25 Grisetti L, Saponaro AA, Sukowati CHC, Tarchi P, Crocè LS, Palmisano S, et al. The expression of Aurora Kinase A and its potential role as a regulator of Programmed Death-Ligand 1 in hepatocellular carcinoma: Implications for immunotherapy and immune checkpoint regulation in hepatocarcinogenesis. Digestive and Liver Disease. 2023 Sept;55:S219–20.

26 Liu Z, Wu B, Liu X, Wu X, Du J, Xia G, et al. CD73/NT5E-mediated ubiquitination of AURKA regulates alcohol-related liver fibrosis via modulating hepatic stellate cell senescence. Int J Biol Sci. 2023;19(3):950–66.

27 Jiang M, Bai M, Xu S, Wang T, Lei J, Xu M, et al. Blocking AURKA with MK-5108 attenuates renal fibrosis in chronic kidney disease. Biochimica et Biophysica Acta (BBA) - Molecular Basis of Disease. 2021 Nov;1867(11):166227.

28 Fu M, Hu Y, Lan T, Guan K-L, Luo T, Luo M. The Hippo signalling pathway and its implications in human health and diseases. Sig Transduct Target Ther. 2022 Nov;7(1). DOI: 10.1038/s41392-022-01191-9

29 Zhao B, Li L, Tumaneng K, Wang C-Y, Guan K-L. A coordinated phosphorylation by Lats and CK1 regulates YAP stability through SCF(beta-TRCP). Genes Dev. 2010 Jan;24(1):72–85.

30 Lu L, Finegold MJ, Johnson RL. Hippo pathway coactivators Yap and Taz are required to coordinate mammalian liver regeneration. Exp Mol Med. 2018 Jan;50(1):e423–e423.

31 Wang J, Sinnett-Smith J, Stevens JV, Young SH, Rozengurt E. Biphasic Regulation of Yes-associated Protein (YAP) Cellular Localization, Phosphorylation, and Activity by G Protein-coupled Receptor Agonists in Intestinal Epithelial Cells: A NOVEL ROLE FOR PROTEIN KINASE D (PKD). J Biol Chem. 2016 Aug;291(34):17988–8005.

32 Moon H, Cho K, Shin S, Kim DY, Han K-H, Ro SW. High Risk of Hepatocellular Carcinoma Development in Fibrotic Liver: Role of the Hippo-YAP/TAZ Signaling Pathway. IJMS. 2019 Jan;20(3):581.

33 Konishi T, Schuster RM, Lentsch AB. Proliferation of hepatic stellate cells, mediated by YAP and TAZ, contributes to liver repair and regeneration after liver ischemia-reperfusion injury. American Journal of Physiology-Gastrointestinal and Liver Physiology. 2018 Apr;314(4):G471–82.

34 Zhou J, Sun C, Yang L, Wang J, Jn-Simon N, Zhou C, et al. Liver regeneration and ethanol detoxification: A new link in YAP regulation of ALDH1A1 during alcohol-related hepatocyte damage. The FASEB Journal. 2022 Apr;36(4). DOI: 10.1096/fj.202101686R

35 Machado MV, Michelotti GA, Pereira TA, Xie G, Premont R, Cortez-Pinto H, et al. Accumulation of duct cells with activated YAP parallels fibrosis progression in non-alcoholic fatty liver disease. Journal of Hepatology. 2015 Oct;63(4):962–70.

36 Salloum S, Jeyarajan AJ, Kruger AJ, Holmes JA, Shao T, Sojoodi M, et al. Fatty Acids Activate the Transcriptional Coactivator YAP1 to Promote Liver Fibrosis via p38 Mitogen-Activated Protein Kinase. Cellular and Molecular Gastroenterology and Hepatology. 2021;12(4):1297–310.

37 Mooring M, Fowl BH, Lum SZC, Liu Y, Yao K, Softic S, et al. Hepatocyte Stress Increases Expression of Yes-Associated Protein and Transcriptional Coactivator With PDZ-Binding Motif in Hepatocytes to Promote Parenchymal Inflammation and Fibrosis. Hepatology. 2020 May;71(5):1813–30.

38 Yang Y, Santos DM, Pantano L, Knipe R, Abe E, Logue A, et al. Screening for Inhibitors of YAP Nuclear Localization Identifies Aurora Kinase A as a Modulator of Lung Fibrosis. Am J Respir Cell Mol Biol. 2022 July;67(1):36–49.

39 Chang S-S, Yamaguchi H, Xia W, Lim S-O, Khotskaya Y, Wu Y, et al. Aurora A kinase activates YAP signaling in triple-negative breast cancer. Oncogene. 2017 Mar;36(9):1265–75.

40 Wang P, Gong Y, Guo T, Li M, Fang L, Yin S, et al. Activation of Aurora A kinase increases YAP stability via blockage of autophagy. Cell Death Dis. 2019 June;10(6):432.

41 Somnay K, Wadgaonkar P, Sridhar N, Roshni P, Rao N, Wadgaonkar R. Liver Fibrosis Leading to Cirrhosis: Basic Mechanisms and Clinical Perspectives. Biomedicines. 2024 Sept;12(10):2229.

42 Chan W-K, Chuah K-H, Rajaram RB, Lim L-L, Ratnasingam J, Vethakkan SR. Metabolic Dysfunction-Associated Steatotic Liver Disease (MASLD): A State-of-the-Art Review. J Obes Metab Syndr. 2023 Sept;32(3):197–213.

43 Zhang D, Zhang Y, Sun B. The Molecular Mechanisms of Liver Fibrosis and Its Potential Therapy in Application. IJMS. 2022 Oct;23(20):12572.

44 Roehlen N, Crouchet E, Baumert TF. Liver Fibrosis: Mechanistic Concepts and Therapeutic Perspectives. Cells. 2020 Apr;9(4):875.

45 Ramakrishna G, Rastogi A, Trehanpati N, Sen B, Khosla R, Sarin SK. From Cirrhosis to Hepatocellular Carcinoma: New Molecular Insights on Inflammation and Cellular Senescence. Liver Cancer. 2013;2(3–4):367–83.

46 De Smet V, Eysackers N, Merens V, Kazemzadeh Dastjerd M, Halder G, Verhulst S, et al. Initiation of hepatic stellate cell activation extends into chronic liver disease. Cell Death Dis. 2021 Nov;12(12). DOI: 10.1038/s41419-021-04377-1

47 Taru V, Szabo G, Mehal W, Reiberger T. Inflammasomes in chronic liver disease: Hepatic injury, fibrosis progression and systemic inflammation. Journal of Hepatology. 2024 Nov;81(5):895–910.

48 Xu F, Liu C, Zhou D, Zhang L. TGF-β/SMAD Pathway and Its Regulation in Hepatic Fibrosis. J Histochem Cytochem. 2016 Mar;64(3):157–67.

49 Hanafusa H, Ninomiya-Tsuji J, Masuyama N, Nishita M, Fujisawa J, Shibuya H, et al. Involvement of the p38 Mitogen-activated Protein Kinase Pathway in Transforming Growth Factor-β-induced Gene Expression. Journal of Biological Chemistry. 1999 Sept;274(38):27161–7.

50 Engel ME, McDonnell MA, Law BK, Moses HL. Interdependent SMAD and JNK Signaling in Transforming Growth Factor-β-mediated Transcription. Journal of Biological Chemistry. 1999 Dec;274(52):37413–20.

51 Wong L, Yamasaki G, Johnson RJ, Friedman SL. Induction of beta-platelet-derived growth factor receptor in rat hepatic lipocytes during cellular activation in vivo and in culture. J Clin Invest. 1994 Oct;94(4):1563–9.

52 Yang L, Kwon J, Popov Y, Gajdos GB, Ordog T, Brekken RA, et al. Vascular endothelial growth factor promotes fibrosis resolution and repair in mice. Gastroenterology. 2014 May;146(5):1339-1350.e1.

53 Huang G, Brigstock DR. Regulation of hepatic stellate cells by connective tissue growth factor. Front Biosci (Landmark Ed). 2012 June;17(7):2495–507.

54 Chiu Y-S, Wei C-C, Lin Y-J, Hsu Y-H, Chang M-S. IL-20 and IL-20R1 antibodies protect against liver fibrosis. Hepatology. 2014 Sept;60(3):1003–14.

55 Czaja AJ. Hepatic inflammation and progressive liver fibrosis in chronic liver disease. WJG. 2014;20(10):2515.

56 Gao R, Tang H, Mao J. Programmed Cell Death in Liver Fibrosis. J Inflamm Res. 2023;16:3897–910.

57 Caligiuri A, Gentilini A, Pastore M, Gitto S, Marra F. Cellular and Molecular Mechanisms Underlying Liver Fibrosis Regression. Cells. 2021 Oct;10(10):2759.

58 Zhang C, Sun C, Zhao Y, Ye B, Yu G. Signaling pathways of liver regeneration: Biological mechanisms and implications. iScience. 2024 Jan;27(1):108683.

59 Aoyagi T, Goya T, Imoto K, Azuma Y, Hioki T, Kohjima M, et al. Two types of regenerative cell populations appear in acute liver injury. Stem Cell Reports. 2025 June;20(6):102503.

60 Font-Burgada J, Shalapour S, Ramaswamy S, Hsueh B, Rossell D, Umemura A, et al. Hybrid Periportal Hepatocytes Regenerate the Injured Liver without Giving Rise to Cancer. Cell. 2015 Aug;162(4):766–79.

61 Aravinthan AD, Alexander GJM. Senescence in chronic liver disease: Is the future in aging? Journal of Hepatology. 2016 Oct;65(4):825–34.

62 Ray K. Activation of NF-κB signaling in hepatocytes induces liver fibrosis. Nat Rev Gastroenterol Hepatol. 2012 May;9(5):244–244.

63 Horiguchi N, Ishac EJN, Gao B. Liver regeneration is suppressed in alcoholic cirrhosis: correlation with decreased STAT3 activation. Alcohol. 2007 June;41(4):271–80.

64 Adamek A, Kasprzak A. Insulin-Like Growth Factor (IGF) System in Liver Diseases. IJMS. 2018 Apr;19(5):1308.

65 Ye Q, Liu Y, Zhang G, Deng H, Wang X, Tuo L, et al. Deficiency of gluconeogenic enzyme PCK1 promotes metabolic-associated fatty liver disease through PI3K/AKT/PDGF axis activation in male mice. Nat Commun. 2023 Mar;14(1). DOI: 10.1038/s41467-023-37142-3

66 Lu L, Ma Y, Tao Q, Xie J, Liu X, Wu Y, et al. Hypoxia-inducible factor-1 alpha (HIF-1α) inhibitor AMSP-30 m attenuates CCl4-induced liver fibrosis in mice by inhibiting the sonic hedgehog pathway. Chemico-Biological Interactions. 2025 May;413:111480.

67 Bárcena C, Stefanovic M, Tutusaus A, Joannas L, Menéndez A, García-Ruiz C, et al. Gas6/Axl pathway is activated in chronic liver disease and its targeting reduces fibrosis via hepatic stellate cell inactivation. J Hepatol. 2015 Sept;63(3):670–8.

68 Nishikawa K, Osawa Y, Kimura K. Wnt/β-Catenin Signaling as a Potential Target for the Treatment of Liver Cirrhosis Using Antifibrotic Drugs. IJMS. 2018 Oct;19(10):3103.

69 Ge W-S, Wang Y-J, Wu J-X, Fan J-G, Chen Y-W, Zhu L. β-catenin is overexpressed in hepatic fibrosis and blockage of Wnt/β-catenin signaling inhibits hepatic stellate cell activation. Molecular Medicine Reports. 2014 June;9(6):2145–51.

70 Yang J, Pan G, Guan L, Liu Z, Wu Y, Liu Z, et al. The burden of primary liver cancer caused by specific etiologies from 1990 to 2019 at the global, regional, and national levels. Cancer Medicine. 2022 Mar;11(5):1357–70.

71 Younossi ZM, Kalligeros M, Henry L. Epidemiology of metabolic dysfunction-associated steatotic liver disease. Clin Mol Hepatol. 2025 Feb;31(Suppl):S32–50.

72 Patel S, Kasem F, Flaherty D, Barve A. HCC in MASLD and ALD: Biochemical Pathways, Epidemiology, Diagnosis, and Treatment. BioChem. 2025 June;5(3):19.

73 Forner A, Reig M, Bruix J. Hepatocellular carcinoma. The Lancet. 2018 Mar;391(10127):1301–14.

74 Niu Z-S, Niu X-J, Wang W-H. Genetic alterations in hepatocellular carcinoma: An update. WJG. 2016;22(41):9069.

75 Gallon J, Coto-Llerena M, Ercan C, Bianco G, Paradiso V, Nuciforo S, et al. Epigenetic priming in chronic liver disease impacts the transcriptional and genetic landscapes of hepatocellular carcinoma. Mol Oncol. 2022 Feb;16(3):665–82.

76 Zheng J, Wang S, Xia L, Sun Z, Chan KM, Bernards R, et al. Hepatocellular carcinoma: signaling pathways and therapeutic advances. Sig Transduct Target Ther. 2025 Feb;10(1). DOI: 10.1038/s41392-024-02075-w

77 Jang J-W, Kim J-S, Kim H-S, Tak K-Y, Lee S-K, Nam H-C, et al. Significance of TERT Genetic Alterations and Telomere Length in Hepatocellular Carcinoma. Cancers (Basel). 2021 Apr;13(9):2160.

78 Yeh S-H, Li C-L, Lin Y-Y, Ho M-C, Wang Y-C, Tseng S-T, et al. Hepatitis B Virus DNA Integration Drives Carcinogenesis and Provides a New Biomarker for HBV-related HCC. Cell Mol Gastroenterol Hepatol. 2023;15(4):921–9.

79 Guichard C, Amaddeo G, Imbeaud S, Ladeiro Y, Pelletier L, Maad IB, et al. Integrated analysis of somatic mutations and focal copy-number changes identifies key genes and pathways in hepatocellular carcinoma. Nat Genet. 2012 June;44(6):694–8.

80 Wang K, Wu J, Yang Z, Zheng B, Shen S, Wang R, et al. Hyperactivation of β-catenin signal in hepatocellular carcinoma recruits myeloid-derived suppressor cells through PF4-CXCR3 axis. Cancer Letters. 2024 Apr;586:216690.

81 Xu C, Xu Z, Zhang Y, Evert M, Calvisi DF, Chen X. β-Catenin signaling in hepatocellular carcinoma. J Clin Invest. 2022 Feb;132(4):e154515.

82 Pinyol R, Sia D, Llovet JM. Immune Exclusion-Wnt/CTNNB1 Class Predicts Resistance to Immunotherapies in HCC. Clinical Cancer Research. 2019 Apr;25(7):2021–3.

83 McCubrey JA, Steelman LS, Bertrand FE, Davis NM, Abrams SL, Montalto G, et al. Multifaceted roles of GSK-3 and Wnt/β-catenin in hematopoiesis and leukemogenesis: opportunities for therapeutic intervention. Leukemia. 2014 Jan;28(1):15–33.

84 Diehl JA, Cheng M, Roussel MF, Sherr CJ. Glycogen synthase kinase-3beta regulates cyclin D1 proteolysis and subcellular localization. Genes Dev. 1998 Nov;12(22):3499–511.

85 Zheng H, Li W, Wang Y, Liu Z, Cai Y, Xie T, et al. Glycogen synthase kinase-3 beta regulates Snail and β-catenin expression during Fas-induced epithelial–mesenchymal transition in gastrointestinal cancer. European Journal of Cancer. 2013 Aug;49(12):2734–46.

86 Frame S, Cohen P. GSK3 takes centre stage more than 20 years after its discovery. Biochem J. 2001 Oct;359(Pt 1):1–16.

87 Huang K-T, Huang Y-H, Li P, He B, Chen Z-K, Yu X, et al. Correlation between tuberous sclerosis complex 2 and glycogen synthase kinase 3 beta levels, and outcomes of patients with hepatocellular carcinoma treated by hepatectomy. Hepatol Res. 2014 Oct;44(11):1142–50.

88 Hu Y, Lin X, Zuo S, Luo R, Fang W. Elevated GSK3β expression predicts good prognosis in hepatocellular carcinoma. Int J Clin Exp Pathol. 2018;11(5):2776–83.

89 Yu Z, Gao Y-Q, Feng H, Lee Y-Y, Li MS, Tian Y, et al. Cell cycle-related kinase mediates viral-host signalling to promote hepatitis B virus-associated hepatocarcinogenesis. Gut. 2014 Nov;63(11):1793–804.

90 Street A, Macdonald A, McCormick C, Harris M. Hepatitis C virus NS5A-mediated activation of phosphoinositide 3-kinase results in stabilization of cellular beta-catenin and stimulation of beta-catenin-responsive transcription. J Virol. 2005 Apr;79(8):5006–16.

91 Jin R, Liu W, Menezes S, Yue F, Zheng M, Kovacevic Z, et al. The metastasis suppressor NDRG1 modulates the phosphorylation and nuclear translocation of β-catenin through mechanisms involving FRAT1 and PAK4. J Cell Sci. 2014 July;127(Pt 14):3116–30.

92 Lu W-J, Chua M-S, Wei W, So SK. NDRG1 promotes growth of hepatocellular carcinoma cells by directly interacting with GSK-3β and Nur77 to prevent β-catenin degradation. Oncotarget. 2015 Oct;6(30):29847–59.

93 Lee D, Cho M, Kim E, Seo Y, Cha J-H. PD-L1: From cancer immunotherapy to therapeutic implications in multiple disorders. Molecular Therapy. 2024 Dec;32(12):4235–55.

94 Calderaro J, Rousseau B, Amaddeo G, Mercey M, Charpy C, Costentin C, et al. Programmed death ligand 1 expression in hepatocellular carcinoma: Relationship With clinical and pathological features. Hepatology. 2016 Dec;64(6):2038–46.

95 Xu H, Liang X-L, Liu X-G, Chen N-P. The landscape of PD-L1 expression and somatic mutations in hepatocellular carcinoma. J Gastrointest Oncol. 2021 June;12(3):1132–40.

96 Kudo M. Changing the Treatment Paradigm for Hepatocellular Carcinoma Using Atezolizumab plus Bevacizumab Combination Therapy. Cancers (Basel). 2021 Oct;13(21):5475.

97 Hao L, Li S, Deng J, Li N, Yu F, Jiang Z, et al. The current status and future of PD-L1 in liver cancer. Front Immunol. 2023 Dec;14:1323581.

98 Wang Q, Tan W, Zhang Z, Chen Q, Xie Z, Yang L, et al. FAT10 induces immune suppression by upregulating PD-L1 expression in hepatocellular carcinoma. Apoptosis. 2024 Oct;29(9–10):1529–45.

99 Ding C-H, Yan F-Z, Xu B-N, Qian H, Hong X-L, Liu S-Q, et al. PRMT3 drives PD-L1-mediated immune escape through activating PDHK1-regulated glycolysis in hepatocellular carcinoma. Cell Death Dis. 2025 Mar;16(1):158.

100 Zong Z, Zou J, Mao R, Ma C, Li N, Wang J, et al. M1 Macrophages Induce PD-L1 Expression in Hepatocellular Carcinoma Cells Through IL-1β Signaling. Front Immunol. 2019 July;10. DOI: 10.3389/fimmu.2019.01643

101 Yu X, Li W, Young KH, Li Y. Posttranslational Modifications in PD-L1 Turnover and Function: From Cradle to Grave. Biomedicines. 2021 Nov;9(11):1702.

102 Li C-W, Lim S-O, Xia W, Lee H-H, Chan L-C, Kuo C-W, et al. Glycosylation and stabilization of programmed death ligand-1 suppresses T-cell activity. Nat Commun. 2016 Aug;7(1):12632.

103 Liu J, Xu X, Zhong H, Yu M, Abuduaini N, Zhang S, et al. Glycosylation and Its Role in Immune Checkpoint Proteins: From Molecular Mechanisms to Clinical Implications. Biomedicines. 2024 June;12(7):1446.

104 Wang Y-N, Lee H-H, Hsu JL, Yu D, Hung M-C. The impact of PD-L1 N-linked glycosylation on cancer therapy and clinical diagnosis. J Biomed Sci. 2020 Dec;27(1):77.

105 Tan Y, Xu Q, Wu Z, Zhang W, Li B, Zhang B, et al. Overexpression of PD-L1 is an Independent Predictor for Recurrence in HCC Patients Who Receive Sorafenib Treatment After Surgical Resection. Front Oncol. 2022 Jan;11:783335.

106 Sun G, Liu H, Zhao J, Zhang J, Huang T, Sun G, et al. Macrophage GSK3β-deficiency inhibits the progression of hepatocellular carcinoma and enhances the sensitivity of anti-PD1 immunotherapy. J Immunother Cancer. 2022 Dec;10(12):e005655.

107 Su W-L, Chuang S-C, Wang Y-C, Chen L-A, Huang J-W, Chang W-T, et al. Expression of FOXM1 and Aurora-A predicts prognosis and sorafenib efficacy in patients with hepatocellular carcinoma. Cancer Biomark. 2020;28(3):341–50.

108 Li G, Tian Y, Gao Z. The role of AURKA/miR-199b-3p in hepatocellular carcinoma cells. Clinical Laboratory Analysis. 2022 Dec;36(12). DOI: 10.1002/jcla.24758

109 Zheng D, Li J, Yan H, Zhang G, Li W, Chu E, et al. Emerging roles of Aurora-A kinase in cancer therapy resistance. Acta Pharm Sin B. 2023 July;13(7):2826–43.

110 Lu L, Han H, Tian Y, Li W, Zhang J, Feng M, et al. Aurora kinase A mediates c-Myc's oncogenic effects in hepatocellular carcinoma. Molecular Carcinogenesis. 2015 Nov;54(11):1467–79.

111 Chen C, Song G, Xiang J, Zhang H, Zhao S, Zhan Y. AURKA promotes cancer metastasis by regulating epithelial-mesenchymal transition and cancer stem cell properties in hepatocellular carcinoma. Biochemical and Biophysical Research Communications. 2017 Apr;486(2):514–20.

112 Cui S-Y, Huang J-Y, Chen Y-T, Song H-Z, Huang G-C, De W, et al. The role of Aurora A in hypoxia-inducible factor 1α-promoting malignant phenotypes of hepatocelluar carcinoma. Cell Cycle. 2013 Sept;12(17):2849–66.

113 Gao X, Lai Y, Zhang Z, Ma Y, Luo Z, Li Y, et al. Long Non-coding RNA RP11-480I12.5 Promotes the Proliferation, Migration, and Invasion of Breast Cancer Cells Through the miR-490-3p-AURKA-Wnt/β-Catenin Axis. Front Oncol. 2020 July;10:948.

114 Dar AA, Belkhiri A, El-Rifai W. The aurora kinase A regulates GSK-3beta in gastric cancer cells. Oncogene. 2009 Feb;28(6):866–75.

115 Chen X, Wang K, Jiang S, Sun H, Che X, Zhang M, et al. eEF2K promotes PD-L1 stabilization through inactivating GSK3β in melanoma. J Immunother Cancer. 2022 Mar;10(3):e004026.

116 Schulz D, Stancev I, Sorrentino A, Menevse A-N, Beckhove P, Brockhoff G, et al. Increased PD-L1 expression in radioresistant HNSCC cell lines after irradiation affects cell proliferation due to inactivation of GSK-3beta. Oncotarget. 2019 Jan;10(5):573–83.

117 Yao C-Y, Tao H-T, He J-J, Zhu F-Y, Xie C-Q, Cheng Y-N, et al. NUAK1 acts as a novel regulator of PD-L1 via activating GSK-3β/β-catenin pathway in hepatocellular carcinoma. Mol Med. 2025 Feb;31(1). DOI: 10.1186/s10020-025-01088-7

118 Kim DY. Changing etiology and epidemiology of hepatocellular carcinoma: Asia and worldwide. JLC. 2024 Mar;24(1):622–70.

119 Finn RS, Qin S, Ikeda M, Galle PR, Ducreux M, Kim T-Y, et al. Atezolizumab plus Bevacizumab in Unresectable Hepatocellular Carcinoma. N Engl J Med. 2020 May;382(20):1894–905.

120 Liu H, Cali Daylan AE, Yang J, Tanwar A, Borczuk A, Zhang D, et al. Aurora Kinase A Inhibition Potentiates Platinum and Radiation Cytotoxicity in Non-Small-Cell Lung Cancer Cells and Induces Expression of Alternative Immune Checkpoints. Cancers. 2024 Aug;16(16):2805.

121 Meng B, Zhao X, Jiang S, Xu Z, Li S, Wang X, et al. AURKA inhibitor-induced PD-L1 upregulation impairs antitumor immune responses. Front Immunol. 2023;14:1182601.

122 Nguyen TTT, Gao Q, Mun J-Y, Zhu Z, Shu C, Naim A, et al. Suppressing PD-L1 Expression via AURKA Kinase Inhibition Enhances Natural Killer Cell-Mediated Cytotoxicity against Glioblastoma. Cells. 2024 July;13(13):1155.

123 Fujise K, Nagamori S, Hasumura S, Homma S, Sujino H, Matsuura T, et al. Integration of hepatitis B virus DNA into cells of six established human hepatocellular carcinoma cell lines. Hepatogastroenterology. 1990 Oct;37(5):457–60.

124 Nagamori S, Fujise K, Hasumura S, Homma S, Sujino H, Matsuura T, et al. [Protein secretion of human cultured liver cells]. Hum Cell. 1988 Dec;1(4):382–90.

125 Kawamoto M, Yamaji T, Saito K, Shirasago Y, Satomura K, Endo T, et al. Identification of Characteristic Genomic Markers in Human Hepatoma HuH-7 and Huh7.5.1-8 Cell Lines. Front Genet. 2020;11:546106.

126 Dor I, Namba M, Sato J. Establishment and some biological characteristics of human hepatoma cell lines. Gan. 1975 Aug;66(4):385–92.

127 Aden DP, Fogel A, Plotkin S, Damjanov I, Knowles BB. Controlled synthesis of HBsAg in a differentiated human liver carcinoma-derived cell line. Nature. 1979 Dec;282(5739):615–6.

128 Schneider-Poetsch T, Ju J, Eyler DE, Dang Y, Bhat S, Merrick WC, et al. Inhibition of eukaryotic translation elongation by cycloheximide and lactimidomycin. Nat Chem Biol. 2010 Mar;6(3):209–17.

129 Guo N, Peng Z. MG132, a proteasome inhibitor, induces apoptosis in tumor cells. Asia-Pac J Clncl Oncology. 2013 Mar;9(1):6–11.

130 Xing Y, Lin NU, Maurer MA, Chen H, Mahvash A, Sahin A, et al. Phase II trial of AKT inhibitor MK-2206 in patients with advanced breast cancer who have tumors with PIK3CA or AKT mutations, and/or PTEN loss/PTEN mutation. Breast Cancer Res. 2019 Dec;21(1):78.

131 Bustin SA, Benes V, Garson JA, Hellemans J, Huggett J, Kubista M, et al. The MIQE Guidelines: Minimum Information for Publication of Quantitative Real-Time PCR Experiments. Clinical Chemistry. 2009 Apr;55(4):611–22.

132 Wang B, Hsu C-J, Chou C-H, Lee H-L, Chiang W-L, Su C-M, et al. Variations in the AURKA Gene: Biomarkers for the Development and Progression of Hepatocellular Carcinoma. Int J Med Sci. 2018;15(2):170–5.

133 Hayat R, Manzoor M, Hussain A. Wnt signaling pathway: A comprehensive review. Cell Biology International. 2022 June;46(6):863–77.

134 Mancinelli R, Carpino G, Petrungaro S, Mammola CL, Tomaipitinca L, Filippini A, et al. Multifaceted Roles of GSK-3 in Cancer and Autophagy-Related Diseases. Oxid Med Cell Longev. 2017;2017:4629495.

135 Duda P, Akula SM, Abrams SL, Steelman LS, Martelli AM, Cocco L, et al. Targeting GSK3 and Associated Signaling Pathways Involved in Cancer. Cells. 2020 Apr;9(5):1110.

136 Kazi A, Xiang S, Yang H, Delitto D, Trevino J, Jiang RHY, et al. GSK3 suppression upregulates β-catenin and c-Myc to abrogate KRas-dependent tumors. Nat Commun. 2018 Dec;9(1):5154.

137 Baumgart S, Chen N-M, Zhang J-S, Billadeau DD, Gaisina IN, Kozikowski AP, et al. GSK-3β Governs Inflammation-Induced NFATc2 Signaling Hubs to Promote Pancreatic Cancer Progression. Mol Cancer Ther. 2016 Mar;15(3):491–502.

138 Lin J, Song T, Li C, Mao W. GSK-3β in DNA repair, apoptosis, and resistance of chemotherapy, radiotherapy of cancer. Biochim Biophys Acta Mol Cell Res. 2020 May;1867(5):118659.

139 Gou Q, Dong C, Xu H, Khan B, Jin J, Liu Q, et al. PD-L1 degradation pathway and immunotherapy for cancer. Cell Death Dis. 2020 Nov;11(11):955.

140 Yin Y, Kong D, He K, Xia Q. Aurora kinase A regulates liver regeneration through macrophages polarization and Wnt/β-catenin signalling. Liver International. 2022 Feb;42(2):468–78.

141 Lee S, Choi EJ, Cho EJ, Lee YB, Lee J-H, Yu SJ, et al. Inhibition of PI3K/Akt signaling suppresses epithelial-to-mesenchymal transition in hepatocellular carcinoma through the Snail/GSK-3/beta-catenin pathway. Clin Mol Hepatol. 2020 Oct;26(4):529–39.

142 Matsuo FS, Andrade MF, Loyola AM, da Silva SJ, Silva MJB, Cardoso SV, et al. Pathologic significance of AKT, mTOR, and GSK3β proteins in oral squamous cell carcinoma-affected patients. Virchows Arch. 2018 June;472(6):983–97.

143 Xi J, Sun Y, Zhang M, Fa Z, Wan Y, Min Z, et al. GLS1 promotes proliferation in hepatocellular carcinoma cells via AKT/GSK3β/CyclinD1 pathway. Experimental Cell Research. 2019 Aug;381(1):1–9.

144 Johnson PJ, Kalyuzhnyy A, Boswell E, Toyoda H. Progression of chronic liver disease to hepatocellular carcinoma: implications for surveillance and management. BJC Rep. 2024 May;2(1). DOI: 10.1038/s44276-024-00050-0

145 Brackenier C, Kinget L, Cappuyns S, Verslype C, Beuselinck B, Dekervel J. Unraveling the Synergy between Atezolizumab and Bevacizumab for the Treatment of Hepatocellular Carcinoma. Cancers (Basel). 2023 Jan;15(2):348.

146 Cacioppo R, Rad D, Pagani G, Gandellini P, Lindon C. Post-transcriptional control drives Aurora kinase A expression in human cancers. 2024 Feb DOI: 10.1101/2024.02.22.581549

147 Wu Y, Liu Z, Xu X. Molecular subtyping of hepatocellular carcinoma: A step toward precision medicine. Cancer Commun (Lond). 2020 Dec;40(12):681–93.

148 De Sousa Abreu R, Penalva LO, Marcotte EM, Vogel C. Global signatures of protein and mRNA expression levels. Mol BioSyst. 2009;10.1039.b908315d.

149 Mobley A, Zhang S, Bondaruk J, Wang Y, Majewski T, Caraway NP, et al. Aurora Kinase A is a Biomarker for Bladder Cancer Detection and Contributes to its Aggressive Behavior. Sci Rep. 2017 Jan;7:40714.

150 Kulbe H, Otto R, Darb-Esfahani S, Lammert H, Abobaker S, Welsch G, et al. Discovery and Validation of Novel Biomarkers for Detection of Epithelial Ovarian Cancer. Cells. 2019 July;8(7):713.

151 Miralaei N, Majd A, Ghaedi K, Peymani M, Safaei M. Integrated pan-cancer of *AURKA* expression and drug sensitivity analysis reveals increased expression of *AURKA* is responsible for drug resistance. Cancer Med. 2021 Sept;10(18):6428–41.

152 Wang B, Hsu C-J, Chou C-H, Lee H-L, Chiang W-L, Su C-M, et al. Variations in the AURKA Gene: Biomarkers for the Development and Progression of Hepatocellular Carcinoma. Int J Med Sci. 2018;15(2):170–5.

153 Cacioppo R, Rad D, Pagani G, Gandellini P, Lindon C. Post-transcriptional control drives Aurora kinase A expression in human cancers. PLoS One. 2024;19(11):e0310625.

154 Cacioppo R, Lindon C. Regulating the regulator: a survey of mechanisms from transcription to translation controlling expression of mammalian cell cycle kinase Aurora A. Open Biol. 2022 Sept;12(9):220134.

155 Ma X, Huang T, Chen X, Li Q, Liao M, Fu L, et al. Molecular mechanisms in liver repair and regeneration: from physiology to therapeutics. Sig Transduct Target Ther. 2025 Feb;10(1):63.

156 Sourisseau T, Maniotis D, McCarthy A, Tang C, Lord CJ, Ashworth A, et al. Aurora-A expressing tumour cells are deficient for homology-directed DNA double strand-break repair and sensitive to PARP inhibition. EMBO Mol Med. 2010 Apr;2(4):130–42.

157 Do T-V, Hirst J, Hyter S, Roby KF, Godwin AK. Aurora A kinase regulates non-homologous end-joining and poly(ADP-ribose) polymerase function in ovarian carcinoma cells. Oncotarget. 2017 Aug;8(31):50376–92.

158 Sharma RK, Chafik A, Bertolin G. Aurora kinase A/AURKA functionally interacts with the mitochondrial ATP synthase to regulate energy metabolism and cell death. Cell Death Discov. 2023 June;9(1):203.

159 Bertolin G, Bulteau A-L, Alves-Guerra M-C, Burel A, Lavault M-T, Gavard O, et al. Aurora kinase A localises to mitochondria to control organelle dynamics and energy production. Elife. 2018 Aug;7:e38111.

160 Li X, Chen W, Jia Z, Xiao Y, Shi A, Ma X. Mitochondrial Dysfunction as a Pathogenesis and Therapeutic Strategy for Metabolic-Dysfunction-Associated Steatotic Liver Disease. IJMS. 2025 Apr;26(9):4256.

161 Hou D, Che Z, Chen P, Zhang W, Chu Y, Liu J. Suppression of AURKA alleviates p27 inhibition on Bax cleavage and induces more intensive apoptosis in gastric cancer. Cell Death Dis. 2018 July;9(8):781.

162 Rio-Vilariño A, Cenigaonandia-Campillo A, García-Bautista A, Mateos-Gómez PA, Schlaepfer MI, Del Puerto-Nevado L, et al. Inhibition of the AURKA/YAP1 axis is a promising therapeutic option for overcoming cetuximab resistance in colorectal cancer stem cells. Br J Cancer. 2024 May;130(8):1402–13.

163 Kim C-L, Lim S-B, Kim K, Jeong H-S, Mo J-S. Phosphorylation analysis of the Hippo-YAP pathway using Phos-tag. Journal of Proteomics. 2022 June;261:104582.

164 Huang Y, Li T, Ems-McClung SC, Walczak CE, Prigent C, Zhu X, et al. Aurora A activation in mitosis promoted by BuGZ. J Cell Biol. 2018 Jan;217(1):107–16.

165 Liu L, Guo C, Dammann R, Tommasi S, Pfeifer GP. RASSF1A interacts with and activates the mitotic kinase Aurora-A. Oncogene. 2008 Oct;27(47):6175–86.

166 Satinover DL, Leach CA, Stukenberg PT, Brautigan DL. Activation of Aurora-A kinase by protein phosphatase inhibitor-2, a bifunctional signaling protein. Proc Natl Acad Sci U S A. 2004 June;101(23):8625–30.

167 Zhao Z-S, Lim JP, Ng Y-W, Lim L, Manser E. The GIT-associated kinase PAK targets to the centrosome and regulates Aurora-A. Mol Cell. 2005 Oct;20(2):237–49.

168 Li Z, Su P, Yu M, Zhang X, Xu Y, Jia T, et al. YAP represses the TEAD–NF-κB complex and inhibits the growth of clear cell renal cell carcinoma. Sci Signal. 2024 July;17(843):eadk0231.

169 Li X, Cho YS, Zhu J, Zhuo S, Jiang J. The Hippo pathway effector YAP inhibits HIF2 signaling and ccRCC tumor growth. Cell Discov. 2022 Oct;8(1):103.

170 Chen C, Zhu D, Zhang H, Han C, Xue G, Zhu T, et al. YAP-dependent ubiquitination and degradation of β-catenin mediates inhibition of Wnt signalling induced by Physalin F in colorectal cancer. Cell Death Dis. 2018 May;9(6):591.

171 Cottini F, Hideshima T, Xu C, Sattler M, Dori M, Agnelli L, et al. Rescue of Hippo coactivator YAP1 triggers DNA damage-induced apoptosis in hematological cancers. Nat Med. 2014 June;20(6):599–606.

172 Yin Y, Kong D, He K, Xia Q. Aurora kinase A regulates liver regeneration through macrophages polarization and Wnt/β-catenin signalling. Liver International. 2022 Feb;42(2):468–78.

173 Fang D, Hawke D, Zheng Y, Xia Y, Meisenhelder J, Nika H, et al. Phosphorylation of beta-catenin by AKT promotes beta-catenin transcriptional activity. J Biol Chem. 2007 Apr;282(15):11221–9.

174 Misztal K, Wisniewska MB, Ambrozkiewicz M, Nagalski A, Kuznicki J. WNT protein-independent constitutive nuclear localization of beta-catenin protein and its low degradation rate in thalamic neurons. J Biol Chem. 2011 Sept;286(36):31781–8.

175 Taurin S, Sandbo N, Qin Y, Browning D, Dulin NO. Phosphorylation of β-Catenin by Cyclic AMP-dependent Protein Kinase. Journal of Biological Chemistry. 2006 Apr;281(15):9971–6.

176 Beurel E, Grieco SF, Jope RS. Glycogen synthase kinase-3 (GSK3): Regulation, actions, and diseases. Pharmacology & Therapeutics. 2015 Apr;148:114–31.

177 Medunjanin S, Schleithoff L, Fiegehenn C, Weinert S, Zuschratter W, Braun-Dullaeus RC. GSK-3β controls NF-kappaB activity via IKKγ/NEMO. Sci Rep. 2016 Dec;6(1):38553.

178 Wang Z, Iwasaki M, Ficara F, Lin C, Matheny C, Wong SHK, et al. GSK-3 promotes conditional association of CREB and its coactivators with MEIS1 to facilitate HOX-mediated transcription and oncogenesis. Cancer Cell. 2010 June;17(6):597–608.

179 Buller CL, Loberg RD, Fan M-H, Zhu Q, Park JL, Vesely E, et al. A GSK-3/TSC2/mTOR pathway regulates glucose uptake and GLUT1 glucose transporter expression. Am J Physiol Cell Physiol. 2008 Sept;295(3):C836-843.

180 Abd-Ellah A, Voogdt C, Krappmann D, Möller P, Marienfeld RB. GSK3β modulates NF-κB activation and RelB degradation through site-specific phosphorylation of BCL10. Sci Rep. 2018 Jan;8(1):1352.

181 Demarchi F, Bertoli C, Sandy P, Schneider C. Glycogen Synthase Kinase-3β Regulates NF-κB1/p105 Stability. Journal of Biological Chemistry. 2003 Oct;278(41):39583–90.

182 Lakshmanan J, Zhang B, Nweze IC, Du Y, Harbrecht BG. Glycogen Synthase Kinase 3 Regulates IL-1β Mediated iNOS Expression in Hepatocytes by Down-Regulating c-Jun. J of Cellular Biochemistry. 2015 Jan;116(1):133–41.

183 Green HF, Nolan YM. GSK-3 mediates the release of IL-1β, TNF-α and IL-10 from cortical glia. Neurochemistry International. 2012 Oct;61(5):666–71.

184 Emma MR, Augello G, Cusimano A, Azzolina A, Montalto G, McCubrey JA, et al. GSK-3 in liver diseases: Friend or foe? Biochimica et Biophysica Acta (BBA) - Molecular Cell Research. 2020 Sept;1867(9):118743.

185 Oksvold MP, Pedersen NM, Forfang L, Smeland EB. Effect of cycloheximide on epidermal growth factor receptor trafficking and signaling. FEBS Letters. 2012 Oct;586(20):3575–81.

186 Oslowski CM, Urano F. Measuring ER Stress and the Unfolded Protein Response Using Mammalian Tissue Culture System. Methods in Enzymology. Elsevier; 2011; pp 71–92.

187 Cao Y, Ye Q, Ma M, She Q-B. Enhanced bypass of PD-L1 translation reduces the therapeutic response to mTOR kinase inhibitors. Cell Rep. 2023 July;42(7):112764.

188 Suresh S, Chen B, Zhu J, Golden RJ, Lu C, Evers BM, et al. eIF5B drives integrated stress response-dependent translation of PD-L1 in lung cancer. Nat Cancer. 2020 May;1(5):533–45.

189 Vranic S, Gatalica Z. PD-L1 testing by immunohistochemistry in immuno-oncology. Biomol Biomed. 2023 Feb;23(1):15–25.

190 Yang Y, Chen D, Zhao B, Ren L, Huang R, Feng B, et al. The predictive value of PD-L1 expression in patients with advanced hepatocellular carcinoma treated with PD-1/PD-L1 inhibitors: A systematic review and meta-analysis. Cancer Med. 2023 Apr;12(8):9282–92.

191 Ng CKY, Dazert E, Boldanova T, Coto-Llerena M, Nuciforo S, Ercan C, et al. Integrative proteogenomic characterization of hepatocellular carcinoma across etiologies and stages. Nat Commun. 2022 May;13(1):2436.

192 Krishnankutty A, Kimura T, Saito T, Aoyagi K, Asada A, Takahashi S-I, et al. In vivo regulation of glycogen synthase kinase 3β activity in neurons and brains. Sci Rep. 2017 Aug;7(1):8602.

193 Mosquera JM, Beltran H, Park K, MacDonald TY, Robinson BD, Tagawa ST, et al. Concurrent AURKA and MYCN gene amplifications are harbingers of lethal treatment-related neuroendocrine prostate cancer. Neoplasia. 2013 Jan;15(1):1–10.

194 Mancini M, De Santis S, Monaldi C, Bavaro L, Martelli M, Castagnetti F, et al. Hyper-activation of Aurora kinase a-polo-like kinase 1-FOXM1 axis promotes chronic myeloid leukemia resistance to tyrosine kinase inhibitors. J Exp Clin Cancer Res. 2019 Dec;38(1):216.

195 Su Z-L, Su C-W, Huang Y-L, Yang W-Y, Sampurna BP, Ouchi T, et al. A Novel AURKA Mutant-Induced Early-Onset Severe Hepatocarcinogenesis Greater than Wild-Type via Activating Different Pathways in Zebrafish. Cancers. 2019 July;11(7):927.

196 Liang M-Q, Yu F-Q, Chen C. C-Myc regulates PD-L1 expression in esophageal squamous cell carcinoma. Am J Transl Res. 2020;12(2):379–88.

197 Wang K, Dai X, Yu A, Feng C, Liu K, Huang L. Peptide-based PROTAC degrader of FOXM1 suppresses cancer and decreases GLUT1 and PD-L1 expression. J Exp Clin Cancer Res. 2022 Sept;41(1):289.

198 Du L, Lee J-H, Jiang H, Wang C, Wang S, Zheng Z, et al. β-Catenin induces transcriptional expression of PD-L1 to promote glioblastoma immune evasion. Journal of Experimental Medicine. 2020 Nov;217(11):e20191115.

199 Jin S, Wang X, Tong T, Zhang D, Shi J, Chen J, et al. Aurora-A enhances malignant development of esophageal squamous cell carcinoma (ESCC) by phosphorylating β-catenin. Molecular Oncology. 2015 Jan;9(1):249–59.

Chapter 7

Research Dissemination and Presentations

List of Publications

Grisetti L, Garcia CJC, Saponaro AA, Tiribelli C, Pascut D. The role of Aurora kinase A in hepatocellular carcinoma: Unveiling the intriguing functions of a key but still underexplored factor in liver cancer. Cell Prolif. 2024; 57(8):e13641. doi:10.1111/cpr.13641

Garcia, C. J. C., Grisetti, L., Tiribelli, C., & Pascut, D. (2024). The ncRNA-AURKA Interaction in Hepatocellular Carcinoma: Insights into Oncogenic Pathways, Therapeutic Opportunities, and Future Challenges. *Life*, *14*(11), 1430. https://doi.org/10.3390/life14111430

Oral and Poster Presentations

POSTER PRESENTATION AT EASL LIVER CANCER SUMMIT, ROTTERDAM, THE NETHERLANDS (22-24 FEBRUARY 2024), FULL BURSARY RECEIVED
Garcia, C., Grisetti, L., Sukowati, C. H. C., Tarchi, P., Bonazza, D., Giacomello, E., Crocè, L. S., Tiribelli, C., & Pascut, D. (2024). The Potential Modulatory Role of Aurora Kinase A on Yes-associated Protein and Glycogen Synthase Kinase-3 Beta in Advanced Chronic Liver Disease

POSTER PRESENTATION AT THE ASIAN PACIFIC ASSOCIATION FOR THE STUDY OF THE LIVER, KYOTO, JAPAN (27-31 MARCH 2024); POSTER PRESENTED BY CO-AUTHOR (UNDERLINE)
Garcia, C., Grisetti, L., Cabral, K. Sukowati, C. H. C., Tarchi, P., Bonazza, D., Giacomello, E., Crocè, L. S., Tiribelli, C., & Pascut, D. (2024). Deciphering the novel functions of Aurora Kinase A in Chronic Liver Disease

POSTER PRESENTATION AT THE INTERNATIONAL LIVER CANCER ASSOCIATION, TORONTO, CANADA; POSTER PRESENTED BY CO-AUTHOR (UNDERLINED)
Garcia, C., Grisetti, L., Sukowati C. H. C., Tarchi P., Bonazza, D., Giacomello, E., Crocè, L. S., Tiribelli, C., & Pascut, D. (2024). The Differential Regulatory Role of Aurora Kinase A in Chronic Liver Disease and Hepatocellular Carcinoma

POSTER PRESENTATION AT EASL LIVER CANCER SUMMIT, PARIS, FRANCE (20-22 FEBRUARY 2025), FULL BURSARY RECEIVED
Garcia, C., Grisetti, L., Tiribelli, C., & Pascut, D. Deciphering the Glycosylation Status of Programmed Cell Death-Ligand 1 and its Regulation by Aurora Kinase A in Hepatocellular Carcinoma

Acknowledgment

This work came to fruition through the guidance and support of my supervisor, Dr. Devis Pascut. I am also profoundly grateful to Prof. Tiribelli for welcoming me as a PhD student at FIF and for his trust that I could carry all the responsibilities of a PhD student.

My heartfelt thanks go to my colleagues as well—especially Luca Grisetti—who helped me learn the ins and outs of the lab when I arrived, working with you has been a pleasure. My deepest gratitude as well to Caecil, Nata, and Pablo for their continuous hard work to collect tissue samples from the hospital. To all the past and present members of FIF, THANK YOU! The memories we share will stay with me.

I am also thankful to my Filipino friends here in Trieste—Melvin, Julia and Romar—for making life here a little less lonely.

I owe immense amount of gratitude to my parents, whose unwavering love and support allowed me to pursue the things I wanted to.

To my dearest friends who have stood by me through the years—Nicole, Aldrin, and Miguel—thank you for your never-ending presence in my life.

To Geoffrey, my fiancé, thank you for walking beside me every step of this journey; I love you to the moon and back—again and again.

To Kodi, my dog; if love could lend time, I would gladly give you ten years of my life so you could live forever. This is for you, too.

Above all, I dedicate this work to my grandmother, whose care and quiet devotion helped shape who I am.